Scuola Internazionale Superiore Studi Avanzati -S.I.S.S.A-

International School for Advanced Studies -I.S.A.S-

Trieste, Italy

Functional characterization of molecular candidates for the calcium-activated chloride channels in the cilia of olfactory sensory neurons.

Thesis submitted for the degree of *"Doctor Philosophiae"*

CANDIDATE

Claudia Sagheddu

SUPERVISOR

Prof. Anna Menini

CO-SUPERVISOR

Dr. Anna Boccaccio

To Giuseppe

Notes

The work described in this Thesis was carried out at the International School for Advanced Studies, Trieste, between November 2006 and October 2010.

The work described in this Thesis is included in:

Calcium-activated chloride currents in olfactory sensory neurons from mice lacking bestrophin-2.
Pifferi S, Dibattista M, Sagheddu C, Boccaccio A, Al Qteishat A, Ghirardi F, Tirindelli R, Menini A.
The Journal of Physiology. 2009 587, 4265-79
I performed caged compounds photolysis patch clamp experiments.

Calcium concentration jumps reveal dynamic ion selectivity of calcium-activated chloride currents in mouse olfactory sensory neurons and TMEM16b-transfected HEK 293T cells.
Sagheddu C, Boccaccio A, Dibattista M, Montani G, Tirindelli R, Menini A.
The Journal of Physiology. 2010 588, 4189–4204
I performed most caged compounds photolysis patch clamp experiments.

ABSTRACT

Olfactory sensory neurons (OSNs) use a Ca^{2+}-activated Cl^- channels amplification mechanism in olfactory transduction. Odor binding to odorant receptors in the cilia of OSNs leads to an increase of intraciliary Ca^{2+} concentration by Ca^{2+} entry through cyclic nucleotide-gated channels. Ca^{2+} activates a Cl^- channel that leads to an efflux of Cl^- from the cilia, contributing to the depolarization in OSNs.

The molecular identity of the olfactory Ca^{2+}-activated Cl^- channel is not definitely established. Bestrophin2 and TMEM16b/anoctamin2 are located at the surface of the olfactory epithelium, in the cilia of OSNs where olfactory transduction takes place.

Moreover when expressed in heterologous systems each of these proteins produces Ca^{2+}-activated Cl^- currents. Both proteins have been indicated as a candidate for being a molecular component of the olfactory Ca^{2+}-activated Cl^- channel.

In the first part of this Thesis we analyzed knockout (KO) mice for bestrophin2. We compared the electrophysiological properties of Ca^{2+}-activated Cl^- currents in OSNs from WT and KO mice for bestrophin2. Our data show that Ca^{2+}-activated Cl^- currents are still present in the cilia of OSNs from KO mice for bestrophin2 and that their properties are not significantly different from those of WT mice. These results indicate that bestrophin2 does not appear to be the main molecular component of the olfactory Ca^{2+}-activated Cl^- channel. Therefore further studies are required to determine the physiological function of the bestrophin2 in the cilia of OSNs.

In the second part of this Thesis we measured functional properties of the native Ca^{2+}-activated Cl^- current in mouse OSNs and compared them with those of TMEM16b/anoctamin2-induced current in transfected HEK cells. We found a similar extracellular blocking potency for some Cl^- channels blockers, a similar anion permeability sequence and a reversal potential time-dependency. Therefore, we conclude that the measured electrophysiological properties are largely similar and further indicate that TMEM16b/anoctamin2 is likely to be a major subunit of the native olfactory Ca^{2+}-activated Cl^- current.

CONTENTS

Abbreviations

AC adenylyl cyclase

ANO anoctamin

BCMCM [6,7-bis (carboxymethoxy) coumarin-4-yl]methyl

BVMD Best vitelliform macular dystrophy

CNG cyclic nucleotide-gated

DPC diphenylamine-2-carboxylate

DIDS 4,4’diisothiocyanostilbene-2,2’-disulphonic acid

DRG dorsal root ganglion

EOG electroolfactogram

FFA flufenamic acid

GPCR G-protein coupled receptor

HEK human embryonic kidney

MeS methanesulfonate

MFA mefenamic acid

NFA niflumic acid

NPPB 5-nitro-2-(3-phenylpropylamino)benzoic acid

OR odorant receptor

OSN olfactory sensory neuron

PDE phosphodiesterase

RPE retinal pigment epithelium

SCN isothiocyanate

SITS 4-acetamido-4’-isothiocyanostilbene- 2.2’-disulphonic acid

TMD transmembrane domain

TMEM transmembrane

1 INTRODUCTION

1.1 Organization of the olfactory system

Chemical senses are responsible for detecting molecules of immense chemical variety from the environment thereby processing specific information concerning food or toxic substances as well as suitable mating partners or predators (reviewed by Firestein, 2001; Tirindelli *et al.*, 2009).

The vertebrate olfactory system is composed of a number of subsystems anatomically segregated within the nasal cavity (reviewed by Breer *et al.*, 2006; Schoenfeld & Cleland, 2005; Ma, 2007; Munger *et al.*, 2009) some well known and others only recently characterized: the main olfactory epithelium, the vomeronasal organ, the Grüneberg ganglion, the septal organ and guanylate cyclase D-containing cells in the main olfactory epithelium (Figure 1.1A). These subsystems are clearly distinguished by the chemosensory receptors they express and the signaling mechanisms they employ to detect and transduce chemosensory stimuli (reviewed by Mombaerts, 1999; Frings, 2001; Breer *et al.*, 2006; Tirindelli *et al.*, 2009); moreover they make distinct neural connections to regions of the olfactory forebrain for processing (reviewed by Munger *et al.*, 2009).

1.1.1 The olfactory epithelium and the olfactory sensory neurons

In vertebrates the main olfactory epithelium lines cartilaginous lamellae, called turbinates, in the posterior nasal cavity. It is a columnar pseudo-stratified neuroepithelium which contains some millions of ciliated olfactory sensory neurons (OSNs), microvillar cells, supporting/sustentacular cells, and basal stem cells (Figure 1.1B) (reviewed by

Breer *et al.*, 2006; Munger *et al.*, 2009; Pifferi *et al.*, 2009*c*). A layer of mucus is secreted by Bowman's glands at the surface of the olfactory epithelium, partially protecting the tissue that is in direct contact with the external environment. The olfactory epithelium has evolved a constitutive mechanism of neurogenesis (Schwob, 2002) to replenish neuronal population lost during natural turnover or after lesions. At the basal germinal layer, globose and horizontal basal cells are thought to contribute to ongoing neurogenesis but the process is poorly understood (Caggiano *et al.*, 1994; Calof *et al.*, 2002; Leung *et al.*, 2007).

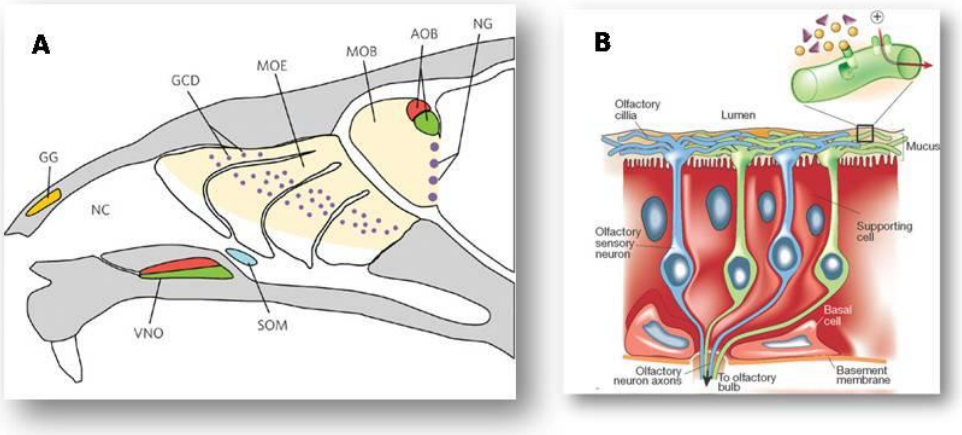

Figure 1.1 *A) Cartoon of olfactory sensory system within the nasal cavity of mouse (From Brennan & Zufall, 2006). MOE, main olfactory epithelium; VNO, vomeronasal organ; GG, Grüneberg ganglion; SOM, septal organ of Masera; GCD, guanylate cyclase D-containing cells in the MOE; NC, nasal cavity; NG, necklace glomeruli; MOB, main olfactory bulb; AOB, accessory olfactory bulb;*
B) Cartoon of the olfactory sensory epithelium primary cells: olfactory sensory neurons, supporting or sustentacular cells and basal stem-cells. Enlargement shows the odor binding at OSNs cilia level (From Firestein, 2001).

Olfactory sensory neurons in mammals are bipolar neurons with the cell body diameter of 5-10 µm (Schild & Restrepo, 1998). The dendrite reaches up to the surface of the tissue with a knob-like ending (diameter 2-3 µm) and several nonmotile cilia (Menco, 1980; Lidow & Menco, 1984; Getchell, 1986; Menco, 1997; Schild & Restrepo, 1998) (Figure 1.2). Cilia are the site of the sensory transduction apparatus (reviewed by Schild & Restrepo, 1998; Nakamura, 2000; Frings, 2001; Kleene, 2008; Pifferi *et al.*, 2009*c*),

their number (20-30) and length (15–50 μm with ~200 nm diameter) increase the cell surface for odor binding (Adamek *et al.*, 1984; Getchell, 1986; Lancet, 1986; Schild & Restrepo, 1998; Kleene, 2008). The axonal processes of OSNs cross the cribriform plate and projects to glomeruli in the olfactory bulb in the most rostral part of central nervous system (Malnic *et al.*, 1999; Mori *et al.*, 1999; Firestein, 2001).

Figure 1.2 *Microphotograph of human olfactory epithelium and olfactory sensory neurons knob/cilia obtained with scanning electron microscopy (From Morrison & Costanzo, 1990).*

1.2 Odor-induced electrical response in olfactory sensory neurons

In 1955 Ottoson published the first analysis of the electrical activity of the olfactory epithelium by electro-olfactogram (EOG) method (Ottoson, 1955). In EOG recording the odor induced potential change is measured on the surface of the olfactory epithelium (Ottoson, 1955; Scott & Scott-Johnson, 2002; Cygnar *et al.*, 2010).

In isolated OSNs, the response to odor stimuli in solution has been well characterized (Kleene, 2008). Most often, the response has been measured under voltage-clamp upon presentation of a brief pulse of odor (Firestein & Werblin, 1989; reviewed by Kleene, 2008). A given neuron responds to a small and unpredictable subset of odors (Grosmaitre

et al., 2006; Zhao *et al.*, 1998; Lagostena & Menini, 2003). Some evidences suggest that more neurons respond to odors when the epithelium is intact (Sicard & Holley, 1984; Duchamp-Viret *et al.*, 2000) whereas success rates are lower in isolated neurons, typically ranging from 3% to 12% in mouse (Lagostena & Menini, 2003; Reisert *et al.*, 2007).

By directing the odor stimulus to various parts of the cell, it has been shown that the sensitivity to odors is largely restricted to the cilia (Kurahashi, 1989; Firestein *et al.*, 1990; Lowe & Gold, 1993; Takeuchi & Kurahashi, 2003) The odor stimulation generates a transient inward receptor current that would be expected to depolarize the neuron *in situ*. The response typically lasts 1 s or more (Takeuchi *et al.*, 2003; reviewed by Kleene, 2008). In mouse and rat, the latency between arrival of the stimulus and the onset of the current is shorter (~160 ms; Reisert & Matthews, 2001; Grosmaitre *et al.*, 2006) than in amphibians (150 to 600 ms; Firestein *et al.*, 1993; Takeuchi & Kurahashi, 2003; Kurahashi, 1989; Firestein & Werblin, 1987). The amplitude of the peak of the receptor current increases proportionally to concentration or duration of the odor stimulus pulse (Takeuchi & Kurahashi, 2002). The relation between odor dose and peak receptor current is generally well fitted by a Hill equation:

$$I = I_{\max} \frac{C^{n_H}}{C^{n_H} + K_{½}^{n_H}}$$

where I_{max} is the maximum macroscopic current, C is the concentration of odor, $K_{½}$ is the half-maximally effective concentration, and n_H is the Hill coefficient (Hille, 2001; Kleene, 2008). For some odors $K_{½}$ ranges from few to hundred μM both in amphibian (Firestein *et al.*, 1993) and mouse OSNs (Grosmaitre *et al.*, 2006), however some studies report OSN response even at nM and pM odor concentration (Frings & Lindemann, 1990; Grosmaitre *et al.*, 2006).

The parameter n_H in Hill equation describes the slope of the dose–response relation. As n_H decreases, the slope also decreases, and the dynamic range (range of stimulus strengths over which the neuron response varies) increases. In isolated amphibian OSNs under whole-cell recording conditions, n_H ranges from 3-10 (Firestein *et al.*, 1993; Takeuchi & Kurahashi, 2005; Tomaru & Kurahashi, 2005), whereas with suction electrode recordings

or perforated patch analysis, n_H is much smaller, 1 to 2 (Ma *et al.*, 1999; Reisert & Matthews, 1999; Grosmaitre *et al.*, 2006).

In physiological solutions, the current-voltage relation of the odor-induced current is nearly linear with a slight outward rectification (Takeuchi & Kurahashi, 2003). The reversal potential is about 0-3 mV (Lowe & Gold, 1993; Takeuchi & Kurahashi, 2003).

1.3 Olfactory transduction

The olfactory transduction of several OSNs involves a canonical cAMP signaling pathway (Figure 1.3) (reviewed by Kleene, 2008; Pifferi *et al.*, 2009*c*). Binding of odorants activates the odorant receptor, which stimulates the rapid synthesis of cAMP by ACIII through a mechanism mediated by the olfaction-specific G protein, $G_{\alpha olf}$.

Cyclic nucleotide-gated (CNG) channels located in the ciliary membrane are directly activated by cAMP, causing a depolarizing influx of Na^+ and Ca^{2+} ions (Nakamura & Gold, 1987). The increase of the intracellular Ca^{2+} concentration generated by Ca^{2+} entry through CNG channels directly gates Ca^{2+}-activated Cl^- channels (Kleene & Gesteland, 1991; Lowe & Gold, 1993; Kurahashi & Yau, 1993; Kleene, 1993*b*).

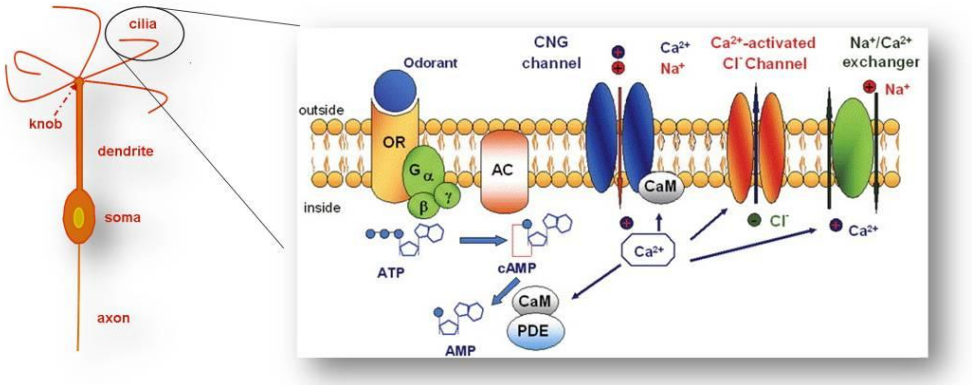

Figure 1.3 *Cartoon of olfactory sensory neuron (OSN) and olfactory transduction. The binding of odorant molecules to ORs induces the G protein-mediated activation of ACIII. cAMP directly gates CNG channels generating a depolarizing influx of Na^+ and Ca^{2+}. Ca^{2+} opens a Cl^- channel that produces a depolarizing efflux of Cl^- (From Pifferi et al. 2006a).*

In OSNs the $Na^+/Ca^{2+}/2Cl^-$ cotransporter NKCC1 (Kaneko *et al.*, 2004; Reisert *et al.*, 2005; Nickell *et al.*, 2006, 2007; Hengl *et al.*, 2010) and probably the Cl^-/HCO_3^- exchanger SLC4A1 (Hengl *et al.*, 2010) maintain an unusually high internal concentration of Cl^- that is in the same range of the Cl^- concentration present in the mucus at the external side of the ciliary membrane (Reuter *et al.*, 1998; Kaneko *et al.*, 2001; Kaneko *et al.*, 2004; Nakamura *et al.*, 1997). Therefore in physiological conditions, the opening of Ca^{2+}-activated Cl^- channels causes an efflux of Cl^- ions from the cilia, corresponding to an inward current that further contributes to the depolarization of OSNs (Kurahashi & Yau, 1993; Lowe & Gold, 1993; Kleene & Gesteland, 1991; Kleene, 1993).

Odor response recovery includes reestablishment of the resting ionic gradients in cilia. A Na^+/Ca^{2+} exchanger (Noé *et al.*, 1997; Reisert & Matthews, 1998) and a plasma membrane Ca^{2+}-ATPase (Antolin *et al.*, 2010) contribute to Ca^{2+} efflux as the odor response terminates (Frings, 2001).

In the next paragraphs the olfactory transduction steps will be discussed in detail.

1.3.1 Odorant receptors

Odorant receptor (OR) proteins belong to the G protein-coupled receptors (GPCRs) family (Buck & Axel, 1991). The number of genes encoding ORs varies considerably among species (reviewed by Mombaerts, 2001; Nei *et al.*, 2008), but they probably represent the largest genes family in the mammalian genome (reviewed by Kaupp, 2010). Most mammals have between 600 and 1,300 OR genes, 12 to 50% of them non-functional pseudogenes (reviewed by Nei *et al.*, 2008). Some ORs with unknown function are also expressed in other cell types and body regions, notably in the kidneys and sperm (Spehr *et al.*, 2003; Pluznick *et al.*, 2009).

OR proteins share common motifs but there is a region of hypervariability in the third, fourth and fifth transmembrane regions (reviewed by Mombaerts, 1999; 2004) thought to be a probable binding site for ligands (reviewed by Nakamura, 2000). Reconstruction of odorant-binding sites would help understanding the molecular mechanisms underlying specificity.

A given OR is expressed only in a small number of olfactory sensory cells (Ressler *et al.*, 1993) and the idea that expression of ORs in OSNs follows the so-called one receptor–one neuron rule is widely accepted but has not been proved. It is better established that each neuron expresses only one of the two alleles of a given OR gene (reviewed by Mombaerts, 2004), with a transcription process that is not yet fully understood (Rodriguez, 2007). The dose–response relationship for a given odor varies considerably among neurons (Firestein *et al.*, 1993; Grosmaitre *et al.*, 2006; reviewed by Kleene, 2008) and different odorants are recognized by unique but overlapping ensembles of ORs (reviewed by Kaupp, 2010).

1.3.2 The G protein

Odorant receptors, like other GPCRs, interact with a G_s protein which is able to stimulate adenylyl cyclase enzymatic activity. The receptor interacts with α subunit of G-protein (G_α), GDP on this subunit is exchanged to GTP, and the βγ-subunit ($G_{\beta\gamma}$) is released from G_α allowing G_α to activate adenylyl cyclase (reviewed by Nakamura, 2000; Pifferi *et al.*, 2009*c*). Jones & Reed (1989) reported that OSNs express a new variant of the G_α, named $G_{\alpha olf}$, localized in olfactory cilia (Menco, 1992). $G_{\alpha olf}$ importance in olfactory transduction has been definitely established by showing that knockout mice for $G_{\alpha olf}$ are anosmic (Belluscio *et al.*, 1998).

1.3.3 The adenylyl cyclase

Odor-induced adenylyl cyclase activity has been shown to depend on GTP presence in olfactory cilia (Pace *et al.*, 1985; Sklar *et al.*, 1986; Shirley *et al.*, 1986).
Adenylyl cyclase found in OSNs by PCR screening (Bakalyar & Reed, 1990) was distinct from before-known AC type I or II, therefore it was named type III (ACIII) (reviewed by Frings, 2001; Nakamura, 2000).
Knockout mice for ACIII are completely anosmic (Wong *et al.*, 2000) supporting the idea that cAMP signaling constitutes the main odor transduction mechanism in OSNs.

1.3.4 The phosphodiesterase

Two phosphodiesterases (PDEs) with distinct cellular localization have been found in OSNs: PDE1C is a Ca^{2+}/calmodulin-stimulated PDE (Yan *et al.*, 1995) mainly enriched in the cilia and dendritic knob (Borisy *et al.*, 1992; Yan *et al.*, 1995; Yan *et al.*, 1996; Menco, 2005) while PDE4A is Ca^{2+} insensitive (Conti & Beavo, 2007) and it is present throughout the cell, but is absent from the cilia (Cherry & Davis, 1995; Juilfs *et al.*, 1997; reviewed by Nakamura, 2000). PDE1C was hypothesized to be critical for rapid termination of the OSN response due to its ciliary localization and Ca^{2+} dependency, while PDE4A was not expected to affect OSN responses as it is excluded from the cilia.

Cygnar & Zhao (2009) showed that double knockout *Pde1c*$^{-/-}$-*Pde4a*$^{-/-}$ mice and not single knockout mice for PDE1C or PDE4A displayed response for odorants with reduced amplitude, prolonged termination, and slower onset kinetic compared to the wild type, in EOG recordings. Their data indicate that PDE1C and PDE4A are both necessary and that removal of cAMP from the cilia is substantially impaired when all PDE activity is eliminated, confirming a previous study by Firestein *et al.* (1991).

1.3.5 The cyclic nucleotide-gated channel

In 1987 Nakamura and Gold showed the presence of a cAMP-gated current in excised patches from olfactory cilia of toad. Such a current was then described in many other species including salamander, frog, newt, rat and mouse (Kurahashi & Kaneko, 1991; Firestein *et al.*, 1991; Frings *et al.*, 1992; Kleene, 1994).

CNG channels are activated by the direct binding of cyclic nucleotides to a large C-terminal cyclic nucleotide-binding domain (reviewed by Pifferi *et al.*, 2006*a*). The gating of CNG channels is not very voltage-dependent (Kaupp & Seifert, 2002).

Olfactory CNG channel affinity for cGMP is higher than cAMP: $K_{½}$ for cAMP is 3 µM in mouse (Michalakis *et al.*, 2006; Song *et al.*, 2008; reviewed by Pifferi *et al.*, 2006*a*), 4.1 µM in rat (Bönigk *et al.*, 1999) and 2 µM in frog (Kleene, 1999); $K_{½}$ for cGMP is 2 µM (reviewed by Nakamura, 2000; Pifferi *et al.*, 2006*a*). The Hill coefficient ranges from

1.3 and 2.3 suggesting that at least 2 molecules of cAMP must bind the channel for gating (reviewed by Kleene, 2008).

With low concentrations of divalent cations on both sides of the membrane, the CNG single channel conductance varies from 8 to 46 pS (Kurahashi & Kaneko, 1991; Larsson *et al.*, 1997; Zufall & Firestein, 1993; Frings *et al.*, 1992; Zufall *et al.*, 1991; reviewed by Kleene, 2008) and the current-voltage relation is almost linear with a slight outward rectification (Bönigk *et al.*, 1999; Kurahashi, 1990; Frings *et al.*, 1992; Kleene, 1993*a*; reviewed by Kleene, 2008).

CNG channels are permeant to all monovalent alkali cations, Na^+, K^+, Li^+, Rb^+ and Cs^+ with similar permeability ratios in rat (Frings *et al.*, 1992) and in newt (Kurahashi, 1990). Extracellular divalent cations like Ca^{2+} and Mg^{2+} are permeant but also block this channel at negative potentials (Nakamura & Gold, 1987; Zufall & Firestein 1993; Kleene, 1995) resulting in a single channel conductance from 0.56 to 1.5 pS (Zufall & Firestein, 1993; Kleene, 1997). A complex of Ca^{2+} and calmodulin at the intracellular side lowers the affinity for cAMP (Liu *et al.*, 1994; Chen & Yau, 1994), resulting in a lowering of its open probability (reviewed by Nakamura, 2000).

Leinders-Zufall *et al.* (1997, 1998) demonstrated that during odorants application resting Ca^{2+} concentration in the cilium increases from 40 nM to 300 nM exclusively from Ca^{2+} entry through the CNG channel (reviewed by Nakamura, 2000).

The first cyclic nucleotide-gated channel was cloned in retinal rods (Kaupp *et al.*, 1989), then in OSNs (Dhallan *et al.*, 1990; Ludwig *et al.*, 1990). Nowadays six CNG channel genes have been identified in mammals (Kaupp & Seifert, 2002), four subunits types A and two subunits types B (reviewed by Pifferi *et al.*, 2006*a*).

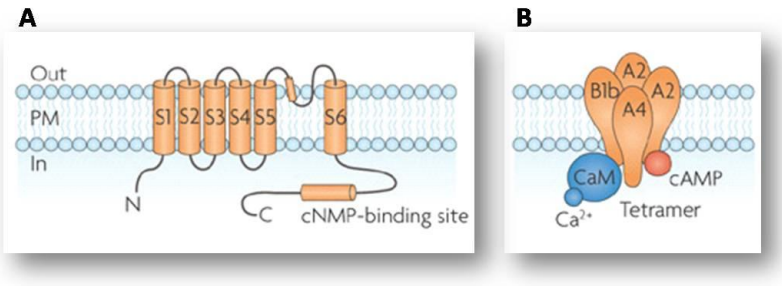

Figure 1.4 *Topology (A) and oligomeric state (B) of cyclic nucleotide-gated channel (CNG). Olfactory CNG is composed by one B1b, one A4 and two A2 subunits (From Kaupp, 2010).*

Olfactory CNG channels consist of two CNGA2, one CNGA4 and one CNGB1 (b splice variant) subunits (Bradley *et al.*, 1994; Liman & Buck, 1994; Sautter *et al.*, 1998) (figure 1.4). CNGA2 knockout mice lack EOG responses to most odorants (Brunet *et al.*, 1996), though showing residual responses to some other odorants (Zhao & Reed, 2001; Lin *et al.*, 2004).

CNG channels are composed of four subunits forming a tetramer with a central pore (figure 1.4). The topology of each subunit is similar to that of the cationic voltage-activated channels with six transmembrane-spanning domains, a pore-loop domain between the fifth and sixth transmembrane domain, and intracellular N- and C-terminal regions (figure 1.4) (reviewed by Pifferi *et al.*, 2006*a*).

1.3.6 Chloride accumulation in olfactory cilia

In cryosections of rat olfactory epithelium Reuter *et al.* (1998) used energy dispersive X-ray micro analysis and estimated the inner Cl^- concentration to be 69 mM and the olfactory mucus Cl^- concentration to be 55 mM, with a calculated equilibrium potential for Cl^- of +6 mV. In intact olfactory epithelium from mice and rats, Kaneko *et al.* (2004) used two-photon fluorescence lifetime imaging microscopy of the Cl^- sensitive dye 6-methoxy-quinolyl acetoethyl ester to measure Cl^- concentration in different compartments. They found 50 mM extracellular Cl^- and 40-50 mM Cl^- concentration in dendritic knobs. Cl^- concentration was less in OSN soma suggesting a gradient for Cl^- accumulation.

Cl^- accumulation process charges the resting cilia to support the excitatory Cl^- efflux in olfactory transduction (reviewed by Kleene, 2008) (see paragraph 1.3.7).

The $Na^+/K^+/2Cl^-$ cotransporter NKCC1 has been shown to be expressed in the cilia of OSNs by proteomic (Stephan *et al.*, 2009; Mayer *et al.*, 2009) and immunological (Hengl *et al.*, 2010) studies. NKCC1 contributes substantially to Cl^- uptake (Kaneko *et al.*, 2004) to maintain the intracellular Cl^- concentration above electrochemical equilibrium (reviewed by Kleene, 2008). NKCC1 is regulated by phosphorylation of four threonine residues in its N terminus by SPAK (Ste20-related proline-alanine-rich) and OSR1 (oxidative-stress response1) kinases (Dowd & Forbush, 2003; Gagnon *et al.*, 2007;

Delpire & Gagnon, 2008). Both SPAK and OSR1 in turn are regulated by the WNK1 and WNK4 kinases (Anselmo *et al.*, 2006; Delpire, 2009).

Recently Hengl *et al.* (2010) clearly showed ciliary expression of NKCC1 and of the entire regulatory complex for Cl^- accumulation in OSNs (see figure 1.5).

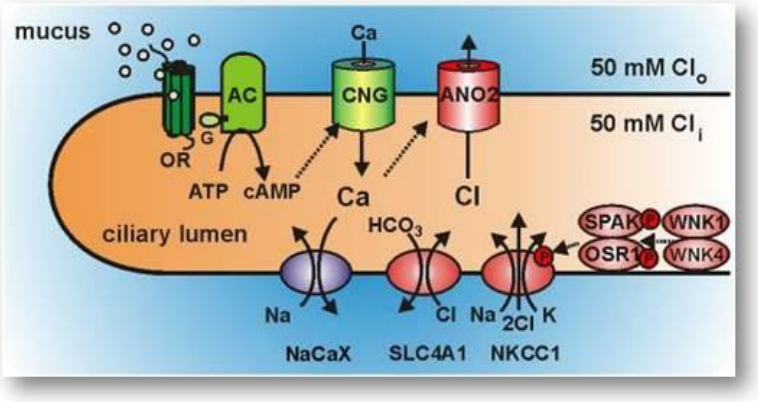

Figure 1.5 *Model for signal amplification strategy of olfactory sensory cilia by Hengl et al. (2010). Transduction proteins for this model are in green and amplification proteins in red.*

Reisert *et al.* (2005) showed that isolated OSNs do not accumulate Cl^- if NKCC1 is eliminated by pharmacological block or genetic removal, but studies in isolated olfactory epithelia (Nickell *et al.*, 2007, 2006) indicated that mice lacking NKCC1 retain approximately 40% to the total Cl^- accumulation. Smith *et al.* (2008) also showed normal olfactory sensitivity of NKCC1 knockout mice measured in behavioral test.

The Cl^-/HCO_3^- exchanger SLC4A1 has been shown to localize to the olfactory cilia (Hengl *et al.*, 2010) where it works as an additional mechanism for ciliary Cl^- uptake.

1.3.7 The calcium-activated chloride channel

The presence of a Ca^{2+}-activated Cl^- conductance in OSNs was first discovered in frog olfactory cilia (Kleene & Gesteland, 1991; Kleene, 1993*b*) and it soon became apparent its importance for olfactory transduction. The Ca^{2+}-activated Cl^- channel

involvement in the response to odorants has been demonstrated in isolated OSNs from amphibians (Kurahashi & Yau, 1993; Firestein & Shepherd, 1995; Zhainazarov & Ache, 1995) and from rats and mice (Lowe & Gold, 1993; Reisert *et al.*, 2005).

Activation of the Ca^{2+}-activated Cl^- channel is subsequent to the influx of Ca^{2+} through the CNG channel (Kleene, 1993*b*) during odor response.

In voltage-clamp experiments it has been shown that a large fraction of the odor-induced inward current is carried by the secondary Cl^- component ranging from 36% in newt and salamander (Kurahashi & Yau, 1993) up to 90% in mice and rats (Lowe & Gold, 1993; Reisert *et al.*, 2005; Nickell *et al.*, 2006; Boccaccio & Menini, 2007) of the total current response.

The current conducted by a single olfactory Cl^- channel is very small and single-channel studies have not been possible. By noise analysis of macroscopic currents, the unit conductance was estimated to be 0.8 pS in frog (Larsson *et al.*, 1997), 1.5 pS in rat (Reisert *et al.*, 2003) and 1.6 pS in mouse (Pifferi *et al.*, 2006*b*).

Half maximal activation ($K_{½}$) by Ca^{2+}, reported for Cl^- conductance, ranges from 2.2 to 4.8 μM Ca^{2+} (Kleene & Gesteland, 1991; Reisert *et al.*, 2003; Pifferi *et al.*, 2006*b*) showing consistent results for amphibians and rodents. In one other study, $K_{½}$ was 26 μM (Hallani *et al.*, 1998), the reason of such a higher value maybe can be related to the unbuffered Ca^{2+} solution used.

Hill coefficient n_H ranges from 2.0 (Kleene & Gesteland, 1991) to 6.6 (Pifferi *et al.* 2006*b*) suggesting that gating of the channel is probably cooperative.

The current-voltage relations in symmetrical Cl^- solutions have been shown to rely on Ca^{2+} concentrations: at 2–3 μM Ca^{2+}, significant outward rectification is apparent, whereas at high Ca^{2+} levels moderate inward rectification is seen (Kleene & Gesteland, 1991; Reisert *et al.*, 2003).

The permeability sequence in inside-out patches are consistent in Reisert *et al.* (2003) (I^- > Br^- > Cl^- > F^-) and in Pifferi *et al.* (2006*b*) (I^- > NO_3^- > Br^- > Cl^- >> MeS^-) with "weak field strength" lyotropic series (Wright & Diamond, 1977; Eisenman & Horn, 1983); indicating that the permeability is primarily determined by the hydration energy of the ion. In this model low electrical field strength is associated to the channel binding site, therefore interactions between permeant ions and the channel are weaker than ion-

water interactions. This is why ions with bigger diameter but well dehydrated pass more easily through the channel pore than smaller water-coated ions. Hallani *et al.* (1998) have shown a different ionic permeability sequence ($Cl^- > F^- > I^- > Br^-$), but these data have not been confirmed by other groups.

Niflumic acid (NFA) 300 µM to 1 mM has been shown to reduce by 70-90% the Ca^{2+}-activated Cl^- current when applied either to the intracellular (Kleene & Gesteland, 1991; Kleene 1993; Reisert *et al.*, 2003; Pifferi *et al.*, 2006*b*) or the extracellular (Lowe & Gold, 1993; Reisert *et al.*, 2005; Pifferi *et al.*, 2006*b*; Boccaccio *et al.*, 2006; Boccaccio & Menini, 2007; Antolin *et al.*, 2010) side of the ciliary membrane.

SITS has been applied at the intracellular side of the olfactory membrane (Kleene & Gesteland, 1991; Pifferi *et al.*, 2006*b*) with a less blocking effect than NFA.

Some other compounds like DIDS, DPC, FFA, have been shown to partially inhibit the olfactory Cl^- current (Kleene & Gesteland, 1991), but very specific blockers for Ca^{2+}-activated Cl^- channels and other Cl^- channels are not known.

The presence of a pair of cationic and anionic currents has been thought to be useful to allow depolarizing current responses in a variety of extracellular ionic environments (Kurahashi & Yau, 1993); in fact ciliary membrane of olfactory neurons is exposed to the external environment in the nasal cavity. This is a possible problem for animals such as fish and amphibians whose fresh water habitat could reduce the extracellular Na^+ concentration and thereby the CNG channels current.

After first studies in amphibians the discovery of the Ca^{2+}-activated Cl^- current in mammals suggested a more general function for this secondary component in olfactory transduction. Ca^{2+}-activated Cl^- current plays the key role of high-gain and low-noise amplifier of the primary CNG current (Kleene, 1997) in olfactory transduction.

1.3.8 Calcium clearance in olfactory cilia

In OSNs cilia free Ca^{2+} levels at rest are ~100 nM (Restrepo *et al.*, 1993; Jung *et al.*, 1994; Leinders-Zufall *et al.*, 1997; Saidu *et al.*, 2009), during the odor response free Ca^{2+} concentration increases ranging from 300 nM (Leinders-Zufall *et al.*, 1998) to 100 µM (Delgado & Bacigalupo, 2004).

The restoration of Ca^{2+} concentrations to pre-stimulus levels (see paragraph 1.3.5) depends on the Na^{+} electrochemical gradient (Reisert & Matthews, 1998; Antolin & Matthews, 2007). Ca^{2+} extrusion mainly occurs via a Na^{+}/Ca^{2+} exchanger (NCX) which has been shown to be present in the olfactory dendrite and cilia (Jung *et al.*, 1994; Noé *et al.*, 1997; Castillo *et al.*, 2007; Pyrski *et al.*, 2007). Accumulation of Na^{+} in cilia produced by exchange with Ca^{2+} is likely to be reversed by a Na^{+}/K^{+}-ATPase which has been identified to be expressed in olfactory cilia (Kern *et al.*, 1991; Lo *et al.*, 1991; Menco *et al.*, 1998; Castillo *et al.*, 2007; Klimmeck *et al.*, 2008; Mayer *et al.*, 2008).

A plasma membrane Ca^{2+}-ATPase (PMCA, also called Ca^{2+} pump) has been supposed to further reduce intraciliary Ca^{2+} as the odor response terminates (Lo *et al.*, 1991; Castillo *et al.*, 2007). Ca^{2+}-ATPase has been localized to the olfactory cilia by immunological (Weeraratne *et al.*, 2006; Castillo *et al.*, 2007) and proteomic (Klimmeck *et al.*, 2008; Mayer *et al.*, 2008) studies.

The quantitative importance of the Ca^{2+}-ATPase appears to be limited compared to the Na^{+}/Ca^{2+} exchanger contribution to ciliary Ca^{2+} clearance in OSN both from amphibians (Reisert & Matthews, 1998; Reisert & Matthews, 2001; Antolin & Matthews, 2007; Kleene, 2009; Antolin *et al.*, 2010) and mouse (Saidu *et al.*, 2009).

Na^{+}/Ca^{2+} exchanger has a lower affinity for Ca^{2+} with ($K_{½} > 1$ µM) than Ca^{2+}-ATPase ($K_{½} < 0.5$ µM) (Carafoli & Brini, 2000). Na^{+}/Ca^{2+} exchanger could therefore reduce most of the high ciliary Ca^{2+} produced during a strong odor response (see paragraph 1.3.5), Ca^{2+}-ATPase could account for only a small fraction of the Ca^{2+} clearance maybe restoring Ca^{2+} down to the OSN basal level (reviewed by Kleene, 2008).

1.4 Calcium-activated chloride channels in other cell types

Ca^{2+}-activated Cl^- currents were first described in the 1980s in *Xenopus* oocytes (Barish, 1983; Miledi, 1982) and salamander photoreceptor inner segments (Bader *et al.*, 1982). To date it is well known that Ca^{2+}-activated Cl^- channels play key roles in several physiological processes including epithelial secretion, membrane excitability in cardiac muscle and neurons, olfactory transduction, regulation of vascular tone (reviewed by Frings *et al.*, 2000; Hartzell *et al.*, 2005).

In oocytes, Ca^{2+}-activated Cl^- channels play a role in the prevention of polyspermy in amphibians (Webb & Nuccitelli, 1985). In fertilized egg, IP_3 production induces a rapid increase in intracellular Ca^{2+} from internal stores. Ca^{2+} activates Cl^- channels resulting in membrane depolarization (reviewed by Hartzell *et al.*, 2005).

In smooth muscle cells, activation of Ca^{2+}-activated Cl^- channels is part of an amplification mechanism in the regulation of the myogenic tone through membrane depolarization (Leblanc *et al.*, 2005; reviewed by Large & Wang, 1996). Activation of Ca^{2+}-activated Cl^- channel is mediated by Ca^{2+} entry through the voltage-gated channels or through the Ca^{2+} released from intracellular stores by IP_3 generated in phospholipase C pathway (Large & Wang, 1996; Davis & Hill, 1999). Ca^{2+}-activated Cl^- channels opening produces a depolarization because chloride equilibrium potential is more positive than the resting potential (Chipperfield & Harper, 2000).

In photoreceptor Ca^{2+}-activated Cl^- channels are localized in inner segment (Bader *et al.*, 1982; Barnes & Hille, 1989; Maricq & Korenbrot, 1988; Lalonde *et al.*, 2008). The depolarization produced by the dark current opens voltage-gated channels located at the synaptic terminal causing a Ca^{2+} influx that activates a large Cl^- conductance. Upon illumination, the dark current turns off, the cell membrane hyperpolarizes, and transmitter release stops (Yau, 1994). The role of Ca^{2+}-activated Cl^- channel in rods is not known, in cones it has been suggested that this current plays a role in modulating lateral inhibition (Barnes & Hille, 1989; Maricq & Korenbrot, 1988; Thoreson & Burkhardt, 1991).

In airway epithelia activation of Ca^{2+}-activated Cl^- channels controls the level of mucous hydration which is important for protection against infection. Basally located transporters accumulate Cl^- in the cell against the electrochemical gradient. Secretion of fluids is

accomplished by apical Cl^- channels that permit Cl^- to flow into the extracellular space down its electrochemical gradient (Kunzelmann *et al.*, 2007).

In dorsal root ganglion (DRG) neurons, spinal cord neurons, and neurons of the autonomic nervous system Ca^{2+}-activated Cl^- channels are thought to regulate neuronal excitability but the mechanism is poorly established (reviewed by Scott *et al.*, 1995). In DRG neurons opening of Ca^{2+}-activated Cl^- channels by Ca^{2+} entry or Ca^{2+} release from stores would depolarize the cell membrane or produce after-depolarization following action potentials (De Castro *et al.*, 1997; reviewed by Scott *et al.*, 1995; Frings *et al.*, 2000; Hartzell *et al.*, 2005)

Proteins constituting Ca^{2+}-activated Cl^- channels in most cells and tissues are still elusive. Ca^{2+}-activated Cl^- currents show heterogeneous biophysical properties, regulatory mechanisms and pharmacology suggesting that different channels are expressed. In many cases, Ca^{2+}-activated Cl^- channels are activated by Ca^{2+} in a wide range of concentrations (Kuruma & Hartzell, 2000; Hartzell *et al.*, 2005; Angermann *et al.*, 2006) and are also voltage-dependent, with membrane depolarization increasing the activity (Nilius *et al.*, 1997; Lalonde *et al.*, 2008; Hartzell *et al.*, 2005). At not saturating Ca^{2+} concentrations they show outwardly rectifying current-voltage relationship, at maximal Ca^{2+} the current-voltage relationship becomes linear (Kuruma & Hartzell, 2000; reviewed by Frings *et al.*, 2000; Hartzell *et al.*, 2005). In some studies Ca^{2+}-activated Cl^- currents are directly activated by Ca^{2+}, in others, activation requires the intervention of a Ca^{2+}/calmodulin-dependent kinase (Arreola *et al.*, 1998; Kaneko *et al.*, 2006).

Despite considerable efforts in the past years these physiologically important ion channels have been difficult to identify at the molecular level. The search for the molecular counterparts for Ca^{2+}-activated Cl^- currents has been difficult first because a favorite system for expression cloning of ion channels, the *Xenopus* oocyte, is not suitable for these channels since these cells express large endogenous Ca^{2+}-activated Cl^- currents. Second, drugs to differentiate Ca^{2+}-activated Cl^- channels from other Cl^- channels lack specificity (De La Fuente *et al.*, 2008). Finally, homology cloning has not been fruitful because none of the known cloned Cl^- channels have properties that suggest clear structural relationships to Ca^{2+}-activated Cl^- channels (reviewed by Hartzell *et al.*, 2009).

To date five candidate proteins have been proposed as the molecular counterparts of Ca^{2+}-activated Cl^- currents: CLCA, ClC-3 and Tweety (reviewed by Hartzell *et al.*, 2005) are briefly described in this section; Bestrophins and TMEM16/Anoctamins (reviewed by Kunzelmann *et al.*, 2009; Hartzell *et al.*, 2009; Flores *et al.*, 2009) will be discussed in detail in the following sections.

CLCA. The Ca^{2+}-activated Cl^- channel (CLCA) family was cloned from a bovine tracheal cDNA expression library (Ran *et al.*, 1992). Transfect ion of various cell types with cDNAs encoding various CLCAs induces Ca^{2+}-dependent currents. However there is great skepticism over the function of CLCAs as chloride channels, because there are too many differences in Ca^{2+} sensitivity, voltage sensitivity and pharmacology with native Ca^{2+}-activated Cl^- channels (reviewed by Eggermont, 2004; Hartzell *et al.*, 2005), and some of them have very high homology to known cell adhesion proteins and some seem to be soluble, secreted proteins (Gruber & Pauli, 1999).

ClC. The ClC-3 is a member of the ClC family of chloride channels and transporters. The properties of the currents reported for ClC-3, however, differ from those typically described for Ca^{2+}-activated Cl^- channels (reviewed by Hartzell *et al.*, 2005) and a normal Ca^{2+}-activated Cl^- channels activity has been shown in parotid acinar cells from a ClC-3 knockout mouse (Arreola *et al.*, 2002).

TWEETY. The human genes hTTYH2 and hTTYH3, with homology to a *Drosophila* gene called tweety, have been shown to encode a Ca^{2+}-regulated maxi-Cl^- channel (Suzuki & Mizuno, 2004; Suzuki, 2006). Big single channel conductance (260 pS) (Suzuki & Mizuno, 2004) and the absence of this channel in cells with classical Ca^{2+}-activated Cl^- currents suggest this is not the favorite candidate (reviewed by Hartzell *et al.*, 2005).

1.5 Bestrophins protein family

Proteins of the bestrophin family have been shown to form Cl^- channels when expressed in heterologous systems (Sun *et al.*, 2002; Tsunenari *et al.*, 2003) and were proposed to be *bona fide* Ca^{2+}-activated Cl^- channels (Qu *et al.*, 2004; Qu *et al.*, 2003; Pusch, 2004; Tsunenari *et al.*, 2006; reviewed by Kunzelmann *et al.*, 2007; Hartzell *et al.*, 2008; Marmorstein *et al.*, 2009).

The electrophysiological properties of Cl^- channels bestrophins were generally investigated after transient heterologous expression in HEK 293 cells (Sun *et al.*, 2002) (Qu *et al.*, 2003; Qu *et al.*, 2004; Pifferi *et al.*, 2006*b*) and other cell types.

Different bestrophins produce currents with different current-voltage relations and kinetics of activation. Human bestrophin1 currents have linear current-voltage relationships, essentially time independent, whereas human bestrophin3 currents strongly inwardly rectify and activate slowly with time (Tsunenari *et al.*, 2003).

The ionic permeability of mouse and *Xenopus* bestrophin2 showed a weak selectivity among various anions with the following permeability sequence: $SCN^- > I^- > Br^- > Cl^- > F^-$ (Qu *et al.*, 2003; Qu *et al.*, 2004; Pifferi *et al.*, 2006*b*), as reported for many Ca^{2+}-activated Cl^- channels (reviewed by Frings *et al.*, 2000; Hartzell *et al.*, 2005).

It is generally agreed that the selectivity of a channel is determined by the channel pore; point mutations in human bestrophin1 and mouse bestrophin2 produce changes in Cl^- channel properties (Pusch, 2004; Qu *et al.*, 2004) such as the ionic permeability and/or the channel gating, supporting strong evidence that bestrophin is responsible for forming the channel. However a new study in airway epithelial cells proposed bestrophins as intracellular store calcium modulator (Barro-Soria *et al.*, 2010; reviewed by Edwards & Kahl, 2010).

Ca^{2+} sensitivity has been investigated for some bestrophins. Human bestrophin1 is activated by increase of intracellular Ca^{2+} concentration with $K_{½}$ ~150 nM (Fischmeister & Hartzell, 2005); mouse bestrophin2 with $K_{½}$ ~200 nM (Qu *et al.*, 2003; Qu *et al.*, 2004). If native bestrophin channels have the same Ca^{2+} sensitivity as these heterologously expressed channels, bestrophin current must be partially activated at all times, because basal free cytosolic Ca^{2+} is typically around 100 nM. Sun *et al.* (2002)

reported that human bestrophin1 current can be rapidly activated by release of Ca^{2+} from caged Ca^{2+}, suggesting a direct activation by Ca^{2+}. The Ca^{2+} binding site might be located in the C-terminus immediately after the last transmembrane domain because this region contains a high density of acidic amino acids that could coordinate positively charged Ca^{2+}. This Asp-rich domain, indicated as a possible Ca^{2+} sensor for bestrophins (Tsunenari *et al.*, 2006), exhibits some similarity with other Ca^{2+}-binding domains like the cytoplasmic Ca^{2+} bowl motif of BK_{Ca} potassium channels (Schreiber & Salkoff, 1997; Bao *et al.*, 2004) and the type 3 (T3) motifs in the C-terminal region of thrombospondins (Carlson *et al.*, 2008).

Because of the significant sequence similarity between the Asp-rich domain and the aforementioned Ca^{2+}-binding domains, it is plausible to hypothesize that Ca^{2+} activation of bestrophins could involve, at least in part, Ca^{2+}-binding to the Asp-rich domain. Molecular dynamics simulations by Kranjc *et al.* (2009) suggest that at least two Ca^{2+}-binding sites could be present in the Asp-rich domain of bestrophins possibly involved in Ca^{2+}-dependent activation of the channel. In the same study they show through electrophysiological experiments that mutations predicted by their model within the bestrophin Asp-rich domain have an impact on the function, decreasing the Ca^{2+}-activated current amplitude.

Single channel properties of endogenous bestrophin have been measured from *Drosophila* S2 cells (Chien *et al.*, 2006). In inside-out patches *Drosophila* bestrophin1 has a single channel conductance of ~2 pS; such a small single channel conductance is a common feature of many Ca^{2+}-activated Cl^- channels expressed in many cell types (reviewed by Frings *et al.*, 2000; Hartzell *et al.*, 2005).

The human genome contains four bestrophin paralogs (hBest1-4) (Stöhr *et al.*, 2002; Tsunenari *et al.*, 2003), whereas mice have three paralogs (mBest1-3) and one pseudogene (Krämer *et al.*, 2004; reviewed by Hartzell *et al.*, 2008). The first member of the family to be discovered, human bestrophin1 (hBest1 or VDM2), was identified (Marquardt *et al.*, 1998; Petrukhin *et al.*, 1998) as the site of mutation in Best vitelliform macular dystrophy (BVMD - Best's disease), a dominantly inherited, early onset form of macular degeneration (reviewed by Hartzell *et al.*, 2008; Kunzelmann *et al.*, 2009). It was assumed that BVMD is caused by a defect in the basolateral retinal pigmented epithelium

(RPE) cells (Sun *et al.*, 2002; Hartzell & Qu, 2003), where human bestrophin1 was shown to be localized (Marmorstein *et al.*, 2000; Bakall *et al.*, 2003; Mullins *et al.*, 2007). However mice with the bestrophin1 gene disrupted (mBest$^{-/-}$) have no retinal pathology and Ca^{2+}-activated Cl^- current in mouse RPE cells is not changed, suggesting bestrophin1 itself could not function as Cl^- channel (Marmorstein *et al.*, 2006).

Experimental data for bestrophin transmembrane topology exist mainly for human bestrophin1, but the high conservation of the predicted transmembrane domains, suggests that all vertebrate bestrophins topologies are similar (reviewed by Hartzell *et al.*, 2008). Bestrophins in all of these species have a conserved N-terminal domain that includes the putative transmembrane regions, and a variable C-terminal domain (reviewed by Hartzell *et al.*, 2008). Two topology models have been proposed for hBest1; according to them, the N- and C-terminal domains of bestrophins would be located at the intracellular side of the membrane and would be connected to five (Tsunenari *et al.*, 2003) or four (Milenkovic *et al.*, 2007) hydrophobic domains forming the channel.

Using mutagenesis and cysteine-accessibility analysis of all amino acids from 69 to 105, Qu and co-workers have shown that TMD2 very likely plays a role in ion selectivity of the mouse bestrophin2 pore. Amino acids in TMD2 closer to the C-terminal (A73C, V78C, S79C, and F80C) react with anionic sulfhydryl reagents more slowly than those closer to the N-terminal suggesting that these residues may form the outer mouth of the channel. This is consistent with the C-terminal end of the putative transmembrane domain being closer to the cytoplasm and deeper in the pore. Several other observations indicate that anionic selectivity is determined by this region of the protein. Replacement of F80 with amino acids of opposite charge had opposite effects on rectification of the current: F80R outwardly rectifies, whereas F80E inwardly rectifies (Qu *et al.*, 2004; Qu *et al.*, 2006). Finally the fact that most of the amino acid substitutions that were made in serine 79 (Qu & Hartzell, 2004) disrupted the channel function in qualitatively similar ways, suggests that this residue plays an important role in the pore (reviewed by Hartzell *et al.*, 2008).

Alternative mechanisms for bestrophin functions have been proposed. Barro-Soria *et al*. (2010) showed that endogenous bestrophin1 primarily resides in the endoplasmic reticulum in airway epithelial cells modulating Ca^{2+} release and uptake from intracellular

stores (reviewed by Edwards & Kahl, 2010). Bestrophin1 has also been demonstrated to be permeable to other anions such as HCO_3^- (Qu & Hartzell, 2008) and γ-aminobutyric acid (GABA) (Lee *et al.*, 2010) showing it could be involved in physiological roles other than chloride flux.

1.5.1 Bestrophin2 as olfactory Ca^{2+}-activated Cl^- channel

Bestrophin2 is expressed in epithelial cells of airways (Barro-Soria *et al.*, 2008), colon (Barro Soria *et al.*, 2009), kidney (Hennig *et al.*, 2008) in the eye (Zhang *et al.*, 2010) and olfactory ciliary epithelium (Pifferi *et al.*, 2006*b*; Klimmeck *et al.*, 2009).
Qu *et al*. (2004) showed that bestrophin2 heterologously expressed was localized at the cell surface and induced similar Ca^{2+}-activated currents in different cell lines (reviewed by Hartzell *et al.*, 2005). Currents induced by bestrophin2 have little or no rectification, with reversal potential as expected for a Cl^- selective current and the same anionic permeability sequence $SCN^- > I^- > Br^- > Cl^- > F^-$ (Qu *et al*., 2004). Mutations in putative pore domains of bestrophin2 (Qu & Hartzell, 2004) alter the conduction and binding of anions. In wild-type channels, substitution of extracellular Cl^- with SCN^- produced a significant decrease in conductance and a shift of the E_{rev}. The reduced conductance in both the inward and outward directions by extracellular SCN^- suggests that not only is SCN^- less conductive than Cl^-, it is also able to block outward movement of Cl^- (inward current), presumably by binding in the channel pore. With the S79C mutant, in contrast, substitution of SCN^- for Cl^- did not reduce the conductance and the E_{rev} shifting was smaller.

Bestrophin2 has been proposed as the putative molecular counterpart of Ca^{2+}-activated Cl^- channels involved in olfactory transduction (Pifferi *et al.*, 2006*b*). Pifferi *et al.* (2006*b*) found by RT-PCR that Bestrophin2 is expressed in OSNs. Bestrophin2 was detected on the cilia by immunocytochemistry, where it colocalizes with CNGA2, the principal subunit of the olfactory CNG channel that is responsible for the primary transduction current. The biophysical and pharmacological properties of the current induced by heterologous expression of bestrophin2 and those of the native Ca^{2+}-activated Cl^- current from dendritic knob/cilia of mouse olfactory sensory neurons present many

similarities, including the same anion permeability sequence ($I^- > NO_3^- > Br^- > Cl^- > MeS^-$), small estimated single-channel conductance, and the same side-specific blockage by some Cl^- channel blockers (Pifferi *et al.*, 2006*b*). The most significant difference between the two currents was found to be their sensitivity to intracellular Ca^{2+}. In fact, currents were half-maximal at a Ca^{2+} concentration of 0.4 µM for bestrophin2, whereas native currents required a higher Ca^{2+} concentration, 4.7 µM (Pifferi *et al.*, 2006*b*).

Two studies challenged the idea of bestrophin2 role in olfactory transduction. Bakall *et al.* (2008) replaced the first two exons of bestrophin2 with Lac-Z and found expression in colon and ciliary epithelium but not olfactory epithelium. Bestrophin2 knockout mice showed no obvious olfactory deficit, but they show diminished intraocular pressure suggesting that bestrophin2 may be involved in aqueous humor generation.

On the contrary Klimmeck *et al.* (2009) clearly showed that bestrophin2 expression was restricted to the cilia of mature OSN and at all subcellular levels in developing sensory neurons. This group suggested a role for bestrophin2 in the process of neurogenesis, during differentiation and growth of axons and cilia of OSNs.

Bestrophin2 has also been suggested to be a cellular volume-regulated Cl^- channel (Fischmeister & Hartzell, 2005) because it is strongly inhibited by hyperosmotic and stimulated by hyposmotic solutions; and a HCO_3^- channel having a relatively high P_{HCO_3}/P_{Cl} (0.69 ± 0.4 for hBest2 and 0.63 ± 0.3 for mBest2; (Qu & Hartzell, 2008; Yu *et al.*, 2010).

1.6 Anoctamins/TMEM16 protein family

The TMEM16 family of genes was first described in vertebrates by bioinformatic analyses (Katoh & Katoh, 2003). TMEM16 proteins are well conserved among eukaryotes; humans and mice have 10 genes named as TMEM16A-K, sharing considerable homology (Galindo & Vacquier, 2005). TMEM16A amino acid sequence identity with TMEM16B is larger than 60%, ~40% for TMEM16C, D, and E; whereas TMEM16F, G, H, J, and K, with 20 – 30% identity, probably represent a more distant subgroup of proteins.

S. cerevisiae's sole TMEM16 homologue, called *Ist2p*, plays a role in salt balance and modulation of intracellular ion concentration (Kim *et al.*, 2005; reviewed by Hartzell *et al.*, 2009). *Drosophila melanogaster* has six paralogues. *Axs* (aberrant x-segregation) is ~35% identical to TMEM16H and K, is localized to the endoplasmic reticulum in early embryos, involved in chromosomal nondisjunction and progression of the meiotic cycle (Zitron & Hawley, 1989; Whyte *et al.*, 1993; Krämer *et al.*, 2003; Galindo & Vacquier, 2005).

All TMEM16 proteins have a similar putative topology, consisting of eight transmembrane segments and intracellular NH_2 and COOH termini; a conserved C-terminal domain of unknown function (DUF590) and a N-linked glycosylation site in the last extracellular loop (except in TMEM16K) (reviewed by Flores *et al.*, 2009; Galietta, 2009; Hartzell *et al.*, 2009; Kunzelmann *et al.*, 2009).

A highly conserved hydrophobic region between TM5 and TM6 that protrudes into the membrane is predicted to form a re-entrant p-loop (except in TMEM16H and K) (Katoh & Katoh, 2004*a*,*b*,*c*; Katoh & Katoh, 2005; Galindo & Vacquier, 2005)

It has been proposed that some members of the TMEM16 family of membrane proteins, TMEM16A and B, are calcium-activated chloride channels (Caputo *et al.*, 2008; Yang *et al.*, 2008; Schroeder *et al.*, 2008; Pifferi *et al.*, 2009*a*; Stephan *et al.*, 2009). Because of their eight transmembrane segments topology and their supposed role in anion transport, TMEM16 proteins were also named 'anoctamins' (Yang *et al.*, 2008); therefore they are also referred as ANO1-10.

Some TMEM16 genes have short splice variant transcripts (Bera *et al.*, 2004; Yang *et al.*, 2008), suggesting the possibility that they could have additional non-channel functions or could fulfill tasks in intracellular compartments (Tsutsumi *et al.*, 2004; Mizuta *et al.*, 2007; Schreiber *et al.*, 2010). Current data suggest that members of the TMEM16 family of proteins are involved in both normal vertebrate development and disease; the existence of multiple TMEM16 paralogs in mice and humans might have evolved to allow tissue-specific expression of proteins with similar functions (Galindo & Vacquier, 2005; Rock & Harfe, 2008; Gritli-Linde *et al.*, 2009).

Several members of the TMEM16 family are overexpressed in different types of cancer (Katoh & Katoh, 2003; Galindo & Vacquier, 2005) and mutation of TMEM16E is

associated with the human disorder gnathodiaphyseal dysplasia (GDD) (Tsutsumi *et al.*, 2004; Mizuta *et al.*, 2007). TMEM16G has been shown to promote adhesion between prostate cancer cells (Das *et al.*, 2007, 2008). Because they are accessible cell surface proteins, TMEM16 proteins are a potential drug target for human diseases (Das *et al.*, 2008; reviewed by Hartzell *et al.*, 2009).

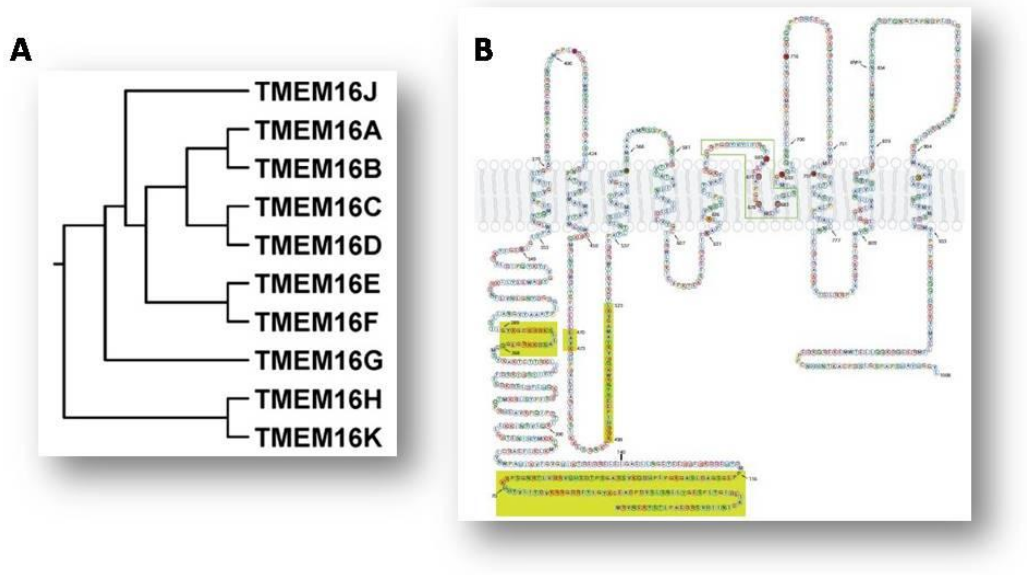

Figure1.6 *A) Phylogenetic tree of human TMEM16 members (From Schroeder et al. 2008). B) TMEM16A protein containing all of its potential alternatively spliced exons (the 'abcd' form, Caputo et al. (2008) Alternatively spliced segments a, b, c and d are shown with a chartreuse background. Single amino acid codes are in circles colored according to the physical properties of the amino acid (green, hydrophilic; pale blue, hydrophobic; red, acidic; magenta, basic; cyan, other ionizable (tyrosine and histidine); yellow, proline; gold, glycine; pink, cysteine) (From Hartzell et al. 2009).*

At this point in time, it has been shown experimentally that TMEM16A and B are calcium-activated chloride channels but it is not clear whether it is the same for all TMEM16 members, and TMEM16H has been shown (Schreiber *et al.*, 2010) to inhibit TMEM16A currents. Also, there are no data showing whether different members of the family form heteromers with other members.

1.6.1 TMEM16A/Anoctamin1

TMEM16A is expressed in many of the tissues that are known to express Ca^{2+}-activated Cl^- currents: airway epithelium and smooth muscle cells, acinar cells of pancreas and salivary glands, proximal kidney tubule epithelium, retina, dorsal root ganglion sensory neurons, and submandibular gland (Huang *et al.*, 2009; Schreiber *et al.*, 2010).

In 2008, three research groups have arrived independently at the identification of TMEM16A as a membrane protein strongly related to the activity of Ca^{2+}-activated Cl^- channels. TMEM16A expressed in different cell systems, HEK-293, FRT cells and *Axolotl* oocytes always leads to the appearance of currents very similar to classical Ca^{2+}-activated Cl^- channels (Caputo *et al.*, 2008; Schroeder *et al.*, 2008; Yang *et al.*, 2008).

At nonmaximal Ca^{2+} concentrations, voltage pulses to positive membrane potentials elicit slow-activating currents. This effect is reversible, as the return to negative membrane potentials causes a deactivation of the current. Accordingly, the steady-state current-voltage relationship under this condition is outwardly rectifying.

At maximal concentration of Ca^{2+}, the channels become fully active at all membrane potentials, and consequently, the relaxation after voltage steps disappear (reviewed by Kunzelmann *et al.*, 2009).

Similar to the case for native Ca^{2+}-activated Cl^- currents, the Ca^{2+} sensitivity of the channel in excised inside-out patches was voltage dependent. At −60 mV the $K_{½}$ for Ca^{2+} was 2.6 μM, whereas it decreased to 0.4 μM at +60 mV (Yang *et al.*, 2008).

Schroeder *et al.*, (2008) shows that expression of xTMEM16A in *Axolotl* oocytes produces currents with multiple components with different reversal potentials. These findings suggest that xTMEM16A has multiple open states that differ in their gating kinetics and ionic selectivity.

At present there are no data about the Ca^{2+} binding site: TMEM16A does not have any obvious E-F hand-like Ca^{2+}-binding sites or IQ-domain CaM binding sites. This could mean that either the protein requires another subunit to confer Ca^{2+} sensitivity or that the Ca^{2+} binding site is a novel type that is not easily recognized. If another subunit is required for Ca^{2+} sensitivity, this subunit must be expressed endogenously in the

expression systems used. (reviewed by Flores *et al.*, 2009; Galietta, 2009; Hartzell *et al.*, 2009; Kunzelmann *et al.*, 2009).

TMEM16A has at least four alternatively spliced exons resulting in proteins having between 712 and 1006 amino acids. The alternatively spliced exons include two at the cytoplasmic N-terminus and two in the first cytoplasmic loop (Caputo *et al.*, 2008; Ferrera *et al.*, 2009). All splice variants produced Ca^{2+}-activated Cl^- currents when expressed in HEK cells, but the variant without any of these segments was not functional (Caputo *et al.*, 2008). This finding suggests that alternative splicing is a mechanism to regulate channel properties and may be the basis for generation of different Ca^{2+}-activated Cl^- channel types with different voltage dependence and Ca^{2+} sensitivity in a tissue-specific manner (Ferrera *et al.*, 2009).

The region between the fifth and sixth transmembrane segments is predicted to form a reentrant loop important for the formation of the channel pore. Mutagenesis of positively charged amino acids localized in this region (Yang *et al.*, 2008) altered ion selectivity of the channel, thus enhancing its permeability to cations. Altered ion selectivity and voltage dependence were also observed by mutagenesis of an arginine and a glutamine in the third and sixth transmembrane domains, respectively (Caputo *et al.*, 2008).

Another characteristic of TMEM16A is its overexpression in human cancers. Its transcript was also identified as expressed at high levels in gastrointestinal stromal tumors and oral squamous cell carcinomas and therefore also named DOG1 (West *et al.*, 2004) and TAOS2 (Huang *et al.*, 2006). The relationship between cancer and a protein with a role in Cl^- transport is not clear. Ca^{2+}-activated Cl^- channels may be important in proliferation, migration, and resistance of cancer cells to apoptotic stimuli (reviewed by Galietta, 2009). TMEM16A was also found to be one of the candidate genes responsible for autosomal recessive hearing impairment (Kalay *et al.*, 2007). This is of interest because during mouse development TMEM16A is strongly expressed in inner ear cells which will later form the organ of Corti, and parts of the stria vascularis (Gritli-Linde *et al.*, 2009). Finally TMEM16A has an important role in the physiology of airway epithelium and is a possible pharmacological target to circumvent the Cl^- transport defect in cystic fibrosis patients.

Rock *et al.* (2008) had reported a TMEM16A knockout mouse. All knockout homozygous mice died within one month of birth showing a severe phenotype characterized by altered formation of tracheal cartilage rings (tracheomalacia). At the moment the reason for tracheal cartilage abnormalities is unknown; it was suggested that the defect in the cartilage rings should be secondary to the improper embryonic stratification of the embryonic tracheal epithelium, which may point out to a functional crosstalk between epithelium and the submucosal tissue during development (reviewed by Flores *et al.* 2009; Galietta, 2009).

Because animals lacking expression of TMEM16A die shortly after birth (Rock *et al.*, 2008), long-term observations are currently not possible.

TMEM16A loss was further analyzed by Ousingsawat *et al.* (2009) in a broad spectrum of epithelial tissues, including airways, colonic epithelium, pancreatic acinar cells, salivary gland cells and hepatocytes, showing TMEM16A contribution to Ca^{2+}-activated whole cell currents and to Ca^{2+}-dependent Cl^- secretion.

Rock *et al.* (2009) found accumulation of mucus in the lumen of tracheas of TMEM16A null mice, suggesting an important function of TMEM16A for mucociliary clearance in mouse airways.

1.6.2 TMEM16B/Anoctamin2

Among the members of the mouse family, TMEM16B is the most similar to TMEM16A, with ~60% amino acid identity (Katoh & Katoh, 2003; Galindo & Vacquier, 2005). TMEM16B transcripts have been found in the retina photoreceptors, in olfactory bulb, olfactory epithelium, pancreas, salivary glands and some brain regions (http://www.brain-map.org).

Large deletions of TMEM16B N-terminus together with von Willebrand factor genes are involved in some cases of the severe von Willebrand disease type 3 (Schneppenheim *et al.*, 2007). Furthermore a recent genome-wide association study (Otowa *et al.*, 2009) in a Japanese population indicated that single nucleotide polymorphisms in TMEM16B gene were significantly associated with panic disorder.

Schroeder *et al.* (2008) and Pifferi *et al.* (2009*a*) reported that TMEM16b generated Ca^{2+}-activated Cl^- currents in *Axolotl* oocytes and HEK 293 cells.

TMEM16b has been pointed to as a promising candidate for the olfactory Cl^- current.

Stephan *et al*. (2009) characterized the mouse olfactory TMEM16b isoform, composed of 24 exons (909 amino acids), with a predicted molecular weight of ~110 kDa. Exon 3, which encodes 33 amino acids in the predicted N-terminal cytoplasmic domain, is lacking in a minority of transcripts in both OSNs and retinal cells, where TMEM16b was first studied (Stöhr *et al.*, 2009). The olfactory TMEM16b variant also lacks the exon 13 (4 amino acids of unknown function) in the first intracellular loop in the retinal variant.

The presence of TMEM16b in OSN has been demonstrated by using different techniques. By in situ hybridization TMEM16b mRNA has been shown to be highly and specifically localized in mature OSNs within the mouse olfactory epithelium (Yu *et al.*, 2005; Hengl *et al.*, 2010; Rasche *et al.*, 2010) and not to the sustentacular or basal stem cell layers.

TMEM16b protein was identified from a proteomic screen of olfactory cilia membrane preparation (Mayer *et al.*, 2009; Stephan *et al.*, 2009; Rasche *et al.*, 2010; Hengl *et al.*, 2010) and by immunocytochemistry it was detected in olfactory epithelium limited to the sensory cilia, where TMEM16b colocalized with marker proteins for olfactory cilia such as acetylated tubulin, CNGA2 (Rasche *et al.*, 2010) and ACIII (Hengl *et al.*, 2010).

Finally in mouse olfactory epithelium infected with adenoviral vector, TMEM16b protein localized primarily in the cilia and dendritic knobs of OSNs (Stephan *et al.*, 2009), demonstrating that TMEM16b is able to use the ciliary targeting machinery.

TMEM16b isoforms from retina (Stöhr *et al.*, 2009; Pifferi *et al.*, 2009*a*) or OSNs (Stephan *et al.*, 2009) expressed in HEK 293 cells produced Ca^{2+}-activated Cl^- current with functional properties similar to the native olfactory Cl^- current when studied both in whole cell configuration (Stöhr *et al.*, 2009; Pifferi *et al.*, 2009*a*); and in inside out patches (Pifferi *et al.*, 2009*a*; Stephan *et al.*, 2009), indicating a possible involvement of TMEM16b in the olfactory signal transduction cascade.

TMEM16b Ca^{2+} sensitivity is slightly voltage-dependent, with a $K_{½}$ that ranges from 1.8 µM (Stephan *et al.*, 2009) to 5.1 µM (Pifferi *et al.*, 2009*a*) at negative potentials and Hill coefficients ~2 (Stephan *et al.*, 2009; Pifferi *et al.*, 2009*a*)

The single channel conductance associated with TMEM16b by noise analysis was estimated to be ~1.2 pS (Pifferi *et al.*, 2009*a*; Stephan *et al.*, 2009).

TMEM16b current–voltage relationship is linear (Pifferi *et al.*, 2009*a*) or with inward rectification (Pifferi *et al.*, 2009*a*; Stephan *et al.*, 2009) in saturating calcium conditions, whereas it shows pronounced outward rectification after activation at sub-saturating calcium concentrations (Pifferi *et al.*, 2009*a*).

Halide permeability sequence for TMEM16b is SCN^- > I^- > NO_3^- > Br^- > Cl^- > MeS > F^- with consistent permeability ratios (P_X/P_{Cl}) in Stephan *et al.* (2009) and Pifferi *et al.* (2009*a*), which are inversely related to the ions hydration energies.

Activation of the TMEM16b channel by different divalent cations: Sr^{2+} efficiently activated a current almost as well as Ca^{2+}, Ba^{2+} activated a small current, and no current was observed upon Mg^{2+} application (Pifferi *et al.*, 2009*a*; Stephan *et al.*, 2009).

TMEM16b current is blocked ~70-80% by the intracellular (Pifferi *et al.*, 2009*a*; Stephan *et al.*, 2009) and extracellular (Pifferi *et al.*, 2009*a*) application of niflumic acid (NFA) in a voltage-independent manner, and the blockage is reversible. Two other fenamates, flufenamic and mefenamic acids (FFA and MFA), as well as NPPB and SITS, only partially blocked the current, whereas DIDS did not have any blocking effect at the intracellular side (Pifferi *et al.*, 2009*a*). NPPB, SITS, and DIDS, produced a 65-80% partial block of both inward and outward currents when applied extracellularly (Pifferi *et al.*, 2009*a*).

The strong similarities between the properties of native Cl^- currents (see paragraph 1.3.7) and currents induced by TMEM16b described here, support the hypothesis that TMEM16b is part of the ciliary Cl^- channel and may contribute to the excitatory current in olfactory transduction.

2 MATERIALS AND METHODS

2.1 Dissociation of mouse olfactory sensory neurons

Mice were handled in accordance with the Italian Guidelines for the Use of Laboratory Animals (Decreto Legislativo 27/01/1992, no. 116) and European Union guidelines on animal research (No. 86/609/EEC).

Olfactory sensory neurons were dissociated enzymatically from the olfactory epithelium of 1 to 3-months-old C57Black wild type or Bestrophin2$^{-/-}$ mice (see paragraph 2.6). Mice were anesthetized with CO_2 inhalation, decapitated, and then the head was hemisected sagittally along the septum to expose olfactory turbinates. The olfactory epithelium was removed and transferred in 1 ml of zero-divalent mammalian Ringer's solution with 200 µM cysteine and 2 U/ml papain (Sigma, Milano, Italy) for 8-10 minutes at room temperature. The olfactory epithelium was minced with fine forceps. The reaction was stopped by adding 0.5 ml of Ringer's solution with 0.1 mg/ml BSA (bovine serum albumin), 0.3 mg/ml leupeptin, and 0.02 mg/ml of DNAseI (all from Sigma, Milano, Italy). After centrifugation (300 g for 5 min) the cells were resuspended in 1 ml of Ringer's solution and plated on glass coverslips (WPI, Sarasota, FL), coated with poly-L-lysine and concanavalin-A TypeV (Sigma, Milano, Italy). Before use, dissociated olfactory sensory neurons were allowed to settle for 60 min at +4°C. Only olfactory sensory neurons with clearly visible cilia were used for the experiments.

2.2 Cell culture and transfection

HEK 293T cells were grown in DMEM (GIBCO) supplemented with 10% FBS (Sigma, Milano, Italy), 100 U/ml penicillin, and 100 µg/ml streptomycin (Sigma, Milano, Italy) at 37ºC in a humidified CO_2 incubator.

The full-length, dominant olfactory isoform of the mouse TMEM16b/anoctamin2 cloned into the pAdTrack-CMV EGFP-expressing vector (Stratagene, LaJolla, CA, Figure 2.1), provided by professor Haiqing Zhao of the Johns Hopkins University in Baltimore (Stephan *et al.*, 2009), was transfected into HEK 293T cells by using FuGENE 6 reagent (Roche Applied Science, Mannheim, Germany) according to the manufacturer's protocol. Transfected cells were identified by EGFP fluorescence and used for electrophysiological recordings from 24 to 48 hours after transfection.

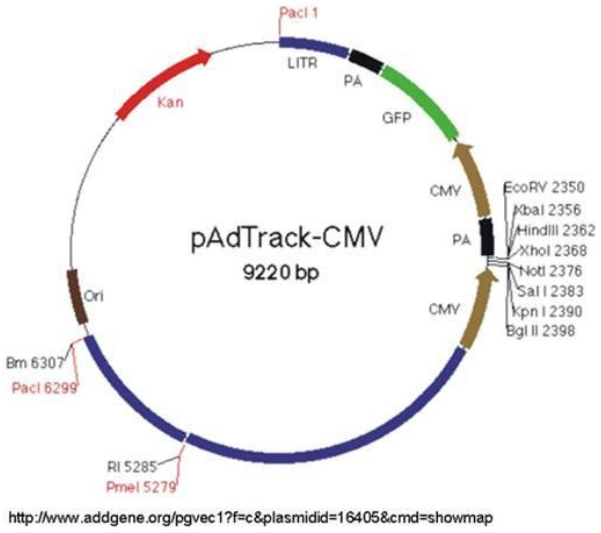

Figure 2.1. *pAdTrack-CMV map (www.addgene.org). The full-length, dominant olfactory isoform of the mouse TMEM16b/anoctamin2 was inserted into the multi cloning site (MCS) between NotI and SalI restriction enzymes (Stephan et al., 2009). Transfected HEK 293T cells were identified by EGFP fluorescence and used for electrophysiological recordings.*

2.3 The experimental set-up for patch clamp recording

Experiments with olfactory sensory neurons and HEK 293T cells transfected with TMEM16b/anoctamin2 were performed on the same experimental setup, shown in Figure 2.2.

The preparation was observed through an oil immersion 100X objective (N.A. 0.17, Zeiss, Milano, Italy) with an Olympus IX70 inverted microscope (Olympus, Japan) placed on an antivibration table (TMC, USA). A homemade Faraday cage provided adequate electrical shielding.

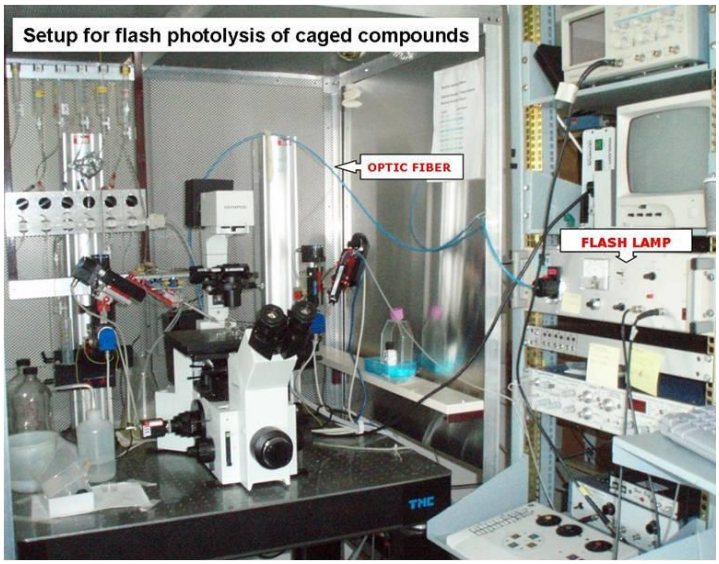

Figure 2.2 *Experimental set up used for patch clamp experiments with photolysis of caged compounds.*

Patch pipettes were made using borosilicate glass (outer diameter 1.65 mm; inner diameter 1.1 mm, WPI, Sarasota, FL, USA) and pulled with a PP83 puller (Narishige, Tokyo, Japan) using a double-stage pull. The diameter of the tip was about 1 µm and the pipette resistances were 3–7 MΩ when filled with the standard intracellular solution.

Pipettes were mounted in a pipette holder with an Ag/AgCl electrode for electrical recording. The holder movements were controlled by an electronic micromanipulator (Luigs & Neumann, Feinmechanick Elektrotechnik GmbH, Ratingen, Germany).

Currents were recorded in the whole cell voltage-clamp mode with an Axopatch 200B patch-clamp amplifier, controlled by Clampex 8 via a Digidata 1332A (Axon Instruments, Union City, CA, USA). Currents were low-pass filtered at 1 kHz and acquired at 2 kHz for experiments with olfactory sensory neurons, or filtered at 5 kHz and sampled at 10 kHz for experiments with transfected HEK 293T cells.

The perfusion system was entirely gravity driven. Solutions were stored in 50 ml syringes and polyethylene tubes were used for connection with the recording chamber. The recording chamber was continuously bathed with mammalian Ringer solution while an aspiration tube, placed at the opposite site and connected with a trap bottle, controlled the level of solution in the recording chamber. The flow of solution was manually controlled by valves.

In experiments in which the Cl^- concentration was changed, the bath was grounded through a 1M KCl agar bridge connected with an Ag/AgCl reference electrode.

All experiments were carried out at room temperature (20 - 24°C).

2.4 Flash photolysis of caged compounds

For flash photolysis of caged compounds a xenon flash-lamp system JML-C2 (Rapp OptoElectronic, Hamburg, Germany) was used coupled with the epifluorescence port of the inverted microscope with a quartz light guide (Boccaccio *et al.*, 2006).

The spot of light had a diameter of about 15 µm to cover only the ciliary region of olfactory sensory neurons (but given the very small size of mouse olfactory sensory neurons it was sometimes technically difficult to restrict the illumination area to the cilia only); or about 50% of the surface of HEK 293T cells (Figure 2.3).

The diameter of the spot was measured by inserting the quartz light guide in an illuminator (Highlight 3100 Olympus) and focusing the spot of the light on the plan of a graduated coverslip. The spot was focused through the oil immersion 100X Zeiss objective used for all the experiments with caged compounds in this thesis.

The released energy at the objective was a few mJ, and this was reduced to an unknown grade of intensity inside the cell.

The flash duration was 1 ms and was kept constant during each experiment. At the beginning of each experiment, the stability of the response was checked by applying repetitive flashes at intervals of about 2 min.

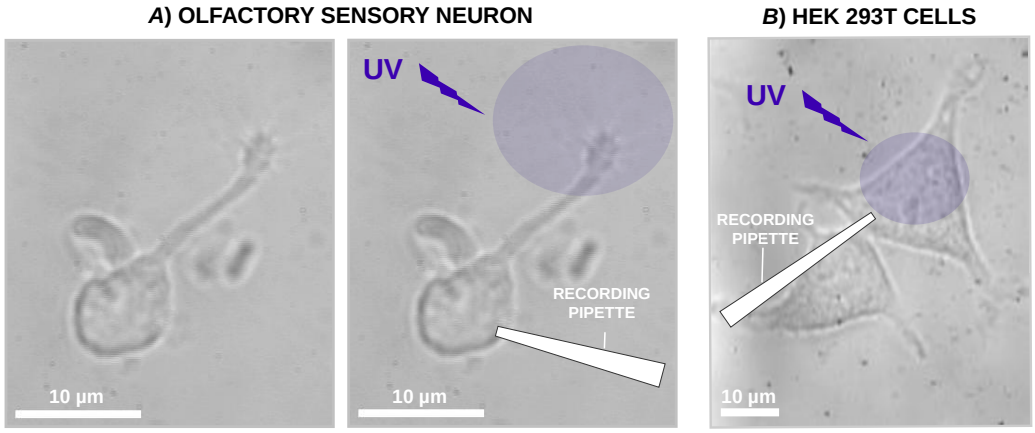

Figure 2.3 *Patch-clamp experiments in the voltage-clamp whole-cell configuration were performed on isolated olfactory sensory neuron with clearly visible cilia (A) or HEK293T cells (B).Caged compounds diffused from the patch pipette into the cell and the physiologically active compound was released with ultraviolet light flashes. The illuminated area is indicated by purple circles.*

2.5 Ionic solutions

Bath solutions with different ionic composition were used for experiments with olfactory sensory neurons and HEK 293T cells, as listed in the following table:

EXTRACELLULAR SOLUTIONS

	NaCl (mM)	KCl (mM)	$CaCl_2$ (mM)	$MgCl_2$ (mM)	EGTA (mM)	HEPES (mM)	Glucose (mM)	Na-pyruv. (mM)
Normal Ringer	140	5	1	1		10	10	1
Low Ca^{2+} Ringer	140	5		1	10	10	10	1

For permeability experiments the NaCl in Normal Ringer was completely replaced with NaSCN, NaBr, NaI, $NaNO_3$, NaMeS or CholineCl

All solutions were adjusted to pH 7.4

Niflumic acid (NFA) and 5-Nitro-2-(3-phenylpropylamino)benzoic acid (NPPB, Tocris) were prepared in dimethyl sulfoxide (DMSO) as stock solutions respectively at 200 mM or 83 mM and diluted to the final concentration in the normal Ringer solution (DMSO alone did not alter the currents); 4,4′-diisothiocyanatostilbene-2,2′-disulfonic acid (DIDS) was directly dissolved in the normal Ringer solution. Different bathing solutions were delivered by using a gravity-fed perfusion system. A slow flow rate was selected in such a way that the position of the cilia of the neurons was not perturbed. A complete solution change was obtained in about 10 s. To measure blocker effects, current recordings were obtained before blocker application (control), 1-2 min after delivery of the solution with the blocker, and 2-5 min after perfusion with Ringer solution without the blocker (washout).

In ionic selectivity experiments NaCl was substituted on an equimolar basis with NaX, where X is the substituted anion, or NaCl was replaced with equimolar choline chloride. Relative permeability of the channels was determined by measuring the shift in reversal potential. The bath was grounded through a 1 M KCl agar bridge connected to a Ag/AgCl reference electrode. Liquid junction potentials were calculated using Clampex's Junction Potential Calculator, based on the JPCalc program developed by Barry (1994; see also http://web.med.unsw.edu.au/phbsoft/LJP_Calculator.htm). Applied membrane potentials were corrected off-line. The liquid junction potential between the pipette and the Ringer solution was calculated. Then, if the bathing solution was changed after reaching the

whole-cell configuration, we calculated the additional liquid junction potential generated between the bathing solution and the 1 M KCl agar bridge. We corrected membrane potentials for the following calculated liquid junction potentials (in mV) in the indicated bathing solutions: -4.6 in Ringer, -4.0 in isothiocyanate Ringer, -4.7 in bromide Ringer, -4.6 in iodide Ringer, -4.3 in nitrate Ringer, -3.0 in methanesulfonate Ringer, -5.3 in Ringer with NaCl replaced with choline chloride.

Intracellular recording solutions for the photorelease of 8-Br-cAMP and calcium are summarized in the following table:

INTRACELLULAR SOLUTIONS

	CsCl	KCl	$CaCl_2$	$MgCl_2$	EGTA	HEPES	MgATP	GTP	K-glucon.	BCMCM 8-Br-cAMP	DMNP-EDTA
	(mM)	(mM)	(mM)	(mM)	(mM)	(mM)	(mM)	(mM)	(mM)	(mM)	(mM)
Caged 8-Br-cAMP		145		4	0.5	10	1	0.1		0.05	
Caged calcium	140		1.5			10					3
Low Cl caged calcium		12				10			133		3

All solutions were adjusted to pH 7.4

The caged 8-Br-cAMP (BCMCM-8-Br-cAMP) was provided by Volker Hagen of the Leibniz-Institute for Molecular Pharmacology in Berlin; Boccaccio *et al.*, 2006). The caged 8-Br-cAMP was dissolved in DMSO at 10 or 50 mM and stored at −20°C for up to 3 months. The final concentration of 50 μM was obtained by diluting an aliquot of the stock solution into the pipette solution.

DMNP-EDTA for the photorelease of caged Ca^{2+} was purchased from Molecular Probes–Invitrogen (West Eugene, OR), and $CaCl_2$ was adjusted with a 0.1 M standard solution from Fluka (Deisenhofen, Germany).

The caged compounds solutions were stored for a few days at −20°C, kept refrigerated in the dark during the experimental session, and were allowed to diffuse freely from the patch pipette into the cytoplasm of the cell for about 2 min after establishment of the whole cell configuration.

Chemicals, except for caged compounds or otherwise stated, were purchased from Sigma.

2.6 mBest2-null mouse line

The mBest2 null mouse line was purchased from Deltagen (USA). The targeting vector was constructed using 0.8-kb (5') and 2.9-kb (3') mouse Best2 genomic DNA fragments as homology arms. The two arms flanked a promoterless lacZ and a neomycin resistant gene cassette (lacZ-neo). Homologous recombination in mouse embryonic stem cells resulted in the insertion of the lacZ-neo cassette, replacing a region spanning exon 1 through a part of exon 3 of the mouse Best2 locus. Germ-line–transmitting chimeric mice generated from the targeted embryonic stem cells were bred with C57Black mice to produce mBest2$^{+/-}$ mice. Intercrossing of heterozygous mice generated Best2$^{-/-}$ mice.

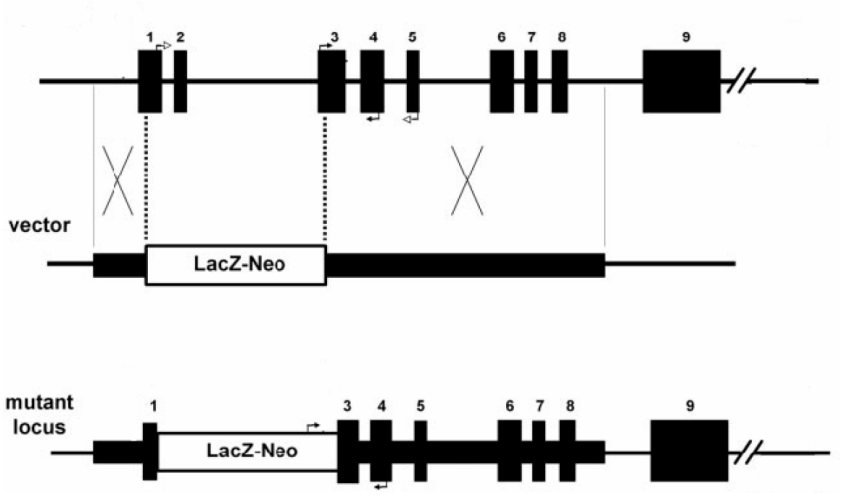

Figure 2. *Targeted disruption of the mouse Best2 gene.*
Schematic representation of wild-type locus, targeting vector, and mutant locus. Thick lines: fragments used for constructing the targeting vector 5' and 3' arms. Thin lines: genomic DNA or vector backbone sequence. Numbered solid boxes: Best2 exons. Labeled boxes: the LacZ and Neo resistance expression cassette. From Deltagen.

2.7 Data analysis

Current amplitudes at each holding potential were calculated by subtracting the value of the baseline. Data are reported as mean ± SEM and N indicates the total number of cells. Statistical significance was determined using Student's t-test, or ANOVA, as appropriate. When a statistically significant difference was determined with ANOVA, a Tukey post hoc test was done to evaluate which data groups showed significant differences. P values <0.05 were considered significant.

Data analysis and figures were made with Igor software (Wavemetrics, Lake Oswego, OR, USA).

3 RESULTS

3.1 Calcium-activated chloride currents in olfactory sensory neurons from mice lacking bestrophin-2.

Pifferi S, Dibattista M, Sagheddu C, Boccaccio A, Al Qteishat A, Ghirardi F, Tirindelli R, Menini A (2009). J Physiol. 587, 4265-79

J Physiol 587.17 (2009) pp 4265–4279

The Journal of Physiology

Calcium-activated chloride currents in olfactory sensory neurons from mice lacking bestrophin-2

Simone Pifferi[1], Michele Dibattista[1], Claudia Sagheddu[1], Anna Boccaccio[1], Ahmed Al Qteishat[1], Filippo Ghirardi[2], Roberto Tirindelli[2] and Anna Menini[1]

[1]*International School for Advanced Studies, Scuola Internazionale Superiore di Studi Avanzati, SISSA, and Italian Institute of Technology, SISSA Unit, Trieste, Italy*

[2]*Section of Physiology, Department of Neuroscience, University of Parma, Parma, Italy*

Olfactory sensory neurons use a chloride-based signal amplification mechanism to detect odorants. The binding of odorants to receptors in the cilia of olfactory sensory neurons activates a transduction cascade that involves the opening of cyclic nucleotide-gated channels and the entry of Ca^{2+} into the cilia. Ca^{2+} activates a Cl^- current that produces an efflux of Cl^- ions and amplifies the depolarization. The molecular identity of Ca^{2+}-activated Cl^- channels is still elusive, although some bestrophins have been shown to function as Ca^{2+}-activated Cl^- channels when expressed in heterologous systems. In the olfactory epithelium, bestrophin-2 (Best2) has been indicated as a candidate for being a molecular component of the olfactory Ca^{2+}-activated Cl^- channel. In this study, we have analysed mice lacking Best2. We compared the electrophysiological responses of the olfactory epithelium to odorant stimulation, as well as the properties of Ca^{2+}-activated Cl^- currents in wild-type (WT) and knockout (KO) mice for Best2. Our results confirm that Best2 is expressed in the cilia of olfactory sensory neurons, while odorant responses and Ca^{2+}-activated Cl^- currents were not significantly different between WT and KO mice. Thus, Best2 does not appear to be the main molecular component of the olfactory channel. Further studies are required to determine the function of Best2 in the cilia of olfactory sensory neurons.

(Received 1 June 2009; accepted after revision 14 July 2009; first published online 21 July 2009)

Corresponding author A. Menini: International School for Advanced Studies, Scuola Internazionale Superiore di Studi Avanzati, SISSA, Via Beirut 2, 34014 Trieste, Italy. Email: menini@sissa.it

Abbreviations Best2, bestrophin-2; CNG, cyclic nucleotide-gated; KO, knockout; WT, wild-type.

In vertebrates, the process of olfactory transduction occurs in sensory neurons, located in the olfactory epithelium in the nasal cavity. Each olfactory sensory neuron bears several cilia departing from the knob-like swelling of the apical part of the dendrite. The cilia are the site of olfactory transduction: odorant molecules bind to specific receptors expressed in the ciliary plasma membrane activating a G protein-coupled transduction cascade. The activation of adenylyl cyclase by the G protein produces an increase in the ciliary concentration of cAMP, which opens cyclic nucleotide-gated (CNG) channels, which produces a primary inward current carried by Na^+ and Ca^{2+} ions (reviewed by Schild & Restrepo, 1998; Menini, 1999; Firestein, 2001; Matthews & Reisert, 2003; Menini *et al.* 2004; Pifferi *et al.* 2006*a*; Kleene, 2008). The increase in Ca^{2+} concentration triggers the gating of Ca^{2+}-activated Cl^- channels that gives rise to a secondary Cl^- current. Since olfactory sensory neurons maintain an elevated intracellular Cl^- concentration, which is in the same range of the Cl^- concentration present in the mucus at the external side of the cilia (Reuter *et al.* 1998; Kaneko *et al.* 2001, 2004), the opening of Ca^{2+}-activated Cl^- channels in the ciliary membrane causes an efflux of Cl^- ions from the cilia, which amplifies the primary inward current (Kleene & Gesteland, 1991; Kleene, 1993; Kurahashi & Yau, 1993; Lowe & Gold, 1993; Kleene, 1997; Boccaccio & Menini, 2007; reviewed by Frings *et al.* 2000; Kleene, 2008; Frings, 2009).

While most of the components of the olfactory transduction cascade have been identified at the molecular level, the molecular identity of Ca^{2+}-activated Cl^- channels is still elusive. In recent years, several proteins have been proposed as possible candidates for Ca^{2+}-activated Cl^-

S. Pifferi and M. Dibattista contributed equally to this study.

DOI: 10.1113/jphysiol.2009.176131

channels, including the families of bestrophins, tweety, CLCA calcium activated chloride channels (reviewed by Hartzell *et al.* 2005, 2009) and, very recently, the anoctamin/transmembrane 16 (TMEM16) protein family (Caputo *et al.* 2008; Schroeder *et al.* 2008; Yang *et al.* 2008; Pifferi *et al.* 2009; Stephan *et al.* 2009).

Proteins of the bestrophin family have been shown to form Cl^- channels when expressed in heterologous systems (Sun *et al.* 2002; Tsunenari *et al.* 2003) and have been proposed to be *bona fide* Ca^{2+}-activated Cl^- channels (Qu *et al.* 2003, 2004; Pusch, 2004), although other reports suggested that they function as regulators of ion transport rather than as ion channels (Rosenthal *et al.* 2006; Yu *et al.* 2008; reviewed by Kunzelmann *et al.* 2007; Hartzell *et al.* 2008; Marmorstein *et al.* 2009).

We have previously shown that bestrophin-2 (Best2) is expressed in the cilia of mouse olfactory sensory neurons, where it colocalizes with CNGA2, the principal subunit of the olfactory CNG channel that is responsible for the primary transduction current (Pifferi *et al.* 2006*b*). Moreover, we have shown that the functional properties of the current induced by heterologous expression of mouse Best2 and those of the native Ca^{2+}-activated Cl^- current from dendritic knob/cilia of mouse olfactory sensory neurons present many similarities, including the same anion permeability sequence, small estimated single-channel conductances, and the same side-specific blockage by some Cl^- channel blockers, although also differences do exist and include a Ca^{2+} sensitivity discrepancy of one order of magnitude (Pifferi *et al.* 2006*b*). However, based on the overall findings, Best2 was indicated to be candidate molecular component of Ca^{2+}-activated Cl^- channels involved in olfactory transduction (Pifferi *et al.* 2006*b*). In the last year knockout mice for Best2 became commercially available opening the possibility of further investigation of the physiological role of Best2. We have therefore analysed the responses of the olfactory epithelium to odorant stimulation and investigated the properties of Ca^{2+}-activated Cl^- currents in wild-type (WT) and knockout (KO) mice lacking Best2. Our results confirm that Best2 is expressed in the cilia of olfactory sensory neurons, but we found that Ca^{2+}-activated Cl^- currents were not significantly different between WT and KO mice, indicating that Best2 is not the main molecular component of the olfactory channel. Further studies are required to determine the physiological role of Best2 in the cilia of olfactory sensory neurons.

Methods

Ethical approval

All animals were handled in accordance with the Italian Guidelines for the Use of Laboratory Animals (Decreto Legislativo 27/01/1992, no. 116) and European Union guidelines on animal research (No. 86/609/EEC). For experiments mice were anaesthetized by CO_2 inhalation and then decapitated.

Animals

Experiments were performed on knockout (KO) mice for *Best2* and wild-type (WT) littermates between 2 and 6 months of age. *Best2* homozygous mutant and WT mice were obtained by breeding heterozygous mutant mice obtained from Deltagen (San Mateo, CA, USA). The generation of these mice has been previously described in detail (Bakall *et al.* 2008).

Cookie test

Mice were left overnight without food with water *ad libitum*. The next day, mice were moved into an opaque cage, while a food pellet (Altromin-R, A. Rieper S.p.A., Vandoies, Bolzano, Italy) was buried in their litter's sawdust, about 2 cm underneath. Then, mice were brought back in their cages and released at the centre of the litter. The time was measured from the moment they were freed to the moment they found the pellet. Results were analysed using the analysis software SPSS 13.0 (SPSS Inc., Chicago, IL, USA) and StatView (SAS Institute Inc., Cary, NC, USA).

RNA isolation and RT-PCR

Total RNA was extracted from the olfactory epithelium of WT and KO mice using standard Clontech procedures (BD Biosciences, Hertfordshire, UK). RNA quality was measured using a NanoDrop1000 Spectrophotometer (ND-1000). Gene expression was examined by RT-PCR from total RNA using primers designed against *Best2*, *CNGA2* and the housekeeping gene *S16*. PCR conditions were as follows: an initial denaturation step of 10 min at 95°C, followed by 35 cycles of 1 min at 94°C, 1 min at 58°C and 1 min at 72°C, and a final extension step of 10 min at 72°C. The products were visualized following agarose gel electrophoresis (1.5%) and DNA was stained with ethidium bromide (10 mg ml^{-1}). Samples without cDNA were used as negative controls. The sequences of the primers used were the following:

Best2 (forward: 5′-AGT CCC AGG AAA CAT AAC AGC TCT C-3′ and reverse: 5′-CTC CCA GCA TCT TCC CTT GGC TCA C-3′);
CNGA2 (forward: 5′-AGG GAA AGG GCA CCA AAA AGA AA-3′ and reverse: 5′-CCA GCA CCA GCC ATA CCA CAA A-3′);

S16 (forward: 5′-GGC AGA CCG AGA TGA ATC CTC A-3′ and reverse: 5′-CAG GTC CAG GGG TCT TGG TCC-3′).

Western blot

Proteins were extracted from olfactory epithelium tissues by RIPA buffer (Millipore, Milan, Italy) and the protein concentration of each sample was determined using the Bio-Rad assay. For Western blotting, 10 μg of protein was separated by gel electrophoresis (SDS-PAG; 12% w/v) and the proteins were electro-blotted onto nitrocellulose filters (Whatman, Germany). Filters were blocked in 1% w/v bovine serum albumin (BSA) in Tris-buffered saline Tween 20 (TBS Tween) and incubated overnight at 4°C with the following primary antibodies: rabbit polyclonal anti-Best2 (1 : 500; Pifferi *et al.* 2006*b*); mouse monoclonal anti-CNGA2 (a gift from F. Müller and U. B. Kaupp, Forschungszentrum Julich, Julich, Germany; Meyer *et al.* 2000), and anti-β-actin (1 : 1000; Sigma, Milan, Italy). Membranes were washed in TBS-Tween before staining with antibodies to the appropriate peroxidase-conjugated secondary antibody, diluted 1 : 1000 in 1% w/v BSA in TBS Tween for 1 h. Blots were developed with the ECL detection system (Amersham, UK).

Immunohistochemistry

The nasal regions were fixed in 4% paraformaldehyde for 4 h at 4°C, decalcified by overnight incubation in 0.5 M EDTA, and then equilibrated in 30% (w/v) sucrose overnight at 4°C for cryoprotection. Coronal sections 16 μm thick were cut on a cryostat and stored at −20°C. Tissue sections were incubated with 0.5% sodium dodecyl sulfate (v/v) in phospate buffered saline (PBS) for 15 min for antigen retrieval, then incubated in blocking solution (2% normal goat serum, 0.2% Triton X-100 in PBS) for 90 min, and incubated overnight at 4°C in primary antibodies diluted in blocking solution. After rinsing in 0.1% (v/v) Tween 20 in PBS, sections were incubated with fluorophore-conjugated secondary antibodies in 0.1% Tween 20 in PBS for 2 h at room temperature and washed. 4′-6-Diamidino-2-phenylindole (DAPI) (0.1 μg ml^{-1}) was used to stain nuclei: tissue sections were incubated for 30 min then washed and mounted with Vectashield (Vector Laboratories, Burlingame, CA, USA).

Primary antibodies were rabbit anti-Best2 (Pifferi *et al.* 2006*b*) and mouse monoclonal anti-CNGA2 (Meyer *et al.* 2000) used at 1 : 50. Secondary antibodies were Alexa 488-conjugated goat anti-rabbit and Alexa 594-conjugated goat anti-mouse diluted to 1 : 200 (Molecular Probes-Invitrogen, Eugene, OR, USA).

Images were visualized by Leica TCS SP2 confocal microscope, acquired using Leica software at 1024 × 1024 pixels resolution and analysed with ImageJ software.

Electro-olfactograms

Electro-olfactogram (EOG) recordings were performed as previously described (Franceschini *et al.* 2009). The mouse head was cut sagitally to expose the medial surface of the olfactory turbinates and EOG recordings were measured at the surface of the olfactory epithelium in response to odorant stimuli in the vapour phase. Each odorant, amylacetate, cineole and acetophenone (Sigma, Milan, Italy), was prepared as 2.5 M stock in DMSO and then diluted with water to the final concentrations used in the experiments. Responses to DMSO alone were less than 0.05 mV. Vapour-phase odorant stimuli were generated by placing 0.9 ml of an odorant solution in a 10 ml glass test-tube capped with a rubber stopper. For stimulation, a 100 ms pulse of the odorant vapour at 8 psi was injected into a continuous stream of humidified air.

Electrophysiological recordings from dissociated olfactory sensory neurons

Olfactory sensory neurons were dissociated enzymatically from the olfactory epithelium of 1- to 2-month-old mice, with a papain–cysteine treatment as previously described (Lagostena & Menini, 2003; Boccaccio *et al.* 2006). Cells were plated on Petri dishes for excised patch recordings, or on glass coverslips coated with poly-L-lysine and concanavalin A (Type V, Sigma, Milan, Italy) for whole-cell recordings with photolysis of caged compounds (Boccaccio *et al.* 2006; Boccaccio & Menini, 2007).

Currents in the whole-cell or in the inside-out voltage-clamp modes were recorded with an Axopatch 1D or an Axopatch 200B amplifier controlled by Clampex 8 or 9 via a Digidata 1322A or 1332A (Axon Instruments, Union City, CA, USA). Patch pipettes were made using borosilicate capillaries (WPI, Sarasota, FL, USA) and pulled with a Narishige PP83 puller (Narishige, Tokyo, Japan). Patch pipettes filled with standard intracellular solutions had resistances of 2–7 MΩ for whole-cell and 7–10 MΩ for excised patch recordings. Currents were low-pass filtered at 1 kHz and acquired at 2 kHz for whole-cell experiments, or filtered at 4 kHz and sampled at 10 kHz for excised patch recordings. All experiments were carried out at room temperature (20–22°C).

For flash photolysis of the caged compounds, we used a xenon flash-lamp system, JML-C2 (Rapp OptoElectronic, Hamburg, Germany), coupled with the epifluorescence port of the microscope with a quartz light guide (Boccaccio *et al.* 2006). The spot of light had a diameter of about 15 μm and was focused on the ciliary region. The interval

between experiments was about 2 min to allow the cell to recover from adaptation.

Rapid solution exchange in inside-out patches was obtained with the perfusion Fast-Step SF-77B (Warner Instrument Corp., Hamden, CT, USA). For current–voltage relations of Ca^{2+}-activated currents, inside-out patches were pre-exposed to the test Ca^{2+} concentration for 500 ms at −100 mV to allow the current to partially inactivate, and then a double voltage ramp from −100 to +100 mV and back to −100 mV was applied at 1 mV ms^{-1}. The two current–voltage relations were averaged and leak currents measured with the same ramp protocol in Ca^{2+}-free solutions were subtracted. The same type of voltage protocol was used to measure current–voltage relations of cAMP-activated currents.

Ionic solutions

For whole-cell recordings, the extracellular mammalian Ringer solution contained (in mM): 140 NaCl, 5 KCl, 1 $CaCl_2$, 1 $MgCl_2$, 10 Hepes, 10 glucose and 1 sodium pyruvate (pH 7.4). The composition of the low Ca^{2+} extracellular solution was similar, except that it contained 10 mM EGTA and no added Ca^{2+}. The whole-cell pipette solution for the photorelease of caged 8-Br-cAMP contained (in mM): 145 KCl, 4 $MgCl_2$, 0.5 EGTA, 10 Hepes, 1 MgATP, 0.1 GTP, 0.05 caged 8-Br-cAMP, (pH 7.4). The caged BCMCM-8-Br-cAMP (Boccaccio *et al.* 2006) was dissolved in DMSO at 10 or 50 mM and stored at −20°C for up to 3 months. The final concentration of 50 μM was obtained by diluting an aliquot of the stock solution into the pipette solution, kept refrigerated in the dark during the experimental session, and stored for a few days at −20°C. The standard pipette solution for the photorelease of caged Ca^{2+} contained (in mM): 3 DMNP-EDTA, 1.5 $CaCl_2$, 140 KCl, and 10 Hepes (pH 7.4). The low Cl^- intracellular solutions for the photorelease of caged Ca^{2+} contained (in mM): 3 DMNP-EDTA, 1.5 $CaCl_2$, 12 KCl, 133 potassium gluconate, and 10 Hepes (pH 7.4). Liquid junction potentials were corrected off-line. DMNP-EDTA was purchased from Molecular Probes–Invitrogen, and $CaCl_2$ was adjusted with a 0.1 M standard solution from Fluka (Deisenhofen, Germany). The caged compounds were allowed to diffuse from the patch pipette into the cytoplasm of an olfactory sensory neuron for about 2 min after establishment of the whole-cell configuration.

For inside-out recordings, the standard solution in the patch pipette contained (in mM): 140 NaCl, 10 HEDTA and 10 Hepes, pH 7.2. In experiments for Ca^{2+} dose–response relations, NaCl was replaced with LiCl to inhibit the Na^+/Ca^{2+} exchanger. The bathing solution at the intracellular side of the patch contained (in mM): 140 NaCl or LiCl, 10 HEDTA and 10 Hepes, pH 7.2, and no added Ca^{2+} for the nominally 0 Ca^{2+} solution, or various added Ca^{2+} concentrations, as calculated with the program WinMAXC (C. Patton), to obtain free Ca^{2+} in the range between 1.5 and 100 μM (Patton *et al.* 2004). The free Ca^{2+} concentrations were experimentally determined by Fura-4F (Molecular Probes–Invitrogen) measurements by using an LS-50B luminescence spectrophotometer (PerkinElmer, Wellesley, MA, USA). To activate CNG channels a solution containing 100 μM cAMP directly dissolved into the 0 Ca^{2+} bathing solution was used.

Chemicals, unless otherwise stated, were purchased from Sigma (Milan, Italy).

Data analysis

Data are reported as means ± standard deviation, with the number of experiments (n) from different mice, cells or membrane patches, as appropriate. The statistical significance of data was evaluated by Student's t-test and P values < 0.05 were considered significant. Data analysis and figures were made with Igor software (Wavemetrics, Lake Oswego, OR, USA).

Results

Expression of *Best2* in the olfactory epithelium

To examine the expression of *Best2*, we performed RT-PCR on total RNA from the olfactory epithelium of WT and KO mice. Specific primers for *Best2*, for the main subunit of the CNG channel *Cnga2*, and for the housekeeping gene *S16* showed that, in WT mice, PCR products of the predicted size were amplified (Best2, 205 bp; CNGA2, 200 bp; S16, 102 bp) (Fig. 1*A*). In KO mice, the 205 bp reaction product, corresponding to *Best2*, was absent, while control genes were normally expressed (Fig. 1*A*). This result confirms the absence of expression of *Best2* in the olfactory epithelium of KO mice.

Best2 immunoreactivity in the olfactory epithelium

To verify the lack of expression of the Best2 protein in the olfactory epithelium of KO mice, we performed both Western blotting and immunohistochemistry (Fig. 1*B* and *C*), using the antibody against Best2 that we have previously generated and characterized (Pifferi *et al.* 2006*b*).

By Western blotting, we identified a 57 kDa band in a membrane fraction of the olfactory epithelium of WT mice, corresponding to the expected molecular weight for the Best2 protein, in agreement with our previous study (Pifferi *et al.* 2006*b*). The 57 kDa band was undetectable in KO animals, while both the 75 and 42 kDa bands, corresponding respectively to CNGA2 and β-actin, were expressed in both mouse lines (Fig. 1*B*).

By immunohistochemistry, we confirmed our previous results showing that Best2 is expressed in the olfactory epithelium of WT mice (Pifferi *et al.* 2006*b*). We found staining at the surface of the olfactory epithelium, at the level of the ciliary layer, where Best2 colocalized with CNGA2 (Fig. 1*C*, top panels). In the olfactory epithelium of KO mice, Best2 immunoreactivity was absent, while CNGA2 was normally expressed at the level of the ciliary layer (Fig. 1*C*, bottom panels). These results demonstrate the loss of the Best2 protein in the olfactory epithelium of KO mice and confirm the specificity of our antibody against this protein.

Behavioural olfactory response

To determine whether deletion of *Best2* caused a behavioural olfactory deficit, mice were examined for olfactory function in a cookie-finding test. In this test, we compared the food-finding ability of WT and KO mice by measuring the latency to locate buried food. Mice were food-deprived with free access to water overnight and then were put in a cage where a food pellet was buried under the litter. None of the mice searched randomly in the litter; conversely, they dug only in the place where the pellet was hidden. The average time necessary to locate the cookie was 55 ± 32 s ($n = 22$) for WT mice, similar to 62 ± 34 s ($n = 22$) for KO animals. These results show that KO mice do not exhibit any gross olfactory deficit, in agreement with previous results (Bakall *et al.* 2008).

Odorant-induced responses in WT and KO mice

To investigate whether disruption of the *Best2* gene modifies the odorant sensitivity of olfactory sensory neurons, we measured odorant-induced changes in voltage across the olfactory epithelium of WT and KO mice. Indeed, the electrical activity of a population of olfactory sensory neurons in response to odorants can be recorded at the surface of the olfactory epithelium as a negative electrical field potential, the electro-olfactogram (EOG) (Ottoson, 1955; Scott & Scott-Johnson, 2002). EOG responses induced by delivering the vapour phase of a 2.5 M amyl acetate solution for 100 ms to the olfactory epithelium were recorded at 13 different locations as indicated in Fig. 2*A*. Although the amplitudes of EOG responses varied according to the different subregions of the olfactory epithelium, amplitudes at each specific location were not significantly different between WT and KO mice (Fig. 2*B*). Similar results were obtained with two

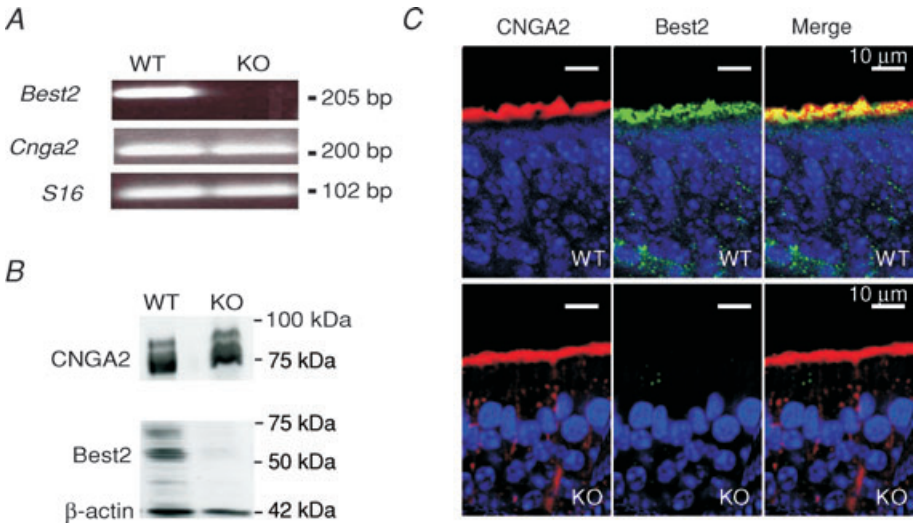

Figure 1. Comparison of Best2 mRNA expression and Best2 immunoreactivity in the mouse olfactory epithelium of WT and KO mice
A, reverse transcription–polymerase chain reaction (RT-PCR) derived cDNA products amplified from RNA of the olfactory epithelium in WT and KO mice using specific primers for *Best2*, *CNGA2* and *S16*, as indicated in the figure. The predicted size of the products for *Best2*, *CNGA2* and *S16* was respectively 205, 200 and 102 base pairs (bp). *B*, Western blot analysis of proteins of the olfactory epithelium in WT and KO mice probed with antibodies against Best2, CNGA2 and β-actin. Bands of the appropriate molecular mass were observed for each protein in WT mice, whereas only bands corresponding to CNGA2 and β-actin were detected in KO mice. The expected molecular mass for Best2, CNGA2 and β-actin was respectively 57, 75 and 42 kDa. *C*, immunostaining of sections of the olfactory epithelium. Confocal micrographs showing Best2 and CNGA2 expression in the ciliary layer of the olfactory epithelium of WT and KO mice. CNGA2 and Best2 co-expression was evident in WT mice, whereas no immunoreactivity to Best2 was detectable in KO mice. Each image on the right was obtained from the merge of the respective left and centre images. Cell nuclei were stained by DAPI.

other commonly used odorants: acetophenone and cineole (data not shown).

We determined the dose–response relation in response to amyl acetate by delivering the vapour phase of odorant solutions at various concentrations to the olfactory epithelium. Figure 2*C* shows representative recordings of EOG responses to amyl acetate in WT and KO mice. The odorant concentration producing 50% of the maximal EOG amplitude was about 10^{-3} M for both WT and KO mice (Fig. 2*D*).

We further analysed the kinetics of the EOG recordings. We measured the latency of the response as the interval between the beginning of the odorant application and the time at which the response reached 1% of its maximal value, the rise time as the time interval between 1% and the peak EOG response, and the termination as the time constant of the exponential fit of the recovery phase of the EOG response from the peak value to 10% of the peak. We did not find any significant difference for any of these parameters between WT and KO mice (Fig. 3).

Thus, no differences were observed between KO and WT mice in EOG recordings, indicating that the absence of Best2 does not significantly affect responses to odorants. However, we cannot exclude the possibility that EOG

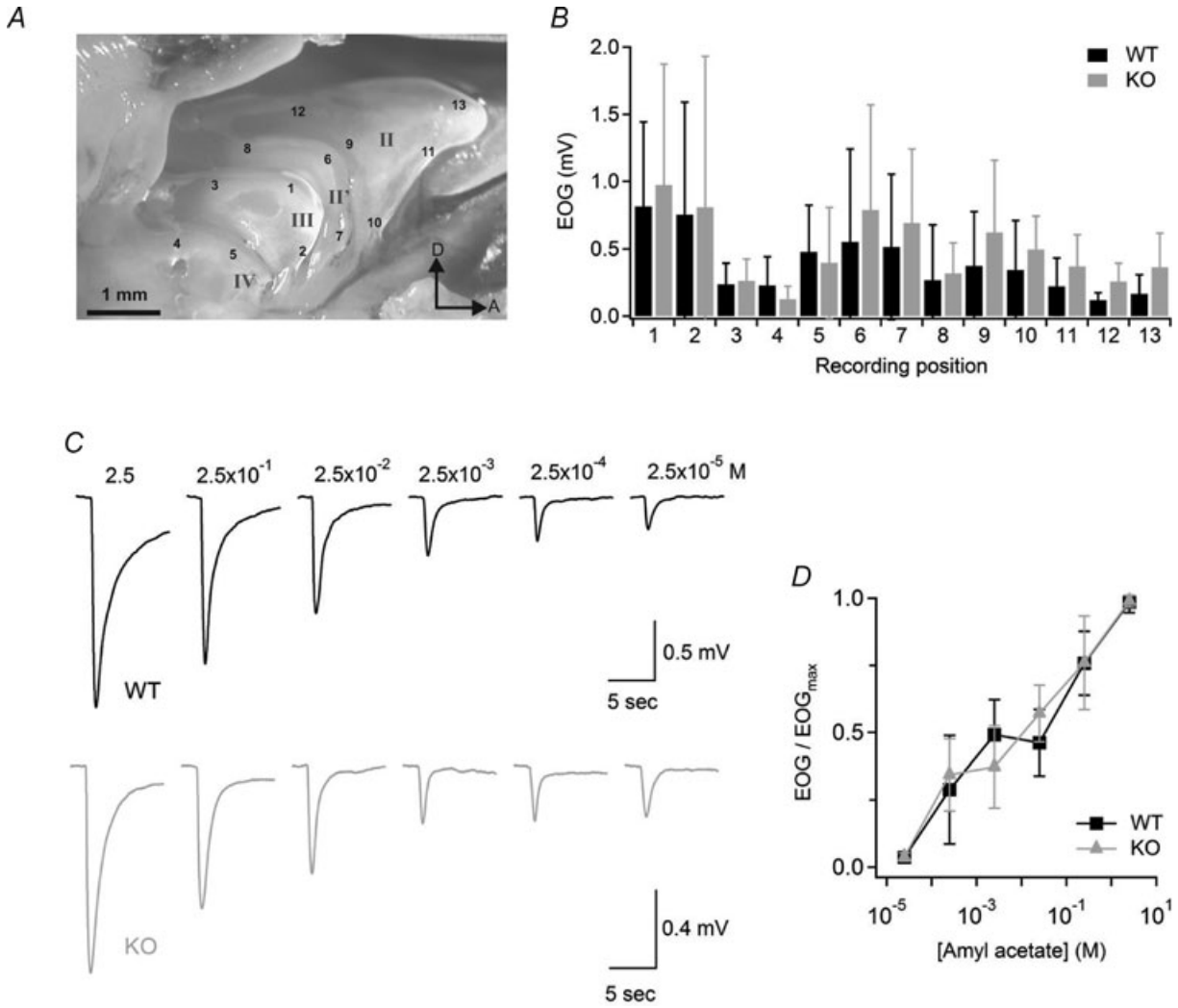

Figure 2. Odorant sensitivity in WT and KO mice

A, photomicrograph of the olfactory turbinate system. Roman numbers designate individual turbinates. Arabic numbers indicate the locations where EOG responses were recorded. D, dorsal; A, anterior. *B*, average EOG amplitudes in response to a 100 ms pulse of odorant vapour from a bottle containing 2.5 M amyl acetate liquid solution measured at the locations indicated in *A* ($n = 7$–14). *C*, representative EOG recordings from WT (black traces) or KO (grey traces) mice in response to 100 ms pulses of amyl acetate vapours. Numbers above traces are the concentrations of amyl acetate solutions in the bottle. EOG recordings were from location 1. *D*, EOG amplitudes were normalized to the value measured in response to the vapour of a 2.5 M amyl acetate solution, averaged, and plotted *versus* amyl acetate concentrations in solution for WT ($n = 14$; black symbols) or KO ($n = 13$, grey symbols) mice. Data points are linked with straight lines.

recordings are similar in WT and KO animals because some compensatory mechanism may modify the intraciliary ion concentrations in KO compared to WT mice. Indeed, although EOG measurements have the advantage of allowing long recordings while leaving the neurons in a relatively unperturbed situation, this technique does not allow the control of the intracellular ionic composition of neurons and of the membrane potential.

Currents in isolated olfactory sensory neurons

To achieve a control of both the intracellular and extracellular ionic compositions, as well as of voltage, we used isolated olfactory sensory neurons and the patch-clamp technique in the whole-cell voltage-clamp configuration. To investigate whether a Ca^{2+}-activated Cl^- current was present in individual olfactory sensory neurons from WT and KO mice, we measured the transduction current directly activating CNG channels in the cilia (Fig. 4). Indeed, the use of odorants to activate the transduction current in isolated olfactory sensory neurons would produce a very low probability of measuring odorant responses (Lagostena & Menini, 2003), due to the fact that each olfactory sensory neuron expresses only one of more than a thousand odorant receptors (for reviews, see Rodriguez, 2007; Malnic, 2007). To activate CNG channels in the cilia, we included caged 8-Br-cAMP in the intracellular solution filling the patch pipette and applied ultraviolet light flashes to the ciliary region to release the physiologically active 8-Br-cAMP. Upon flash photolysis, CNG channels are activated by 8-Br-cAMP allowing the flux of Ca^{2+} ions in the cilia and the subsequent opening of Ca^{2+}-activated Cl^- channels (Boccaccio *et al.* 2006; Boccaccio & Menini, 2007). We have previously shown that the rising phase of the response at −50 mV in Ringer solution containing 1 mM Ca^{2+} was multiphasic, composed of a primary phase of the response due to Na^+ and Ca^{2+} influx through CNG channels and a secondary phase due to Cl^- efflux through Cl^- channels activated by the influx of Ca^{2+}. Moreover, the secondary phase of the response was absent in low extracellular Ca^{2+} or at +50 mV, when the influx of Ca^{2+} through CNG channels is strongly reduced and therefore the contribution of Ca^{2+}-activated Cl^- channels is expected to be negligible (Boccaccio & Menini, 2007).

To investigate the Ca^{2+} dependence of the rising phase of the response in WT and KO mice, we compared responses at −50 mV in extracellular low Ca^{2+} or in 1 mM Ca^{2+} in the same neuron (Fig. 4*A* and *B*). Both in WT and in KO mice the rising phase of the response in low Ca^{2+} was well

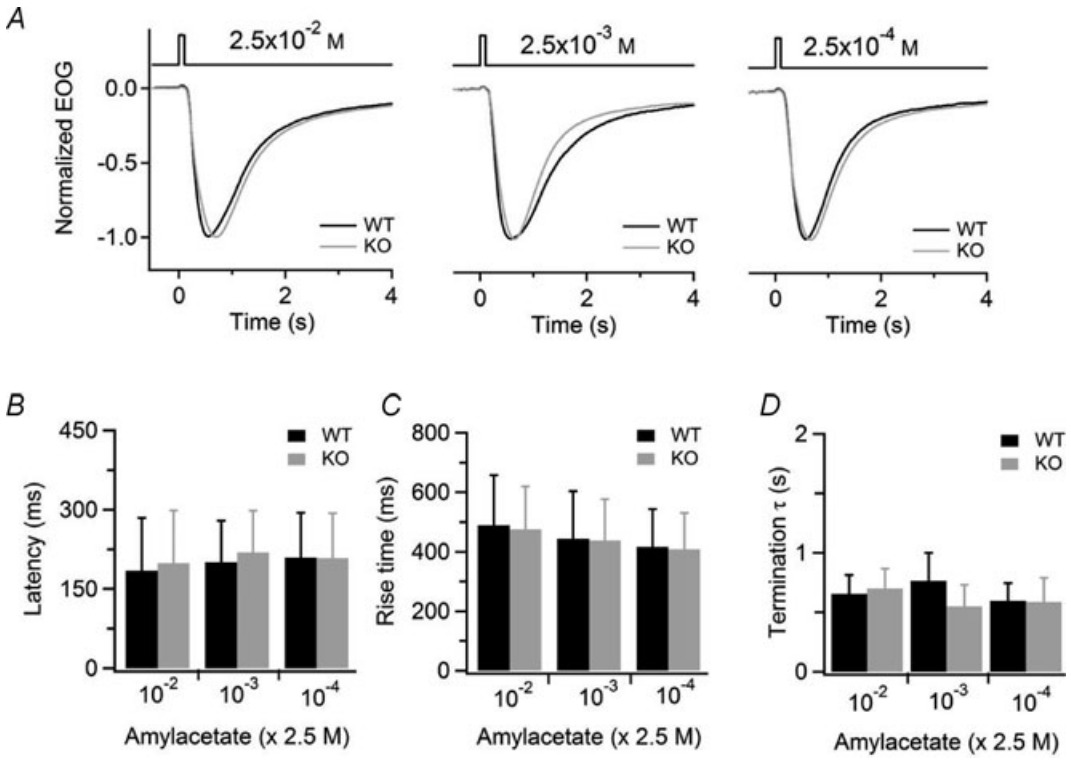

Figure 3. Kinetics analysis of odorant responses in WT and KO mice
A, normalized EOG responses to 100 ms pulses of vapour of the indicated amyl acetate concentration in solution for WT (black traces) or KO (grey traces). *B–D*, average values for latency (*B*), rise time (*C*), and time constant of the termination phase (*D*) were not significantly different in WT and KO animals at each odorant concentration ($n = 10$).

fitted with a single exponential function, while in Ringer solution containing 1 mM Ca^{2+}, the rising phase was slower and could not be described by a single exponential function. To better illustrate the rising phase, traces were normalized to their peak values and plotted superimposed on an expanded time scale in the insets of Fig. 4*A* and *B*. We measured the time necessary for the current to reach 50% of its maximal response, t_{50}, after the delivery of the light flash and found that the average ratio between t_{50} measured in Ringer solution and in low Ca^{2+} at −50 mV was 7.1 ± 3.0 ($n = 4$) for WT, not significantly different from the value of 9.1 ± 3.2 ($n = 5$) for KO.

To further investigate the presence of a Ca^{2+}-activated Cl^- current, we compared currents in Ringer solution containing 1 mM Ca^{2+} at +50 or −50 mV in the same neuron (Fig. 4*C* and *D*). At +50 mV the influx of Ca^{2+} through CNG channels is greatly reduced and the outward current is mainly carried by K^+ ions, whose permeation through CNG channels is similar to that of Na^+ ions (reviewed in Kaupp & Seifert, 2002). Both in WT and KO, the rising phase at +50 mV could be well described by a single exponential function, whereas more than one current component was present at −50 mV, as discussed above. The different rising components are illustrated in more detail in the insets of Fig. 4*C* and *D*. The rising time of the response was measured, as described above, as t_{50}, and we found that the ratio between t_{50} at +50 and at −50 mV was 0.27 ± 0.13 ($n = 3$) for WT, not significantly different from the value of 0.22 ± 0.07 ($n = 4$) for KO. Furthermore, in the same set of experiments, the ratio

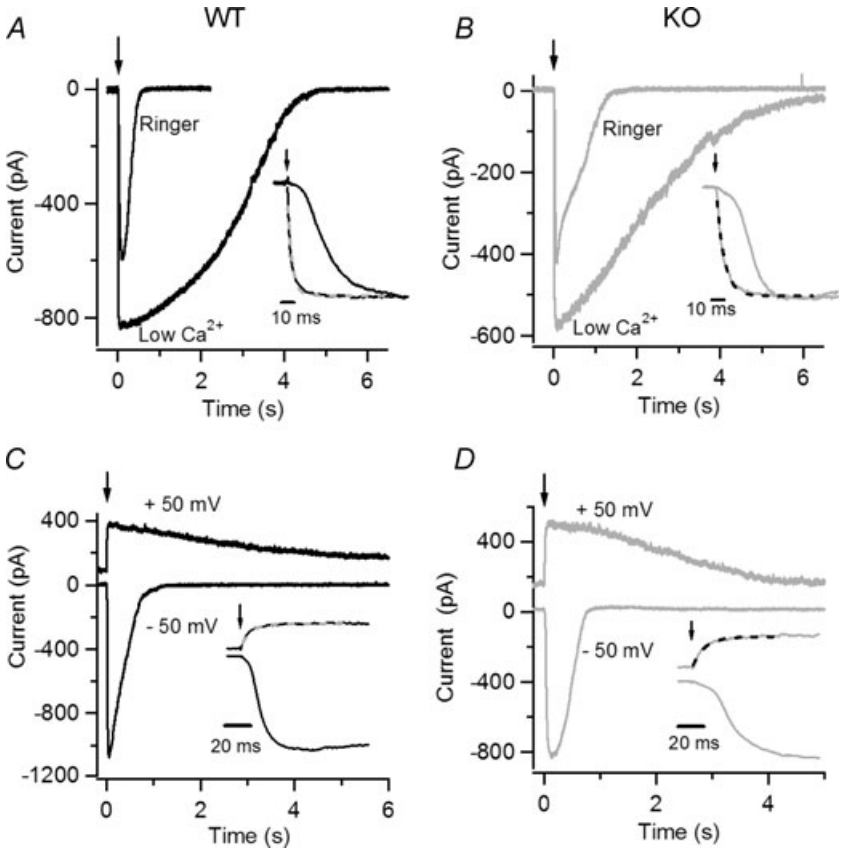

Figure 4. Current responses induced by photorelease of 8-Br-cAMP in isolated olfactory sensory neurons from WT and KO mice

Currents recorded from isolated mouse olfactory sensory neurons in the whole-cell voltage-clamp configuration in response to photorelease of 8-Br-cAMP in the cilia. An ultraviolet flash was applied at the time indicated by each arrow. *A* and *B*, an isolated olfactory sensory neuron from WT (*A*, black traces) and KO (*B*, grey traces) mice was bathed in Ringer solution containing 1 mM Ca^{2+} or in nominally 0 Ca^{2+} at the holding potential of −50 mV. Insets: responses were scaled to their maximum value and plotted superimposed on an expanded time scale. The rising phase of the response in 0 Ca^{2+} solution was fast and was well fitted by a single exponential (dashed lines), with $\tau = 3.6$ ms for WT and $\tau = 6.2$ ms for KO. Traces in Ringer solution and 0 Ca^{2+} in each panel were recorded from the same neuron. *C* and *D*, currents in an isolated olfactory sensory neuron from WT (*C*, black traces) and KO (*D*, grey traces) mice at the holding potential of −50 or +50 mV. Insets: current responses plotted on an expanded time scale, displayed a multiphasic rising phase at −50 mV, whereas at +50 mV the rising phase was well fitted by a single exponential (dashed lines, $\tau = 7.7$ ms for WT and $\tau = 10.9$ ms for KO mice). Traces at −50 and +50 mV in each panel were recorded from the same neuron.

between peak current amplitude at +50 and −50 mV was 0.35 ± 0.08 ($n = 3$) for WT, not significantly different from 0.43 ± 0.30 ($n = 4$) for KO mice.

These results show that in isolated olfactory sensory neurons from both mouse lines the transduction current comprises a primary CNG current and a secondary Ca^{2+}-activated current that is expected to be carried by Cl^- ions (Boccaccio & Menini, 2007).

To directly measure Ca^{2+}-activated currents in WT and KO mice, we photoreleased Ca^{2+} in the cilia (Fig. 5). To determine if Ca^{2+}-activated currents were carried by Cl^-, we measured the reversal potentials in the presence of various Cl^- concentrations. In a first set of experiments, we measured the reversal potential in almost symmetrical Cl^- solutions (Fig. 5*A* and *B*), while in a second set of experiments we reduced the intracellular Cl^- concentration by replacing most Cl^- with gluconate (Fig. 5*C* and *D*). The average reversal potential in symmetrical Cl^- solutions for WT, -0.8 ± 1.6 mV ($n = 5$), was not significantly different from that measured in KO, -0.5 ± 3.2 mV ($n = 4$) (Fig. 5*E*). The average reversal potential in the low intracellular Cl^- solution was shifted toward more negative values, as expected for Cl^- channels in our ionic conditions, and was similar for WT, -37.0 ± 1.2 mV ($n = 5$), and KO, -41.7 ± 5.6 mV ($n = 5$) (Fig. 5*E*). These results confirm that Ca^{2+}-activated Cl^- channels were present in olfactory sensory neurons from both WT and KO mice.

Currents in inside-out excised membrane patches from dendritic knob/cilia

To obtain a precise control of the concentrations of cyclic nucleotides and Ca^{2+} at the intracellular side of the transduction channels, we conducted patch-clamp experiments on excised membrane patches from the dendritic knob of dissociated olfactory sensory neurons with visible cilia of WT and KO mice. As previously noted (Reisert *et al.* 2003), cilia were sometimes sucked into the tip of the patch pipette and therefore the excised patches

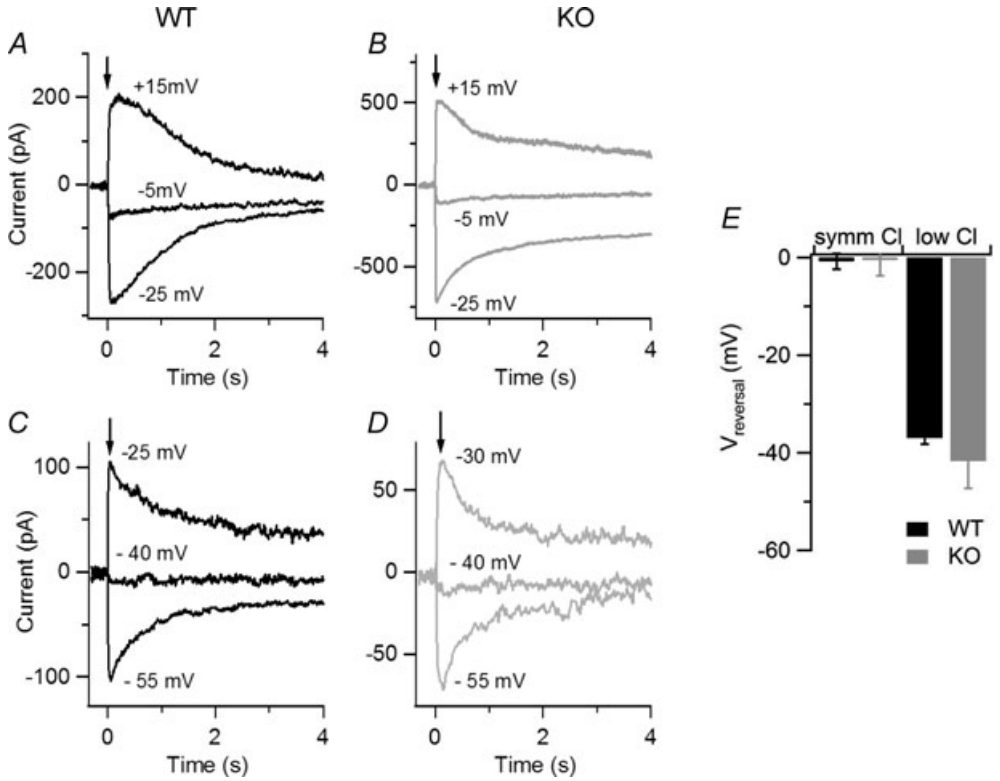

Figure 5. Current responses induced by photorelease of Ca^{2+} in isolated olfactory sensory neurons from WT and KO mice

Currents recorded from isolated mouse olfactory sensory neurons in the whole-cell voltage-clamp configuration in response to photorelease of caged Ca^{2+} (DMNP-EDTA) in the cilia. An ultraviolet flash was applied at the time indicated by each arrow to release the physiologically active Ca^{2+} into the ciliary region. *A* and *B*, currents from olfactory sensory neurons were recorded in symmetrical Cl^- solutions from WT (*A*, black traces) and KO (*B*, grey traces) mice. Currents in each panel were evoked on the same isolated olfactory sensory neuron at the indicated holding potentials, corrected for junction potentials. *C* and *D*, similar experiments were repeated when most (see Methods section) Cl^- in the intracellular solution was replaced with gluconate. *E*, average reversal potentials in symmetrical Cl^- solutions and in low Cl^- solutions.

contained membranes from both the dendritic knob and from the cilia.

To investigate the presence of CNG and Ca^{2+}-activated Cl^- currents, inside-out excised membrane patches, at the holding potential of −50 mV, were first exposed to a solution containing 100 μM cAMP in the absence of divalent cations. The same patch was then exposed to a solution containing 100 μM Ca^{2+} (Fig. 6*A* and *B*).

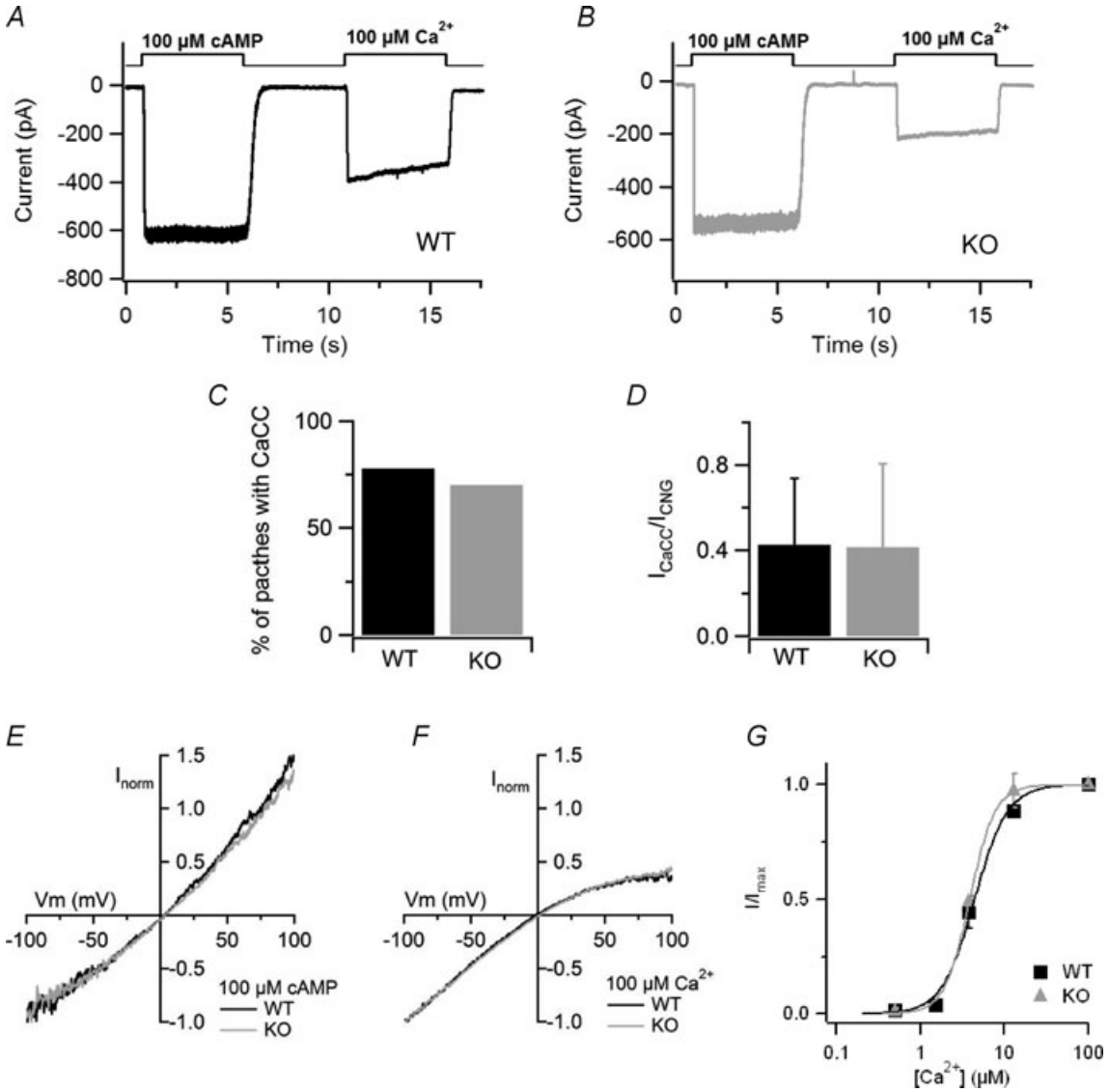

Figure 6. Recordings of CNG and Ca^{2+}-activated Cl^- currents in inside-out membrane patches
A and *B*, the cytoplasmic side of membrane patches excised from dendritic knob/cilia of olfactory sensory neurons from WT mice (*A*) and KO mice (*B*) was exposed to 100 μM cAMP, in the absence of divalent cations, to activate the CNG channels, and to 100 μM Ca^{2+} to activate the Cl^- channels. Divalent cations were absent from the patch pipette solution. The holding potential was −50 mV. *C*, percentage of membrane patches with detectable Ca^{2+}-activated Cl^- currents with respect to the presence of CNG currents in WT and KO mice. *D*, average ratios between Ca^{2+}-activated Cl^- currents and CNG currents in patches from WT ($n = 6$) and KO ($n = 11$) mice. *E*, comparison of representative current–voltage relations of the CNG current activated by 100 μM cAMP in WT (black trace) or KO (grey trace) patches. Voltage ramp from −100 to +100 mV. Currents were normalized to the value at −100 mV. *F*, comparison of representative current–voltage relations of the Cl^- current activated by 100 μM Ca^{2+} in WT (black trace) or KO (grey trace) patches. Voltage ramps from −100 to +100 mV. Currents were normalized to the value at −100 mV. *G*, dose–response relations were measured exposing patches to various free Ca^{2+} concentrations. The holding potential was −50 mV. Peak currents at each Ca^{2+} concentrations were normalized to the average current measured in the presence of 100 μM Ca^{2+} before and after each test Ca^{2+} concentration. Normalized currents were plotted *versus* Ca^{2+} concentrations, and fitted to the Hill equation. For WT mice $K_{1/2}$ was 4.4 μM, and n_H was 2.2 ($n = 3$). For KO mice $K_{1/2}$ was 3.8 μM, and n_H was 2.9 ($n = 3$).

We found that, both in WT and KO mice, about 75% of the membrane patches that showed detectable CNG currents also had Ca^{2+}-activated Cl^- currents (Fig. 6*C*). We observed a great variability in current amplitudes in both mouse lines: at −50 mV, currents in WT mice varied from absolute values of 29 to 795 pA for CNG currents, and from 16 to 495 pA for Ca^{2+}-activated Cl^- currents, while currents in KO mice varied from absolute values of 56 to 902 pA for CNG currents, and from 9 to 212 pA for Ca^{2+}-activated Cl^- currents. Since it has been previously shown that Ca^{2+}-activated Cl^- currents in olfactory sensory neurons exhibit a rundown over time, while CNG currents remain quite constant (Reisert *et al.* 2003), both currents were measured within 30 s after patch excision. The average CNG current at −50 mV was 327 ± 305 pA ($n = 7$) in WT animals, not significantly different from the value of 209 ± 254 pA ($n = 14$) in KO mice. For Ca^{2+}-activated Cl^- currents the average amplitude at −50 mV was 113 ± 15 pA ($n = 7$) in WT animals, also not significantly different from the value of 44 ± 64 pA ($n = 14$) in KO mice. To obtain an estimate of the relative density of channels we measured the ratio between Ca^{2+}-activated Cl^- currents and CNG currents in each membrane patch. The average ratio between Ca^{2+}-activated Cl^- currents and CNG currents was 0.42 ± 0.31 ($n = 7$) in WT animals, not significantly different from the value of 0.41 ± 0.39 ($n = 14$) calculated in KO mice (Fig. 6*D*). These results show that Ca^{2+}-activated Cl^- currents are present in inside-out patches from the dendritic knob/cilia of KO mice.

To further compare other biophysical properties of the transduction channels in WT and KO mice, we measured the rectification properties of the two types of currents. Currents were activated by 100 μM cAMP (Fig. 6*E*) or by 100 μM Ca^{2+} (Fig. 6*F*) using voltage ramps from −100 to +100 mV and normalized to the value at −100 mV. As shown in Fig. 6*E* and *F*, normalized current–voltage relations from WT and KO mice superimposed. The average ratio between currents at +50 and −50 mV for CNG currents was 1.13 ± 0.15 ($n = 5$) in WT animals, not significantly different from the value of 1.15 ± 0.15 ($n = 10$) calculated in KO mice. For Ca^{2+}-activated Cl^- currents the average ratio between currents at +50 and −50 mV was 0.52 ± 0.20 ($n = 5$) in WT animals, also not significantly different from the value of 0.52 ± 0.08 ($n = 6$) in KO mice.

Since it has been previously shown (Reisert *et al.* 2003) that, in addition to rundown, Ca^{2+}-activated Cl^- currents in olfactory sensory neurons also exhibit a reversible time-dependent decrease in amplitude during the exposure to a constant Ca^{2+} concentration (Fig. 6*A* and *B*), we measured the ratio between current amplitudes measured at the peak and after 5 s of 100 μM Ca^{2+} exposure. We found that the ratio was 0.80 ± 0.10 ($n = 6$) in WT mice, not significantly different from the value of 0.78 ± 0.13 in KO animals ($n = 12$).

Finally, to measure the Ca^{2+} sensitivity of the Cl^- channel in WT and KO mice, we obtained dose–response relations by activating currents with various Ca^{2+} concentrations in excised membrane patches (Fig. 6*G*). Experiments were performed after the rapid phase of rundown, when currents reached an almost steady-state value and, to take into account a remaining slow phase of the rundown that was present in some membrane patches, currents at each test Ca^{2+} concentration were normalized to the average current activated by 100 μM Ca^{2+} before and after each test Ca^{2+} concentration. Normalized currents measured at −50 mV were plotted *versus* Ca^{2+} concentration and fitted by the Hill equation: $I/I_{max} = c^{n_H}/(c^{n_H} + K_{1/2}^{n_H})$, where c is the Ca^{2+} concentration, $K_{1/2}$ the Ca^{2+} concentration producing half-maximal current activation, and n_H is the Hill coefficient. At −50 mV, the $K_{1/2}$ was 4.4 μM for WT, similar to 3.8 μM for KO mice, and n_H was 2.2 and 2.9 for WT and KO animals, respectively (Fig. 6*G*). $K_{1/2}$ and n_H values were not significantly different between WT and KO mice.

Thus, electrophysiological properties of Ca^{2+}-activated Cl^- currents in inside-out membrane patches from dendritic knob/cilia of olfactory sensory neurons are not significantly different between WT and KO mice.

Discussion

Expression of Best2 in the ciliary layer of the olfactory epithelium

In this study, we confirmed that Best2 is expressed in the ciliary layer of olfactory sensory neurons and that the antibody against Best2 we previously developed (Pifferi *et al.* 2006*b*) is specific for this protein, as demonstrated by the absence of immunostaining in the olfactory epithelium of KO mice. Thus, these data, together with those of a very recently published study (Klimmeck *et al.* 2009) in which the expression of Best2 in the olfactory epithelium was extensively investigated, solve the reported controversy (Hartzell *et al.* 2008; Marmorstein *et al.* 2009) as to whether mouseBest2 is indeed expressed in the olfactory epithelium. In fact, Bakall *et al.* (2008), by employing immunoistochemistry in the same mouse lines of the present study, found expression of the Best2 protein in the colon and in the eye (in the non-pigmented epithelia cells of the ciliary body) of WT mice, but not in the olfactory epithelium, although they detected a *Best2* transcript. A possible explanation of the different results between the laboratories is likely to reside in the different antibodies that were used. Indeed, Bakall *et al.* (2008) reported that their antibody was not working in Western blot. On the other side, concerning the immunohistochemistry, it must be noted that no positive controls of the immunostaining

in the olfactory epithelium were shown by Bakall *et al.* (2008) and therefore it cannot be excluded that, since cilia are very fragile, they were absent from the olfactory epithelium slices.

Physiological role of Best2

Since Best2 is expressed in the cilia of olfactory sensory neurons (Pifferi *et al.* 2006*b*), the site of olfactory transduction, and it has been previously demonstrated that Best2 forms Ca^{2+}-activated Cl^- channels when expressed in heterologous systems (Qu *et al.* 2004; Qu & Hartzell, 2004; Pifferi *et al.* 2006*b*), we conducted experiments to investigate the physiological role of Best2 in olfactory transduction by comparing the properties of WT mice with those of KO mice. Since a previous study has shown that KO mice showed no obvious olfactory deficits, as detected by the cookie test (Bakall *et al.* 2008), we also repeated this type of behavioural test and found results in agreement with those previously published. However, it cannot be concluded from these experiments that Best2 is not required for normal olfactory sensitivity, as more detailed behavioural studies, as for example the study of olfactory behavioural thresholds as reported in mice lacking NKCC1 (Smith *et al.* 2008), would be required to reach such a conclusion. In addition, it is important to note that, as previously pointed out by Smith *et al.* (2008), it is still unknown whether a deficit in Ca^{2+}-activated Cl^- current would produce a reduction in olfactory sensitivity, and it is possible that the secondary Cl^- current may not be required at all for normal olfactory sensitivity. Indeed, it is possible that the primary current through CNG channels is sufficient for normal olfactory sensitivity.

We analysed the responses to odorants of the olfactory epithelium and found no differences in the odorant sensitivity or kinetics properties measured by EOG recordings in WT and KO mice. Moreover, at the level of single olfactory sensory neurons, a Ca^{2+}-activated Cl^- channel component was also measured by using photolysis of caged 8-Br-cAMP or of caged Ca^{2+} localized to the cilia of olfactory sensory neurons of KO mice. Finally, a Ca^{2+}-activated Cl^- current was still present in excised inside-out patches from knob/cilia of olfactory sensory neurons of KO mice, with electrophysiological properties similar to those of WT mice.

Thus, we determined that the absence of expression of Best2 in the ciliary layer of the olfactory epithelium does not significantly alter the electrophysiological properties of the olfactory epithelium. These results indicate that Best2 may not be the main molecular component of the olfactory Ca^{2+}-activated Cl^- channel, although we cannot exclude the possibility that in KO mice some compensatory mechanisms may act to replace the function of the missing protein. However, it must also be noted here that, although the protein Best2 has been proposed as a candidate for being a molecular component of the olfactory Ca^{2+}-activated Cl^- channel, very recent studies reported that the anoctamin/TMEM16 family of membrane proteins display many features of native Ca^{2+}-activated Cl^- channels (Caputo *et al.* 2008; Schroeder *et al.* 2008; Yang *et al.* 2008). In addition, it has been shown, by *in situ* hybridization, that TMEM16B is expressed in the mature sensory neurons of the mouse olfactory epithelium (Yu *et al.* 2005), and it is a prominent protein in the rat olfactory ciliary proteome (transmembrane protein 16B isoform 2, Supplementary Table S1 in Mayer *et al.* 2009). Stephan *et al.* (2009) also identified TMEM16B (Anoctamin 2, ANO2) in a proteomic screen of ciliary membranes and showed that the fusion protein TMEM16B-EGFP localized to the cilia when expressed *in vivo* using an adenoviral vector. In addition, Stephan *et al.* (2009) provided evidence that the electrophysiological properties of this protein are remarkably similar to those of native olfactory Ca^{2+}-activated Cl^- channels.

We have also recently characterized the electrophysiological properties of the mouse TMEM16B expressed in a heterologous system and found that the channel properties are remarkably similar to those of the native Ca^{2+}-activated Cl^- channels (Pifferi *et al.* 2009). Indeed, while we have previously pointed out that a significant difference between Best2 and the native olfactory channel was a Ca^{2+} sensitivity difference of one order of magnitude, with a Ca^{2+} concentration for half-maximal activation at -50 mV of 0.4 μM for Best2 and a higher concentration of 4.7 μM for native channels (Pifferi *et al.* 2006*b*), we recently showed that the $K_{1/2}$ for Ca^{2+} in TMEM16B-induced currents was 4.9 μM, similar to the native channel. Further studies will have to establish whether TMEM16B is a component of the olfactory Ca^{2+}-activated Cl^- channel.

In this study, we have shown that Best2 is expressed in the olfactory ciliary layer, but it does not appear to be the main molecular component of the Ca^{2+}-activated Cl^- current. What is then the physiological role of Best2 in the olfactory epithelium? In addition to functioning as Ca^{2+}-activated Cl^- channels when expressed heterologously, mouse Best2 and other bestrophins have also been shown to be activated by osmotic cell swelling in the absence of Ca^{2+}, indicating that they may be cell volume regulators (Fischmeister & Hartzell, 2005; Chien & Hartzell, 2007). Furthermore, Best1 can interact with the voltage-gated Ca^{2+} channel Cav1.3 and modulate its biophysical properties (Rosenthal *et al.* 2006; Yu *et al.* 2008), indicating that some bestrophins could also act as regulators of other ion channels. In the eye, Best2 is expressed in the non-pigmented epithelium and, using the same mouse line employed in the present study, it was found that KO mice have a diminished

intraocular pressure compared to WT mice (Bakall *et al.* 2008). A very recent study suggested that Best2 is involved in the control of aqueous dynamics (Zhang *et al.* 2009).

In the olfactory epithelium, Klimmeck *et al.* (2009) have recently investigated in detail the expression pattern of Best2 comparing results from adult and postnatal day 1 (P1) mice. In adult mice, whose olfactory epithelium contains mainly mature olfactory sensory neurons, Best2 expression was found in the cilia of these neurons. In P1 mice, where most olfactory sensory neurons are still immature, strong Best2 signals were detected at all subcellular levels of the developing neurons. Based on these observations, Klimmeck *et al.* (2009) suggested a physiological role for Best2 related to neurogenesis, in which Best2 may act as a volume-regulated anion channel contributing to the coordinated extension of cell volume in developing sensory neurons.

In the olfactory cilia, it is possible to speculate that Best2 may subserve different functions as, for example, the maintenance of the local ionic homeostasis, also preventing volume changes resulting from the exposure to exogenous osmotically active solutions. It is also possible to envisage that Best2 could contribute to setting the correct chloride concentration in the mucous layer of the olfactory epithelium.

In summary, we now have unequivocal confirmation that Best2 is expressed in the cilia of mature olfactory sensory neurons, thus cutting out all the controversies about its presence in the olfactory epithelium. Nevertheless, the function of Best2 remains elusive and further studies will be required to determine its physiological role.

References

Bakall B, McLaughlin P, Stanton JB, Zhang Y, Hartzell HC, Marmorstein LY & Marmorstein AD (2008). Bestrophin-2 is involved in the generation of intraocular pressure. *Invest Ophthalmol Vis Sci* **49**, 1563–1570.

Boccaccio A, Lagostena L, Hagen V & Menini A (2006). Fast adaptation in mouse olfactory sensory neurons does not require the activity of phosphodiesterase. *J Gen Physiol* **128**, 171–184.

Boccaccio A & Menini A (2007). Temporal development of cyclic nucleotide-gated and Ca^{2+}-activated Cl^{--} currents in isolated mouse olfactory sensory neurons. *J Neurophysiol* **98**, 153–160.

Caputo A, Caci E, Ferrera L, Pedemonte N, Barsanti C, Sondo E, Pfeffer U, Ravazzolo R, Zegarra-Moran O & Galietta LJ (2008). TMEM16A, a membrane protein associated with calcium-dependent chloride channel activity. *Science* **322**, 590–594.

Chien LT & Hartzell HC (2007). *Drosophila* bestrophin-1 chloride current is dually regulated by calcium and cell volume. *J Gen Physiol* **130**, 513–524.

Firestein S (2001). How the olfactory system makes sense of scents. *Nature* **413**, 211–218.

Fischmeister R & Hartzell HC (2005). Volume sensitivity of the bestrophin family of chloride channels. *J Physiol* **562**, 477–491.

Franceschini V, Bettini S, Pifferi S, Rosellini A, Menini A, Saccardi R, Ognio E, Jeffery R, Poulsom R & Revoltella RP (2009). Human cord blood CD133+ stem cells transplanted to nod-scid mice provide conditions for regeneration of olfactory neuroepithelium after permanent damage induced by dichlobenil. *Stem Cells* **27**, 825–835.

Frings, S (2009). Chloride-based signal amplification in olfactory sensory neurons. In *Physiology and Pathology of Chloride Transporters and Channels in the Nervous System. From Molecules to Diseases*, ed. Alvarez-Leefmans FJ & Delpire E. Elsevier–Academic Press, San Diego.

Frings S, Reuter D & Kleene SJ (2000). Neuronal Ca^{2+}-activated Cl^{--} channels: homing in on an elusive channel species. *Prog Neurobiol* **60**, 247–289.

Hartzell C, Putzier I & Arreola J (2005). Calcium-activated chloride channels. *Annu Rev Physiol* **67**, 719–758.

Hartzell HC, Qu Z, Yu K, Xiao Q & Chien LT (2008). Molecular physiology of bestrophins: multifunctional membrane proteins linked to best disease and other retinopathies. *Physiol Rev* **88**, 639–672.

Hartzell HC, Yu K, Xiao Q, Chien LT & Qu Z (2009). Anoctamin/TMEM16 family members are Ca^{2+}-activated Cl^- channels. *J Physiol* **587**, 2127–2139.

Kaneko H, Nakamura T & Lindemann B (2001). Noninvasive measurement of chloride concentration in rat olfactory receptor cells with use of a fluorescent dye. *Am J Physiol Cell Physiol* **280**, C1387–C1393.

Kaneko H, Putzier I, Frings S, Kaupp UB & Gensch T (2004). Chloride accumulation in mammalian olfactory sensory neurons. *J Neurosci* **24**, 7931–7938.

Kaupp UB & Seifert R (2002). Cyclic nucleotide-gated ion channels. *Physiol Rev* **82**, 769–824.

Kleene SJ (1993). Origin of the chloride current in olfactory transduction. *Neuron* **11**, 123–132.

Kleene SJ (1997). High-gain, low-noise amplification in olfactory transduction. *Biophys J* **73**, 1110–1117.

Kleene SJ (2008). The electrochemical basis of odor transduction in vertebrate olfactory cilia. *Chem Senses* **33**, 839–859.

Kleene SJ & Gesteland RC (1991). Calcium-activated chloride conductance in frog olfactory cilia. *J Neurosci* **11**, 3624–3629.

Klimmeck D, Daiber PC, Brühl A, Baumann A, Frings S & Möhrlen F (2009). Bestrophin 2: an anion channel associated with neurogenesis in chemosensory systems. *J Comp Neurol* **515**, 585–599.

Kunzelmann K, Milenkovic VM, Spitzner M, Soria RB & Schreiber R (2007). Calcium-dependent chloride conductance in epithelia: is there a contribution by bestrophin? *Pflugers Arch* **454**, 879–889.

Kurahashi T & Yau KW (1993). Co-existence of cationic and chloride components in odorant-induced current of vertebrate olfactory receptor cells. *Nature* **363**, 71–74.

Lagostena L & Menini A (2003). Whole-cell recordings and photolysis of caged compounds in olfactory sensory neurons isolated from the mouse. *Chem Senses* **28**, 705–716.

Lowe G & Gold GH (1993). Nonlinear amplification by calcium-dependent chloride channels in olfactory receptor cells. *Nature* **366**, 283–286.

Malnic B (2007). Searching for the ligands of odorant receptors. *Mol Neurobiol* **35**, 175–181.

Marmorstein AD, Cross HE & Peachey NS (2009). Functional roles of bestrophins in ocular epithelia. *Prog Retin Eye Res* **28**, 206–226.

Matthews HR & Reisert J (2003). Calcium, the two-faced messenger of olfactory transduction and adaptation. *Curr Opin Neurobiol* **13**, 469–475.

Mayer U, Kuller A, Daiber PC, Neudorf I, Warnken U, Schnolzer M, Frings S & Mohrlen F (2009). The proteome of rat olfactory sensory cilia. *Proteomics* **9**, 322–334.

Menini A (1999). Calcium signalling and regulation in olfactory neurons. *Curr Opin Neurobiol* **9**, 419–426.

Menini A, Lagostena L & Boccaccio A (2004). Olfaction: from odorant molecules to the olfactory cortex. *News Physiol Sci* **19**, 101–104.

Meyer MR, Angele A, Kremmer E, Kaupp UB & Muller F (2000). A cGMP-signaling pathway in a subset of olfactory sensory neurons. *Proc Natl Acad Sci U S A* **97**, 10595–10600.

Ottoson D (1955). Analysis of the electrical activity of the olfactory epithelium. *Acta Physiol Scand Suppl* **35**, 1–83.

Patton C, Thompson S & Epel D (2004). Some precautions in using chelators to buffer metals in biological solutions. *Cell Calcium* **35**, 427–431.

Pifferi S, Boccaccio A & Menini A (2006*a*). Cyclic nucleotide-gated ion channels in sensory transduction. *FEBS Lett* **580**, 2853–2859.

Pifferi S, Dibattista M & Menini A (2009). TMEM16B induces chloride currents activated by calcium in mammalian cells. *Pflugers Arch* (in press; doi: 10.1007/s00424-009-0684-9).

Pifferi S, Pascarella G, Boccaccio A, Mazzatenta A, Gustincich S, Menini A & Zucchelli S (2006*b*). Bestrophin-2 is a candidate calcium-activated chloride channel involved in olfactory transduction. *Proc Natl Acad Sci U S A* **103**, 12929–12934.

Pusch M (2004). Ca^{2+}-activated chloride channels go molecular. *J Gen Physiol* **123**, 323–325.

Qu Z, Fischmeister R & Hartzell C (2004). Mouse bestrophin-2 is a bona fide Cl^- channel: identification of a residue important in anion binding and conduction. *J Gen Physiol* **123**, 327–340.

Qu Z & Hartzell C (2004). Determinants of anion permeation in the second transmembrane domain of the mouse bestrophin-2 chloride channel. *J Gen Physiol* **124**, 371–382.

Qu Z, Wei RW, Mann W & Hartzell HC (2003). Two bestrophins cloned from *Xenopus laevis* oocytes express Ca^{2+}-activated Cl^- currents. *J Biol Chem* **278**, 49563–49572.

Reisert J, Bauer PJ, Yau KW & Frings S (2003). The Ca-activated Cl channel and its control in rat olfactory receptor neurons. *J Gen Physiol* **122**, 349–363.

Reuter D, Zierold K, Schroder WH & Frings S (1998). A depolarizing chloride current contributes to chemoelectrical transduction in olfactory sensory neurons in situ. *J Neurosci* **18**, 6623–6630.

Rodriguez I (2007). Odorant and pheromone receptor gene regulation in vertebrates. *Curr Opin Genet Dev* **17**, 465–470.

Rosenthal R, Bakall B, Kinnick T, Peachey N, Wimmers S, Wadelius C, Marmorstein A & Strauss O (2006). Expression of bestrophin-1, the product of the VMD2 gene, modulates voltage-dependent Ca^{2+} channels in retinal pigment epithelial cells. *FASEB J* **20**, 178–180.

Schild D & Restrepo D (1998). Transduction mechanisms in vertebrate olfactory receptor cells. *Physiol Rev* **78**, 429–466.

Schroeder BC, Cheng T, Jan YN & Jan LY (2008). Expression cloning of TMEM16A as a calcium-activated chloride channel subunit. *Cell* **134**, 1019–1029.

Scott JW & Scott-Johnson PE (2002). The electroolfactogram: a review of its history and uses. *Microsc Res Tech* **58**, 152–160.

Smith DW, Thach S, Marshall EL, Mendoza MG & Kleene SJ (2008). Mice lacking NKCC1 have normal olfactory sensitivity. *Physiol Behav* **93**, 44–49.

Stephan AB, Shum EY, Hirsh S, Cygnar KD, Reisert J & Zhao H (2009). ANO2 is the cilial calcium-activated chloride channel that may mediate olfactory amplification. *Proc Natl Acad Sci U S A* (in press; doi: 10.1073/pnas.0903304106).

Sun H, Tsunenari T, Yau KW & Nathans J (2002). The vitelliform macular dystrophy protein defines a new family of chloride channels. *Proc Natl Acad Sci U S A* **99**, 4008–4013.

Tsunenari T, Sun H, Williams J, Cahill H, Smallwood P, Yau KW & Nathans J (2003). Structure-function analysis of the bestrophin family of anion channels. *J Biol Chem* **278**, 41114–41125.

Yang YD, Cho H, Koo JY, Tak MH, Cho Y, Shim WS, Park SP, Lee J, Lee B, Kim BM, Raouf R, Shin YK & Oh U (2008). TMEM16A confers receptor-activated calcium-dependent chloride conductance. *Nature* **455**, 1210–1215.

Yu K, Xiao Q, Cui G, Lee A & Hartzell HC (2008). The best disease-linked Cl^- channel hBest1 regulates Ca_V1 (L-type) Ca^{2+} channels via src-homology-binding domains. *J Neurosci* **28**, 5660–5670.

Yu TT, McIntyre JC, Bose SC, Hardin D, Owen MC & McClintock TS (2005). Differentially expressed transcripts from phenotypically identified olfactory sensory neurons. *J Comp Neurol* **483**, 251–262.

Zhang Y, Davidson BR, Stamer WD, Barton JK, Marmorstein LY & Marmorstein AD (2009). Enhanced inflow and outflow rates despite lower IOP in bestrophin-2-deficient mice. *Invest Ophthalmol Vis Sci* **50**, 765–770.

Author contributions

S.P., M.D., A.B., A.AQ., R.T. and A.M. contributed to conception and design of the experiments, drafting and revision of the manuscript. M.D. did the immunohistochemistry. F.G. and R.T. did the behavioural test. A.AQ performed RT-PCR and WB analysis. S.P., C.S. and A.B. did the electrophysiology experiments.

S.P., C.S., A.B. and A.M. analyzed the data. S.P., M.D., R.T., A.B. and A.M. wrote the manuscript. All authors approved the final version to be published.

Acknowledegments

We thank C. Degrassi and M. Stebel for animal care; J. Franzot for genotyping mice; L. Masten for technical help; F. Müller and U. B. Kaupp (Forschungszentrum Jülich, Jülich, Germany) for the gift of the CNGA2 monoclonal antibody; V. Hagen (Leibniz-Institut für Molekulare Pharmakologie, Berlin, Germany) for kindly providing caged cyclic nucleotides. This study was supported by grants from the Italian Ministry of Research (MIUR) and from the Italian Institute of Technology.

Authors' present addresses

S. Pifferi: Max Delbrück Center for Molecular Medicine (MDC), Berlin-Buch, Germany.
A. Boccaccio: Italian Institute of Technology, Department of Neuroscience and Brain Technologies, Genova, Italy.

3.2 Calcium concentration jumps reveal dynamic ion selectivity of calcium-activated chloride currents in mouse olfactory sensory neurons and TMEM16b-transfected HEK 293T cells.

Sagheddu C, Boccaccio A, Dibattista M, Montani G, Tirindelli R, Menini A (2010). J Physiol. 588, 4189–4204

J Physiol 588.21 (2010) pp 4189–4204

The Journal of Physiology

Calcium concentration jumps reveal dynamic ion selectivity of calcium-activated chloride currents in mouse olfactory sensory neurons and TMEM16b-transfected HEK 293T cells

Claudia Sagheddu[1], Anna Boccaccio[1,2], Michele Dibattista[1], Giorgia Montani[3], Roberto Tirindelli[3] and Anna Menini[1]

[1] *International School for Advanced Studies, Scuola Internazionale Superiore di Studi Avanzati, SISSA, and Italian Institute of Technology, SISSA Unit, Trieste, Italy*

[2] *Institute of Biophysics, Consiglio Nazionale delle Ricerche, Genova, Italy*

[3] *Section of Physiology, Department of Neuroscience, University of Parma, Parma, Italy*

Ca^{2+}-activated Cl^- channels play relevant roles in several physiological processes, including olfactory transduction, but their molecular identity is still unclear. Recent evidence suggests that members of the transmembrane 16 (TMEM16, also named anoctamin) family form Ca^{2+}-activated Cl^- channels in several cell types. In vertebrate olfactory transduction, TMEM16b/anoctamin2 has been proposed as the major molecular component of Ca^{2+}-activated Cl^- channels. However, a comparison of the functional properties in the whole-cell configuration between the native and the candidate channel has not yet been performed. In this study, we have used the whole-cell voltage-clamp technique to measure functional properties of the native channel in mouse isolated olfactory sensory neurons and compare them with those of mouse TMEM16b/anoctamin2 expressed in HEK 293T cells. We directly activated channels by rapid and reproducible intracellular Ca^{2+} concentration jumps obtained from photorelease of caged Ca^{2+} and determined extracellular blocking properties and anion selectivity of the channels. We found that the Cl^- channel blockers niflumic acid, 5-nitro-2-(3-phenylpropylamino)benzoic acid (NPPB) and DIDS applied at the extracellular side of the membrane caused a similar inhibition of the two currents. Anion selectivity measured exchanging external ions and revealed that, in both types of currents, the reversal potential for some anions was time dependent. Furthermore, we confirmed by immunohistochemistry that TMEM16b/anoctamin2 largely co-localized with adenylyl cyclase III at the surface of the olfactory epithelium. Therefore, we conclude that the measured electrophysiological properties in the whole-cell configuration are largely similar, and further indicate that TMEM16b/anoctamin2 is likely to be a major subunit of the native olfactory Ca^{2+}-activated Cl^- current.

(Received 17 June 2010; accepted after revision 8 September 2010; first published online 13 September 2010)

Corresponding author A. Menini: International School for Advanced Studies, Scuola Internazionale Superiore di Studi Avanzati, SISSA, Via Bonomea 265, 34136 Trieste, Italy. Email: menini@sissa.it

Abbreviations DIDS, 4,4′-diisothiocyanatostilbene-2,2′-disulfonic acid; HEK, human embryonic kidney; MeS^-, methanesulfonate; NFA, niflumic acid; NPPB, 5-nitro-2-(3-phenylpropylamino)benzoic acid; SCN^-, isothiocyanate; TMEM16, transmembrane 16.

Introduction

In several cell types, an increase in intracellular Ca^{2+} concentration produces the activation of chloride channels that, depending on the electrochemical gradient of Cl^-, will cause depolarization or hyperpolarization of the cell membrane. Ca^{2+}-activated Cl^- channels were first identified in *Xenopus* oocytes (Miledi, 1982; Barish, 1983) and in the inner segment of salamander photoreceptors (Bader *et al.* 1982), and afterwards in many other cell types, including olfactory sensory neurons (Kleene & Gesteland, 1991; Kleene, 1993; Kurahashi

DOI: 10.1113/jphysiol.2010.194407

& Yau, 1993). These channels are involved in a large variety of physiological processes, including generation of the fertilization potential in *Xenopus* oocytes, regulation of synaptic transmission in photoreceptors, and signal amplification in olfactory sensory neurons (reviewed by Frings *et al.* 2000; Hartzell *et al.* 2005; Kleene, 2008; Frings, 2009*a*,*b*).

Despite the physiological relevance of Ca^{2+}-activated Cl^- channels, their molecular identity remained largely elusive. Several molecular candidates have been proposed for these channels, but none of them completely reproduced the properties of native Ca^{2+}-activated Cl^- currents (reviewed by Hartzell *et al.* 2005; Duran *et al.* 2010). In 2008, three independent studies reported evidence suggesting that some members of the family of TMEM16/anoctamins are likely to be the molecular determinants of Ca^{2+}-activated Cl^- currents in some cell types (Caputo *et al.* 2008; Schroeder *et al.* 2008; Yang *et al.* 2008; reviewed by Flores *et al.* 2009; Galietta, 2009; Hartzell *et al.* 2009; Kunzelmann *et al.* 2009).

In olfactory sensory neurons, Ca^{2+}-activated Cl^- currents are measured, together with cAMP-activated currents, in the cilia (Kleene & Gesteland, 1991; Kleene, 1993), where they play an important role in the amplification of the response to odorants, constituting up to 90% of the transduction current (Kurahashi & Yau, 1993; Lowe & Gold, 1993; Boccaccio & Menini, 2007). Indeed, the process of olfactory transduction occurs in the cilia of olfactory sensory neurons, where a second messenger cascade is activated by the binding of odorant molecules to odorant receptors and leads to the production of cAMP and the opening of cAMP-activated channels (reviewed by Schild & Restrepo, 1998; Lowe & Gold, 1993; Menini, 1999; Matthews & Reisert, 2003; Menini *et al.* 2004; Pifferi *et al.* 2006*a*, 2009*c*; Kleene, 2008; Tirindelli *et al.* 2009). Since olfactory sensory neurons maintain an unusually elevated intracellular concentration of Cl^- (Reuter *et al.* 1998; Kaneko *et al.* 2001, 2004), the influx of Ca^{2+} through cAMP-activated channels in the cilia produces an efflux of Cl^- through Ca^{2+}-activated Cl^- channels, contributing to the odorant-induced depolarization (Kleene & Gesteland, 1991; Kleene, 1993, 1997, 2008; Kurahashi & Yau, 1993; Lowe & Gold, 1993; Boccaccio & Menini, 2007; reviewed by Frings *et al.* 2000; Frings, 2009*a*,*b*; Pifferi *et al.* 2009*c*).

At present, several lines of evidence indicate that TMEM16b/anoctamin2 is the best candidate for being the main molecular component of the olfactory Ca^{2+}-activated Cl^- channels in the cilia. Indeed, *in situ* hybridization studies showed that TMEM16b/anoctamin2 is expressed in mature sensory neurons of the mouse olfactory epithelium (Yu *et al.* 2005); proteomic screenings identified TMEM16b/anoctamin2 as a prominent protein of olfactory ciliary membranes (Stephan *et al.* 2009; Hengl *et al.* 2010; Rasche *et al.* 2010); the fusion protein TMEM16b/anoctamin2–EGFP localized to the cilia when expressed *in vivo* using an adenoviral vector (Stephan *et al.* 2009); immunohistochemistry showed the localization of TMEM16b/anoctamin2 to the ciliary region (Hengl *et al.* 2010; Rasche *et al.* 2010); functional properties measured by patch-clamp recordings from excised inside-out membrane patches of TMEM16b/anoctamin2 expressed in HEK 293T cells or from the dendritic knobs and ciliary region of olfactory sensory neurons are very similar (Pifferi *et al.* 2009*a*; Stephan *et al.* 2009).

However, to identify the channel protein it is necessary to prove that all the functional properties of native channels are reproduced by the candidate protein. At present, several electrophysiological properties of native olfactory Ca^{2+}-activated Cl^- currents are still unknown. Indeed, while the properties of native olfactory channels in the excised cilium (Kleene & Gesteland, 1991; Kleene, 1993) or in the excised inside-out membrane patches have been extensively investigated (Reisert *et al.* 2003; Pifferi *et al.* 2006*b*, 2009*b*; Stephan *et al.* 2009), those of the native channels in isolated olfactory sensory neurons are poorly known. Moreover, currents in excised patches exhibited a pronounced rundown as well as inactivation/desensitization in the presence of a constant Ca^{2+} concentration (Reisert *et al.* 2003), while whole-cell recordings appeared to be more stable (Boccaccio & Menini, 2007; Takeuchi *et al.* 2009).

Niflumic acid or 4-acetamido-4-isothiocyanato-stilben-2, 2-disulfonate (SITS; Kurahashi & Yau, 1993; Lowe and Gold, 1993) are commonly used as extracellular blockers of Ca^{2+}-activated Cl^- channels in intact olfactory sensory neurons, but the extracellular blocking potencies of several other compounds have not been measured. Moreover, the ion selectivity of the native channels in isolated olfactory sensory neurons has not been estimated yet, except for showing that the current is carried by Cl^- ions (Kurahashi & Yau, 1993; Takeuchi *et al.* 2009).

The goal of this study was to measure the unknown electrophysiological properties of the native olfactory Ca^{2+}-activated Cl^- channels and to obtain a side-by-side comparison with the recently cloned TMEM16b/anoctamin2 (Stephan *et al.* 2009) heterologously expressed in HEK 293T cells. Channels were directly activated by rapidly increasing the intracellular Ca^{2+} concentration by flash photolysis of caged Ca^{2+}.

Our results show that Ca^{2+}-activated Cl^- currents measured in the whole-cell configuration in olfactory sensory neurons were largely similar to those induced by the candidate protein, contributing further support to the hypothesis that TMEM16b/anoctamin2 is a major constituent of the olfactory Ca^{2+}-activated Cl^- channel.

Methods

Ethical approval

All animals were handled in accordance with the Italian Guidelines for the Use of Laboratory Animals (Decreto Legislativo 27/01/1992, no. 116) and European Union guidelines on animal research (No. 86/609/EEC). For experiments mice were killed by cervical dislocation or anaesthetized with CO_2 inhalation and then decapitated.

RNA extraction and RT-PCR

RNA was extracted from the olfactory epithelium of FVB mice and purified using Trizol reagent (Invitrogen Milano, Italy). About 2 μg of total RNA served as template for oligo-dT primed first strand cDNA synthesis with Im-Prom-II Reverse Transcriptase (Promega, Milano, Italy). PCR was performed in Mastercycler Personal (Eppendorf, Milano, Italy) using AmpliBiotherm DNA polymerase, 3 mM $MgCl_2$, 0.2 mM for each dNTPs and 200 pmol forward/reverse target-specific oligonucleotide primers. Cycling parameters consisted of an initial denaturation step (95°C, 2 min) followed by 35 cycles each of these included a denaturation (95°C, 30 s), a primer annealing (50°C, 30 s), and an extension (72°C, 30 s) step. Reaction was completed by a final extension step at 72°C for 5 min. Semiquantitative analysis of RNA expression was performed on agarose gel after electrophoresis using the NIS-Elements Advanced Research software (Nikon, Firenze, Italy).

Primers were designed to amplify a 650–700 bp DNA sequence, which is predicted to encode a region of the C-terminal intracellular domain of TMEM16/anoctamins. The chromosomic region corresponding to the amplicon DNA sequences spans over five exons and four introns.

The following primer sequences were used to amplify target DNAs:

TMEM16a/anoctamin1: bases 1826–2493, fwd: 5′-ACGTGTACATCTTCCGCTCTTT-3′ (Tm 58°C), rev: 5′ GATCTGAACCTCATAGCCCAG-3′ (Tm 59°C);
TMEM16b/anoctamin2: bases 1694–2358, fwd: 5′-ATGTCTACGTGTTCGACGGTTA-3′ (Tm 58°C) rev: 5′-AAACTGAACCTCCTGGTCGAA (Tm 57°C);
TMEM16c/anoctamin3: bases 2009–2652, fwd: 5′-ACAATAAACTTTTTGAGCGGTG-3′ (Tm 54°C) rev: 5′-GTAACCAGATTTTCCCATACC-3′ (Tm 55°C);
TMEM16d/anoctamin4: bases 1361–2052, fwd: 5′-ACTTGAGATTGATAAACAGGTG-3′ (Tm 54°C) rev: 5′-GTACTTCAGAGGGGTTCCTGA-3′ (Tm 59°C);
TMEM16e/anoctamin5: bases 1739–2382, fwd: 5′-ACACATATATGTTCAACATATGGA-3′ (Tm 54°C), rev: 5′-GGTGACGAAGTCTTTTTTCTC-3′) (Tm 55°C);
TMEM16f/anoctamin6: bases 1751–2418, fwd: 5′-CAGTGTACTTGCTGGGCAAATA-3′ (Tm 57°C), rev: 5′-CAAGGTATAGTTACCAAGCCC-3′(Tm 57°C);
TMEM16g/anoctamin7: bases 1685–2340, fwd: 5′-ACCACACCTTGTTTGGAATCC-3′ (Tm 57°C), rev: 5′-GTAAGTCGGAGAATAGTGTCC 3′ (Tm 57°C);
TMEM16h/anoctamin8: bases 1962–2665, fwd: 5′-CGAAGAAGACGATGAGCCTGA-3′ (Tm 71°C), rev: 5′-CCTGCCGCTCGTGCCGCTTGA-3′ (Tm 61°C);
TMEM16j/anoctamin9: bases 1331–2004, fwd: 5′-CCACGCGCCTGGCTGGCCTGTG-3′ (Tm 63°C), rev: 5′-CACGGTCACGTTTTCTTGGCC-3′ (Tm 54°C);
TMEM16k/anoctamin10: bases 1298–1894, fwd: 5′-TGGCCACACTCCTGATCACCTC-3′ (Tm 59°C), rev: 5′-AAGATTCGAATTCCAATCTGG-3′ (Tm 67°C);
OMP (olfactory marker protein): bases 1–1079, fwd: 5′-CCCTGCTGGCCAAAGCTGGAA-3′ (Tm 63°C), rev: 5′-GTCTCTAAAGCTGTAGGGAGA-3′ (Tm 58°C);
Vmn2r70, bases 1011–1704, fwd: 5′-TTACAGTAGTG-AATTTTCCTTTGC-3′ (Tm 55°C), rev: 5′-TTGGAGGCAGAGAGTATGGTGTTC (Tm 63°C).

All amplicons were separated by agarose gel electrophoresis, the corresponding bands were excised and the DNA extracted and purified (Qiagen gel extraction Kit, Milano, Italy) and subsequently subcloned in pGEMt-easy vector (Promega) for sequencing.

Immunohistochemistry

Immunostainings of olfactory epithelium were performed as previously described (Pifferi *et al.* 2009*b*). Primary antibodies were: mouse monoclonal anti-TMEM16b (1:1; provided by H. Stöhr, Universität Regensburg, Regensburg, Germany; Stöhr *et al.* 2009) and rabbit anti-adenylyl cyclase III (1:300, Santa Cruz Biotechnology, SantaCruz, CA, USA; cat. no. sc-558). Secondary antibodies were: Alexa 488-conjugated goat anti-mouse and Alexa 594-conjugated goat anti-rabbit diluted to 1:300 (Molecular Probes-Invitrogen, West Eugene, OR, USA).

Images were visualized by Leica TCS SP2 confocal microscope (Leica Microsystems, Milano, Italy) acquired using Leica software at 1024 × 1024 pixels resolution and analysed with ImageJ software. Images were not modified other than to balance brightness and contrast.

Dissociation of mouse olfactory sensory neurons

Olfactory sensory neurons were dissociated enzymatically from the olfactory epithelium of 1- to 3-month-old C57 Black mice with a method similar to that previously described (Lagostena & Menini, 2003; Boccaccio *et al.*

2006). The olfactory epithelium was removed and transferred in 1 ml of zero-divalent mammalian Ringer solution with 200 μM cystein and 2 U ml^{-1} papain (Sigma, Milano, Italy) for 8–10 min at room temperature. The olfactory epithelium was minced with fine forceps. The reaction was stopped by adding 0.5 ml of Ringer solution with 0.1 mg ml^{-1} bovine serum albumin (BSA), 0.3 mg ml^{-1} leupeptin and 0.02 mg ml^{-1} of DNaseI (all from Sigma). After centrifugation (300 *g* for 5 min) the cells were resuspended in 1 ml of Ringer solution and plated on glass coverslips (WPI, Sarasota, FL, USA), coated with poly-L-lysine and concanavalin-A Type V (Sigma). Before use, dissociated olfactory sensory neurons were allowed to settle for 60 min at +4°C.

Only olfactory sensory neurons with clearly visible cilia were used for the experiments.

Heterologous expression of TMEM16b/anoctamin2

The full-length, dominant olfactory isoform of the mouse TMEM16b/anoctamin2 cloned into the expression vector pAdtrack-CMV (Stratagene, LaJolla, CA, USA) with an independent expression cassette for EGFP (provided by Haiqing Zhao of the Johns Hopkins University in Baltimore (Stephan *et al.* 2009), was transfected into HEK 293T cells using FuGENE 6 reagent (Roche Applied Science, Mannheim, Germany) according to the manufacturer's protocol. Transfected cells were identified by EGFP fluorescence and used for electrophysiological recordings from 24 to 48 h after transfection.

Patch-clamp recordings

Olfactory sensory neurons or HEK 293T cells transfected with TMEM16b/anoctamin2 were observed with an inverted microscope (Olympus IX70, Milano, Italy) with an oil immersion ×100 objective (Zeiss, Milano, Italy).

Currents in the whole-cell voltage-clamp mode were recorded with an Axopatch 200B patch-clamp amplifier, controlled by Clampex 8 via a Digidata 1322A (Axon Instruments, Union City, CA, USA). Patch pipettes were made using borosilicate capillaries (WPI) and pulled with a Narishige PP83 puller (Narishige, Tokyo, Japan). Pipette resistances were 3–7 MΩ when filled with the standard intracellular solution. Currents were low-pass filtered at 1 kHz and acquired at 2 kHz for experiments with olfactory sensory neurons, or filtered at 5 kHz and sampled at 10 kHz for experiments with transfected HEK 293T cells. All experiments were carried out at room temperature (20–24°C).

Ionic solutions and perfusion system

The extracellular mammalian Ringer solution contained (in mM): 140 NaCl, 5 KCl, 1 $CaCl_2$, 1 $MgCl_2$, 10 Hepes, 10 glucose and 1 sodium pyruvate (pH 7.4). The pipette solution contained (in mM): 140 CsCl, 3 DMNP–EDTA, 1.5 $CaCl_2$ and 10 Hepes (pH 7.4). The caged Ca^{2+} compound DMNP–EDTA was purchased from Molecular Probes–Invitrogen, and $CaCl_2$ was adjusted with a 0.1 M standard solution from Fluka (Deisenhofen, Germany). Pipette solution aliquots were stored for a few days at −20°C and kept refrigerated in the dark during the experimental session. Caged Ca^{2+} was allowed to diffuse from the patch pipette into the cell cytoplasm for at least 2 min after establishment of the whole-cell configuration.

Niflumic acid (NFA) and 5-nitro-2-(3-phenylpropylamino)benzoic acid (NPPB, Tocris Bioscience, Bristol, UK) were prepared in dimethyl sulfoxide (DMSO) as stock solutions at 200 mM or 83 mM, respectively, and diluted to the final concentration of 400 μM and 100 μM, respectively, in the bathing solution (DMSO alone did not alter the currents); 4,4′-diisothiocyanatostilbene-2,2′-disulfonic acid (DIDS) was directly dissolved in the bathing solution to 1 mM.

Different bathing solutions were delivered by using a gravity-fed perfusion system. A slow flow rate was selected in such a way that the position of the cilia of the neurons was not perturbed. A complete solution change was obtained in about 10 s. To measure blocker effects, current recordings were obtained before blocker application (control), 1–2 min after delivery of the solution with the blocker, and 2–5 min after perfusion with Ringer solution without the blocker (washout).

For ionic selectivity experiments, Cl^- was substituted with other anions by replacing NaCl on an equimolar basis with NaX, where X is the substituted anion, or NaCl was replaced with equimolar choline chloride.

The bath was grounded through a 1 M KCl agar bridge connected to a Ag–AgCl reference electrode. Liquid junction potentials were calculated using Clampex's Junction Potential Calculator, based on the JPCalc program developed by Barry (1994; see also http://web.med.unsw.edu.au/phbsoft/LJP_Calculator.htm). Applied membrane potentials were corrected off-line. The liquid junction potential between the pipette and the Ringer solution was calculated. Then, if the bathing solution was changed after reaching the whole-cell configuration, we calculated the additional liquid junction potential generated between the bathing solution and the 1 M KCl agar bridge. We corrected membrane potentials for the following calculated liquid junction potentials (in mV) in the indicated bathing solutions: −4.6 in Ringer solution, −4.0 in isothiocyanate Ringer solution, −4.7 in bromide Ringer solution, −4.6 in iodide Ringer solution, −4.3 in nitrate Ringer solution, −3.0 in methanesulfonate Ringer

solution, −5.3 in Ringer solution with NaCl replaced with choline chloride.

Chemicals, unless otherwise stated, were purchased from Sigma.

Photolysis of caged Ca^{2+}

For flash photolysis of caged Ca^{2+}, we used a xenon flash-lamp JML-C2 system (Rapp OptoElectronic, Hamburg, Germany) coupled with the epifluorescence port of the microscope with a quartz light guide as previously described (Boccaccio *et al.* 2006; Boccaccio & Menini, 2007). The spot of light had a diameter of about 15 μm and was focused on the ciliary region of olfactory sensory neurons or to cover about 50% of the surface of HEK 293T cells. The flash duration was less than 1.5 ms and was kept constant during each experiment. At the beginning of each experiment, the stability of the response was checked by applying repetitive flashes at intervals of about 2 min. Neurons or cells that did not reach a stable response to two or three flashes were discarded.

Data analysis

Data analysis and figures were made with Igor software (Wavemetrics, Lake Oswego, OR, USA). A single exponential function was fitted to the rising phase for monophasic current responses. Current recordings at each holding potential were plotted by subtracting the value of the baseline.

Data are reported as mean ± S.E.M. and the total number of cells (n). Statistical significance was determined using unpaired t tests, or ANOVA, as appropriate. When a statistically significant difference was determined with ANOVA, a Tukey *post hoc* test was done to evaluate which data groups showed significant differences. P values < 0.05 were considered significant.

Results

Expression of TMEM16s/anoctamins in the olfactory epithelium

To analyse the expression of each TMEM16/anoctamin in the olfactory epithelium, we performed RT-PCR using intron-spanning primers for amplifying DNA encoding a fragment of the C-terminal intracellular domain of each family member (Fig. 1).

We found expression in the olfactory epithelium for TMEM16a/anoctamin1, b/2, f/6, j/9 and k/10 (Fig. 1*A*). To semiquantify the expression of the different TMEM16/anoctamin isotypes in the olfactory epithelium, we amplified the OMP sequence in the same reaction. Results indicated that TMEM16a/anoctamin1, b/2 and j/9 are abundantly expressed, and f/6 and k/10 are moderately expressed (Fig. 1*D*). To further investigate the expression of TMEM16c/anoctamin3, d/4, e/5, g/7 and h/8 (undetectable in Fig. 1*A* and *D*) we loaded them in a much larger amounts and found a positive expression of d/4 and g/7 (Fig. 1*B*). No expression could be detected for TMEM16c/anoctamin3, e/5 and h/8 (Fig. 1*A* and *B*) although they are abundantly expressed in the whole E16 embryo (Fig. 1*C*). To validate the PCR results, all amplicons were directly sequenced after purification from agarose gel.

To examine the localization of TMEM16b/anoctamin2 in the olfactory epithelium, we performed immunohistochemistry experiments on cryosections of the olfactory epithelium by using an anti-TMEM16b antibody (Stöhr *et al.* 2009). We found staining at the surface of

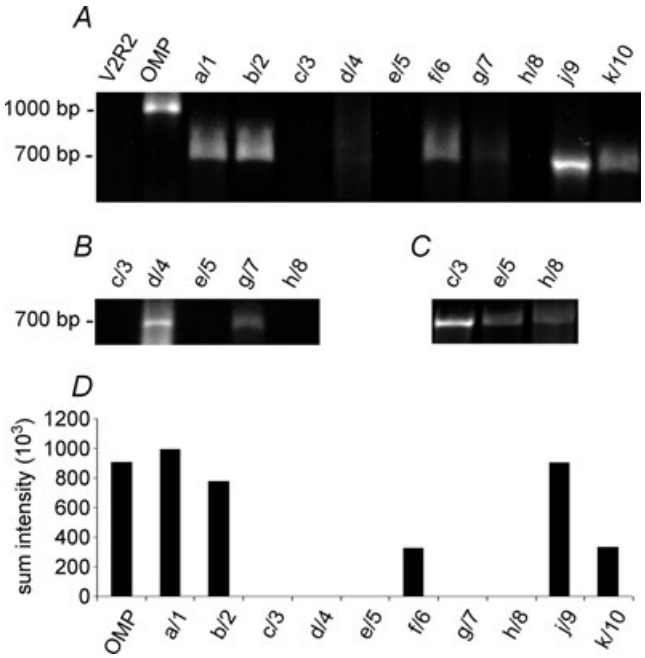

Figure 1. Expression of TMEM16s/anoctamins in the olfactory epithelium
A, olfactory transcripts of the TMEM16/anoctamin isoforms 1–10 were detected by RT-PCR (35 cycles) and sequencing. Specificity was confirmed by negative (olfactory epithelium cDNA amplified with primer for vomeronasal receptors, V2R2s) and positive (olfactory epithelium cDNA amplified with primers for OMP) controls. All lanes were loaded with the same amount of reaction product (5 μl) to obtain a semiquantitative evaluation of the TMEM16/anoctamin expression as represented in *D*. *B,* TMEM16c/anoctamin3, d/4, e/5, g/7 and h/8 (apparently undetectable in *A*) were loaded in a much larger amount and showed a lower but positive expression of d/4 and g/7. *C,* primer specificity for TMEM16c/anoctamin3, e/5 and h/8 (not detected in the olfactory epithelium) was confirmed by RT-PCR on cDNA from the whole embryo (E16). *D*, semiquantitative analysis of the TMEM16/anoctamin expression in the olfactory epithelium for the experiment shown in *A*.

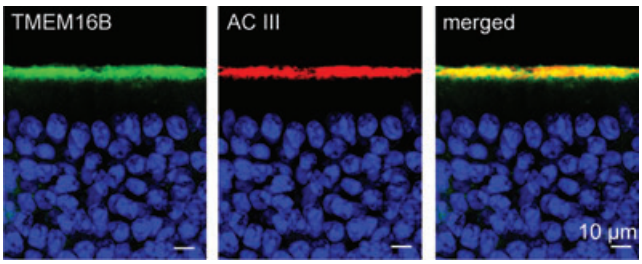

Figure 2. Localization of TMEM16b/anoctamin2 at the surface of the olfactory epithelium
Immunostaining of sections of the olfactory epithelium. Confocal micrographs showing TMEM16b and adenylyl cyclase III (AC3) expression at the surface of the olfactory epithelium. Cell nuclei were stained by DAPI. The image on the right was obtained from the merge of the left and centre images. Scale bar is 10 μm in all panels.

the olfactory epithelium, where TMEM16b/anoctamin2 largely co-localized with adenylyl cyclase III (Fig. 2), a protein that is mainly expressed in the cilia of olfactory sensory neurons (Menco *et al.* 1992, 1994; reviewed by Menco, 1997). However, we cannot exclude the presence of TMEM16b/anoctamin2 also in the microvilli of sustentacular cells at the surface of the olfactory epithelium. Therefore, our experiments are in agreement with previous results, obtained with different antibodies, showing that TMEM16b/anoctamin2 is expressed at the site of olfactory transduction (Hengl *et al.* 2010; Rasche *et al.* 2010).

Extracellular blockers of native Ca^{2+}-activated currents in olfactory sensory neurons

The most commonly used extracellular blocker of Ca^{2+}-activated Cl^- current in intact olfactory sensory neurons is NFA at concentrations ranging between 300 and 500 μM (Kleene, 1993; Boccaccio *et al.* 2006; Boccaccio & Menini, 2007; Takeuchi *et al.* 2009), while the extracellular blocking potencies of several other compounds are still unknown. We measured the effect of adding 400 μM NFA, 100 μM NPPB or 1 mM DIDS at the extracellular side of olfactory sensory neurons, while activating the current by producing a sudden Ca^{2+} concentration increase by photorelease of caged Ca^{2+} in the ciliary region at the holding potential of −50 mV.

Figure 3*A* illustrates the typical NFA blockage of the current activated by a Ca^{2+} concentration jump produced by an ultraviolet flash applied at the time indicated in the upper panels. The maximal current amplitude was reduced to about 17% of its value before blocker application, and the effect was reversed after perfusion with Ringer solution without NFA (87% recovery), in agreement with previous data (Kleene, 1993; Boccaccio *et al.* 2006; Boccaccio & Menini, 2007; Takeuchi *et al.* 2009). To better illustrate the variability of results among neurons, we normalized the responses for each neuron in the presence and after washout of the blocker to the value measured before blocker application (Fig. 3, right panels). On average, the amplitude in the presence of 400 μM NFA was 13% of the control value. After perfusion with Ringer solution without the blocker, the current recovered on average to 63% of its control value.

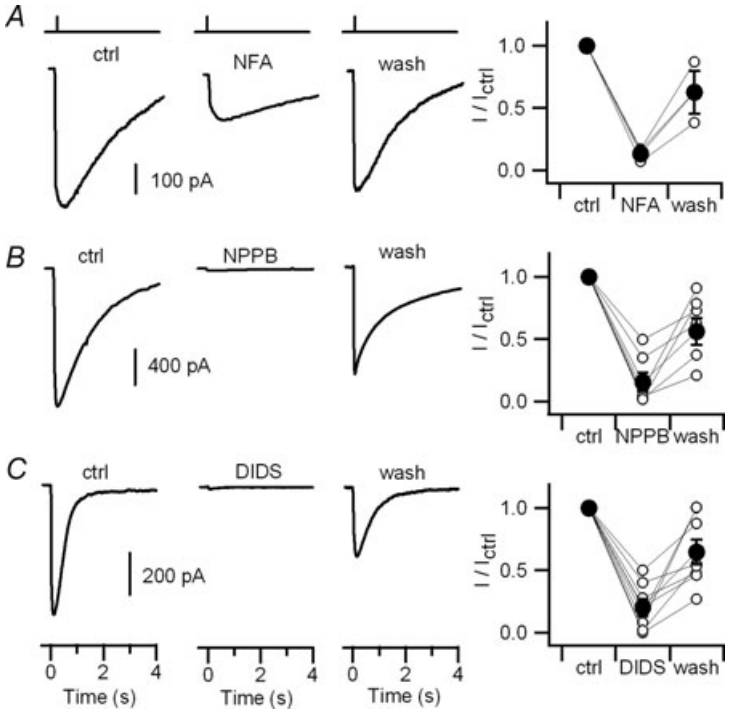

Figure 3. Olfactory sensory neurons: extracellular blockage of currents activated by photorelease of caged Ca^{2+} in the cilia
Currents recorded in the whole-cell voltage-clamp configuration in response to sudden jumps in Ca^{2+} concentration obtained with photorelease of caged Ca^{2+}. Ultraviolet light flashes were applied on the ciliary region at the times indicated by the vertical bars in the upper panels. The holding potential was −50 mV. The following blockers were used: *A*, 400 μM NFA; *B*, 100 μM NPPB; *C*, 1 mM DIDS. Current recordings were obtained before blocker application (control), 1–2 min after application of the indicated blockers, and 2–5 min after the removal of blockers (washout). Panels on the right show peak currents measured in the presence of each blocker and after washout, normalized to the control value before blocker application for each neuron (open circles). Average ratios are plotted as filled circles.

Figure 3*B* shows recordings from an olfactory sensory neuron in which the extracellular addition of 100 μM NPPB produced a strong block to 2% of its control value with an almost complete recovery after washout (79% recovery). In another neuron (Fig. 3*C*), 1 mM DIDS also blocked the Ca^{2+}-activated current (2% of its control value) while the recovery was only partial (53% of control value).

On average, the current amplitude in the presence of 100 μM NPPB or 1 mM DIDS was, respectively, 16% or 20% of the control value (Fig. 3*B* and *C*, panels on the right). After washout of NPPB or DIDS, the current recovered on average to about 60% of its control value for both blockers (56% for NPPB and 65% for DIDS).

These results show that 100 μM NPPB and 1 mM DIDS may also be used as efficient blockers of the Ca^{2+}-activated current in olfactory sensory neurons (see also Fig. 5).

Comparison of extracellular blockers of Ca^{2+}-activated currents in HEK 293T cells expressing TMEM16b/anoctamin2 and in olfactory sensory neurons

To compare the pharmacological profile of the native olfactory Ca^{2+}-activated current with that of the protein that is at present the best molecular candidate for being the olfactory channel, we used the same experimental conditions described in the previous section, uncaging caged Ca^{2+} in HEK 293T cells transfected with TMEM16b/anoctamin2.

As shown in Fig. 4*A*–*C*, each test compound partially blocked the Ca^{2+}-activated current. On average, the current amplitude in the presence of 400 μM NFA, 100 μM NPPB or 1 mM DIDS was, respectively, 10%, 42% or 26% of the control value. After washout of the blockers, the current recovered on average to 54% (NFA), 62% (NPPB) or 64% (DIDS) of its control value.

Since the current after washout from the blockers presented some variability, to better compare the blocking efficiencies for the native and the TMEM16b/anoctamin2-induced currents, we normalized the blocked current to the average between control and washout for each experiment (Fig. 5). Ca^{2+}-activated currents were reduced on average to the following percentages: 69% for NFA, 81% for NPPB, 76% for DIDS in olfactory sensory neurons, to be compared with 84% for NFA, 51% for NPPB and 70% for DIDS in HEK 293T cells transfected with TMEM16b/anoctamin2.

The blocking potencies of the three test compounds (measured both with respect to control, Figs 3 and 4, or to the average between control and washout, Fig. 5), were not significantly different in olfactory sensory neurons, while in HEK 293T cells NFA blocked more potently than NPPB.

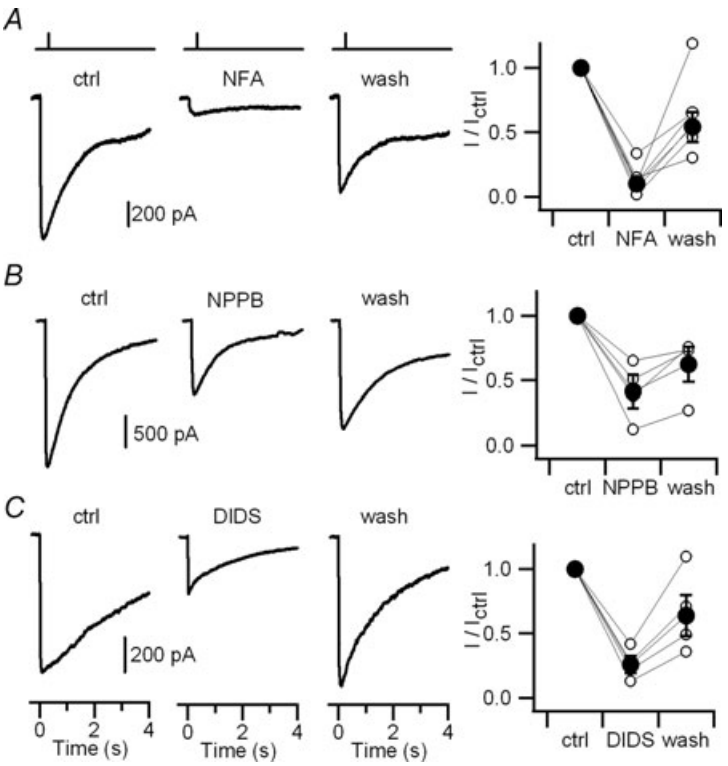

Figure 4. TMEM16b-transfected HEK 293T cells: extracellular blockage of currents activated by photorelease of caged Ca^{2+}
Currents recorded in the whole-cell voltage-clamp configuration in response to photorelease of caged Ca^{2+}. Ultraviolet light flashes were applied on HEK cells at the times indicated by the vertical bars in the upper panels. The holding potential was −50 mV. As in Fig. 3, the following blockers were used: *A*, 400 μM NFA; *B*, 100 μM NPPB; *C*, 1 mM DIDS. Current recordings were obtained before blocker application (control), 1–2 min after application of the indicated blockers, and 2–5 min after the removal of blockers (washout). Panels on the right show peak currents measured in the presence of each blocker and after washout, normalized to the control value before blocker application for each neuron (open circles). Average ratios are plotted as filled circles.

Anion selectivity of native Ca^{2+}-activated currents in olfactory sensory neurons

To measure the ion selectivity of Ca^{2+}-activated currents in the whole-cell configuration, we photoreleased caged Ca^{2+} in the ciliary region, and recorded the current at various holding potentials while changing the ion composition in the extracellular solution. To avoid contributions from Ca^{2+}-activated K^+ currents the intracellular monovalent cation was Cs^+.

In a first set of experiments, the intracellular and extracellular Cl^- concentrations were very similar ($[Cl^-]_o = 149$ mM, $[Cl^-]_i = 143$ mM) and the calculated equilibrium potential for Cl^- was -1.0 mV. Figure 6*A* shows currents in response to Ca^{2+} concentration jumps obtained by photorelease of Ca^{2+} when an olfactory sensory neuron was held at the indicated holding potentials from -15 to $+15$ mV. The rise time of the response was fast and was fitted by a single exponential with $\tau = 27$ ms at $+5$ mV and $\tau = 29$ ms at -5 mV.

Figure 6*B* shows current–voltage relations measured at various times after Ca^{2+} photorelease. The V_{rev} extrapolated from each current–voltage relation did not significantly change with time and was 0.4 mV, close to the expected Cl^- equilibrium potential (-1.0 mV). The average V_{rev} from several neurons was 1.0 ± 1.1 mV ($n = 13$).

Although V_{rev} was very close to the calculated equilibrium potential for Cl^-, a non-selective cation current might also contribute to the Ca^{2+}-activated current. If Ca^{2+}-activated channels are permeable to cations, the replacement of Na^+ by choline, a large organic cation that is usually impermeant in cation channels, should cause a large shift of the V_{rev} (Franciolini & Nonner, 1994; Qu & Hartzell, 2000; Hille, 2001). Instead, we found that the average V_{rev} measured in the presence of 140 mM choline chloride remained close to 0 mV, with an average value of 0.4 ± 0.6 mV ($n = 3$; data not shown), indicating that the Ca^{2+}-activated current was indeed mainly carried by Cl^-.

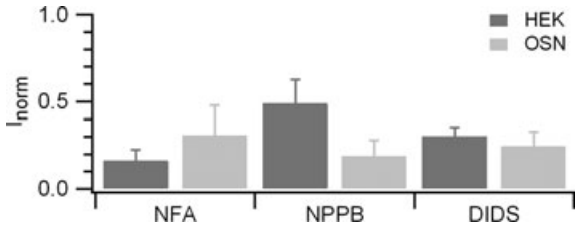

Figure 5. Comparison of extracellular blockage of Ca^{2+}-activated currents
Average ratios of currents measured in the presence of each blocker normalized to the average between control and washout currents. Experiments were from olfactory sensory neurons (OSN, $n = 3$–8) or from HEK 293T cells transfected with TMEM16b/anoctamin2 (HEK, $n = 4$–6). The block efficacy of different compounds was not significantly different in olfactory sensory neurons (ANOVA, $F = 0.33$, $P = 0.72$). In contrast in HEK 293T cells, blockage by NFA was significantly bigger from NPPB block (ANOVA, Tukey test $P < 0.05$), but not different from DIDS block. However, current blockages in olfactory sensory neurons and in HEK 293T cells were not significantly different (unpaired *t* test).

To measure the selectivity among anions we replaced 140 mM NaCl in the Ringer solution with $NaNO_3$, NaI, NaSCN, NaBr or NaMeS and estimated the V_{rev} in the presence of each anion. After each anion substitution, the Ringer bathing solution still contained 9 mM Cl^-, producing a calculated equilibrium potential for Cl^- of $+70.2$ mV.

Figure 6*C* shows recordings in the presence of nitrate Ringer solution. Surprisingly, multiple current components were clearly evident at several holding potentials. At -29 mV, a fast outward current ($\tau = 15$ ms) with a peak amplitude of $+45$ pA, was followed by a slower current component reaching a value of 0 pA about 250 ms after the flash and -75 pA at 2.5 s, as illustrated in Fig. 6*D*.

Current–voltage relations were measured at various times after Ca^{2+} photorelease (Fig. 6*E*) and the V_{rev} extrapolated from each current–voltage relation was plotted as a function of time in Fig. 6*F*. The V_{rev} in nitrate Ringer solution showed a time dependence with a gradual shift from a value of -34 mV at 50 ms, toward a less negative value of about -24 mV during the following 2–4 s.

In the presence of $NaNO_3$, we measured a time-dependent shift of V_{rev} in each of four tested neurons. The average V_{rev} in the presence of NO_3^- was -28.6 ± 2.5 mV ($n = 4$) for the fast current component, and -17.3 ± 3.6 mV ($n = 4$) for the current component measured at 2–4 s. The shift of V_{rev} toward more negative values upon substitution of Cl^- with NO_3^- indicates that NO_3^- was more permeant than Cl^-.

Substitution of chloride Ringer with iodide Ringer solution also revealed the presence of multiple current components (Fig. 7*A*). At -25 mV a fast outward current with a peak amplitude of $+270$ pA 17 ms after the flash, was followed by a slower component reaching a value of -150 pA within 2 s from flash release. At -35 mV a fast inward current component with a value of -270 pA at 50 ms was followed by an additional slower component that reached -500 pA within 2 s (Fig. 7*B*). Thus, also in iodide Ringer solution, V_{rev} was time dependent, with a gradual shift from -30 mV at 50 ms, to -18 mV at 2–4 s (Fig. 7*C*).

A similar time dependence of V_{rev} was measured in isothiocyanate Ringer solution (from -36 to -21 mV for the experiment in Fig. 7*C*). In the presence of bromide Ringer solution, V_{rev} had a small time dependence (from -17 to -14 mV for the experiment in Fig. 7*C*), only in 2 out of 6 olfactory sensory neurons.

The average reversal potential of the fast component was -30.5 ± 3 mV ($n = 6$) in the presence of I^-, -42 ± 5.5 mV ($n = 4$) in SCN^- and -13.8 ± 2.2 mV ($n = 6$) for Br^-.

When chloride Ringer was replaced by methanesulfonate Ringer solution, current recordings showed that MeS^- was much less permeant than Cl^-; indeed V_{rev} was +34 mV and remained fairly constant at different times (Fig. 7*C*). The average reversal potential was $+31.6 \pm 4.3$ mV ($n = 5$). The selectivity sequence was $SCN^- \approx I^- \approx NO_3^- > Br^- > Cl^- > MeS^-$ (Fig. 10).

These results demonstrate that the current activated by Ca^{2+} photorelease in the ciliary region of olfactory sensory neurons is anion selective and that for some anions V_{rev} gradually shifted with time toward less negative values.

Anion selectivity of Ca^{2+}-activated currents in HEK 293T cells expressing TMEM16b/anoctamin2

To investigate whether Ca^{2+}-activated currents induced by TMEM16b/anoctamin2 in HEK 293T cells exhibits a time-dependent V_{rev} in the presence of some anions, we used the same experimental protocols as in olfactory sensory neurons.

Figure 8*A* shows recordings from a cell in chloride Ringer solution. As in olfactory sensory neurons, the rise time of the response to photorelease of Ca^{2+} in NaCl was fast and was well fitted by a single exponential with $\tau = 14$ ms at +20 mV and $\tau = 4$ ms at −20 mV. Current–voltage relations measured at various times (Fig. 8*B*) showed that the estimated V_{rev} was −0.2 mV and was not time

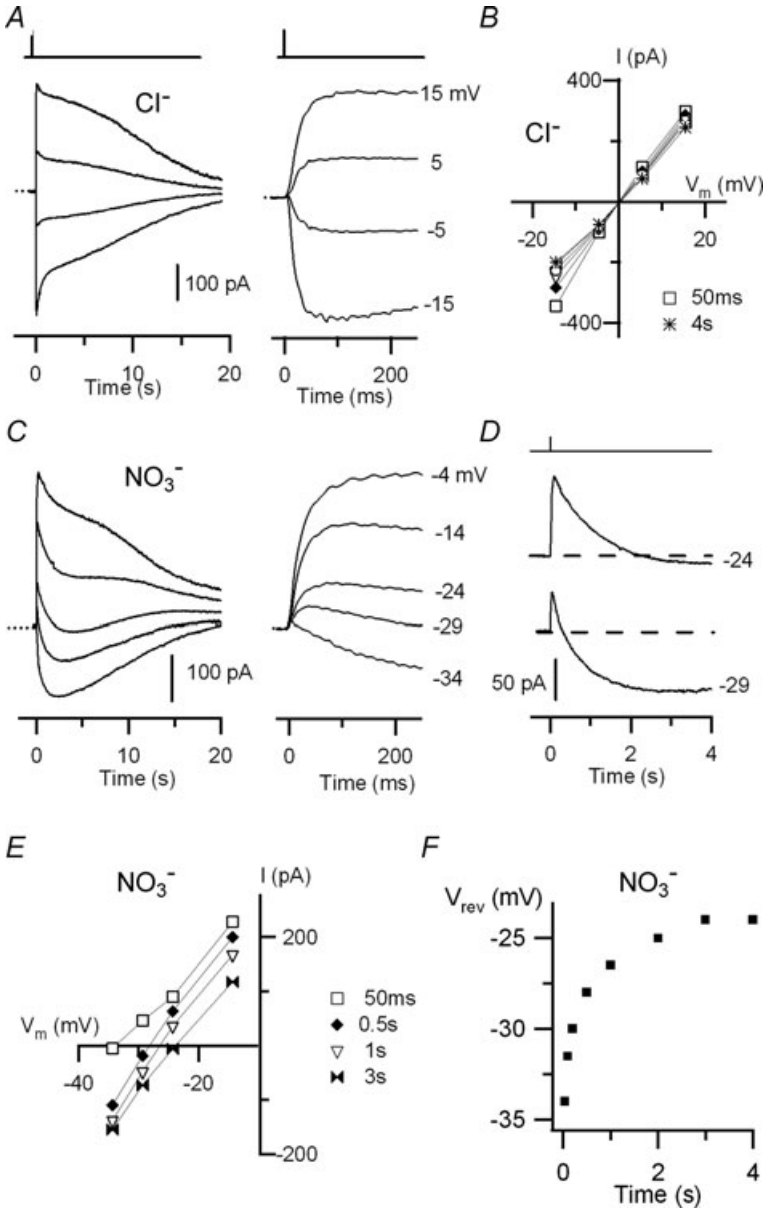

Figure 6. Olfactory sensory neurons: current responses induced by photorelease of Ca^{2+} in the presence of external Cl^- or NO_3^-
Currents recorded from isolated mouse olfactory sensory neurons in the whole-cell voltage-clamp configuration in response to photorelease of caged Ca^{2+} in the cilia at the time indicated by the vertical bars at the top. *A*, currents from an olfactory sensory neuron were recorded in almost symmetrical Cl^- solutions at the indicated holding potentials and plotted on different time scales. The dotted line indicates the zero current level. *B*, current–voltage relations measured from recordings in *A* at different times from the flash: 50 ms square, 0.5 s diamond, 1 s triangle, 2 s circle, 3 s double triangle, 4 s asterisk. *C*, currents from another olfactory sensory neuron recorded in the presence of external NO_3^- at the indicated holding potentials and plotted on different time scales. The dotted line indicates the zero current level. *D*, recordings in external NO_3^- at −24 and −29 mV are shown on a different scale to better illustrate the time dependence of V_{rev}. *E*, current–voltage relations in external NO_3^- measured from recordings in *C* at different times from the flash: 50 ms open square, 0.5 s diamond, 1 s triangle, 3 s double triangle. *F*, V_{rev} as a function of time for external NO_3^- from recordings in *C*.

dependent. Its average value was -0.7 ± 0.7 mV ($n = 21$). Moreover, when NaCl was replaced by choline chloride the average V_{rev} was -0.5 ± 0.6 mV, $n = 4$ (data not shown), similar to that in NaCl, indicating that the current was mainly carried by Cl^-, as in olfactory sensory neurons.

In the presence of nitrate Ringer solution multiple current components were evident (Fig. 8*C*). The current amplitude at -20 mV was $+230$ pA 70 ms after the flash and -18 pA at 2.5 s (Fig. 8*D*). Current–voltage relations as a function of time (Fig. 8*E*) indicate that V_{rev} gradually shifted with time from -29 mV to about -20 mV at 2–4 s (Fig. 8*F*). On average, V_{rev} in the presence of NO_3^- was -26.8 ± 1.5 mV ($n = 4$) for the fast current component, and -19.5 ± 4.8 mV ($n = 4$) for the current component measured at 2–4 s.

Figure 9 shows a summary of results obtained with the other anions: in iodide Ringer solution (Fig. 9*A* and *B*), at -20 mV a fast current component of $+140$ pA was measured at 200 ms, followed by a slower component reaching -20 pA at 5 s. A fast and a slow component were also evident at -40 mV, with a value of -100 pA at 80 ms that reached -430 pA within 4 s. The time dependence of V_{rev} for I^- is illustrated in Fig. 9*C*, where V_{rev} shifted from -26 to -18 mV at 2–4 s.

V_{rev} also had a significant time-dependent shift in isothyocianate Ringer solution (from -38.5 to -18 mV for the experiment in Fig. 9*C*), while the shift was smaller in bromide Ringer solution (from -11.2 to -7 mV for the experiment in Fig. 9*C*).

The average reversal potential of the fast component was -34.9 ± 1.8 mV ($n = 4$) in the presence of I^-, -29.0 ± 4.0 mV ($n = 5$) in SCN^- and -15.7 ± 0.4 mV ($n = 5$) in Br^-.

Figure 9*C* shows that recordings in methanesulphonate Ringer solution exhibited a single current component with a time-independent V_{rev} of $+27$ mV. The average V_{rev} was $+39.7 \pm 4.6$ mV ($n = 6$) confirming that MeS^- is less permeant than Cl^-.

Figure 10 summarizes the average V_{rev} of the fast component in olfactory sensory neurons and in HEK 293T cells expressing TMEM16b/anoctamin2. For both types of currents the selectivity sequence was the following: $SCN^- \approx I^- \approx NO_3^- > Br^- > Cl^- > MeS^-$.

Furthermore, these results show that, similarly to olfactory sensory neurons, also in HEK 293T cells expressing TMEM16b/anoctamin2, the V_{rev} gradually shifted as a function of time toward less negative values in the presence of external NO_3^-, I^-, SCN^- and, to a lesser extent, in Br^-, while it did not change with time in Cl^- and in MeS^-.

Discussion

Expression of TMEM16b/anoctamin2 in the ciliary layer

In this study, we show by RT-PCR that TMEM16b/anoctamin2 and some other members of the TMEM16/anoctamin family are expressed in the olfactory epithelium. Our results are in agreement with other reports showing the presence not only of TMEM16b/anoctamin2, but also of a/1 and k/10, whereas not all studies agree on other family members (Stephan *et al.* 2009; Rasche *et al.* 2010). Indeed, we identified also the presence of d/4, g/7 and j/9 that could not be detected in other reports (Rasche *et al.* 2010). Differences might

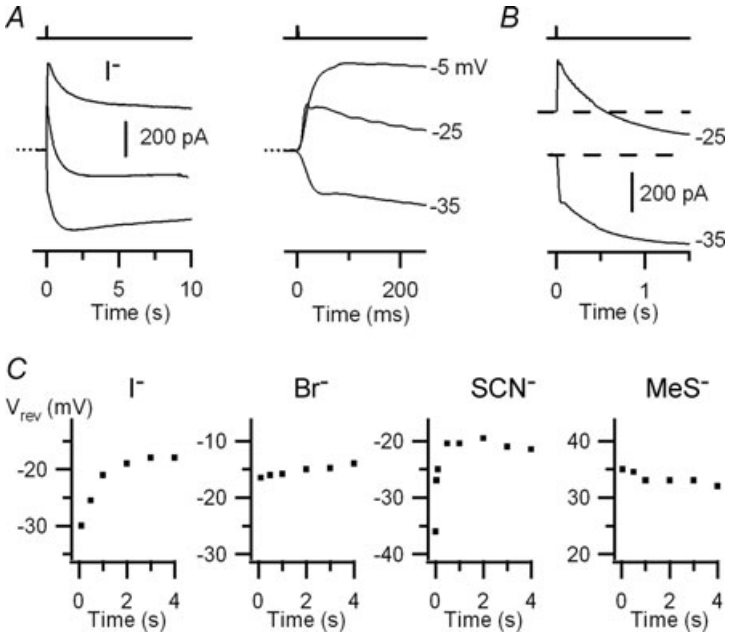

Figure 7. Olfactory sensory neurons: current responses induced by photorelease of Ca^{2+} in external I^-, SCN^-, Br^- or MeS^-
A, currents recorded at the indicated holding potentials from an olfactory sensory neuron bathed in external iodide Ringer solution. The dotted line indicates the zero current level. *B*, recordings in external I^- at -25 and -35 mV are shown on a different scale to better illustrate the time dependence of V_{rev}. *C*, V_{rev} as a function of time for external I^- (from the recordings in *A*), Br^-, SCN^- and MeS^-, each from a different neuron.

be due to several reasons. The discrepancy for d/4 and g/7 might reflect a higher efficiency of our amplification reaction since both are likely to be poorly expressed in the olfactory epithelium. The different result for j/9 that, in our hands, appears abundantly expressed in the olfactory epithelium, is unlikely to be caused by the recognition of a different isoform, as oligonucleotide primers employed by Rasche and colleagues are internal to ours. It remains plausible that the modality for tissue collection may reveal an important variable to explain this inconsistency, although in our study, olfactory epithelia were isolated by distinct operators without appreciable differences in the final results.

Although not all studies agree on the specific family members, at present, only the mRNA of TMEM16b/anoctamin2 has been shown to be specific to mature olfactory sensory neurons by *in situ* hybridization (Yu *et al.* 2005), and proteomic screening of ciliary membranes (Mayer *et al.* 2009; Stephan *et al.* 2009) revealed only TMEM16b/anoctamin2 as a prominent protein in the olfactory cilia. Finally, the expression of TMEM16b/anoctamin2 in the ciliary layer of olfactory sensory neurons, has been independently confirmed by immunohistochemistry in our study, using the antibody developed by Stöhr *et al.* (2009), and in other recent reports using two other different antibodies (Hengl *et al.* 2010; Rasche *et al.* 2010).

Taken together, all these results indicate that TMEM16b/anoctamin2 is strongly expressed in the cilia of olfactory sensory neurons, where olfactory transduction takes place, while some other members of the family might be present at a lower level or in other cell types.

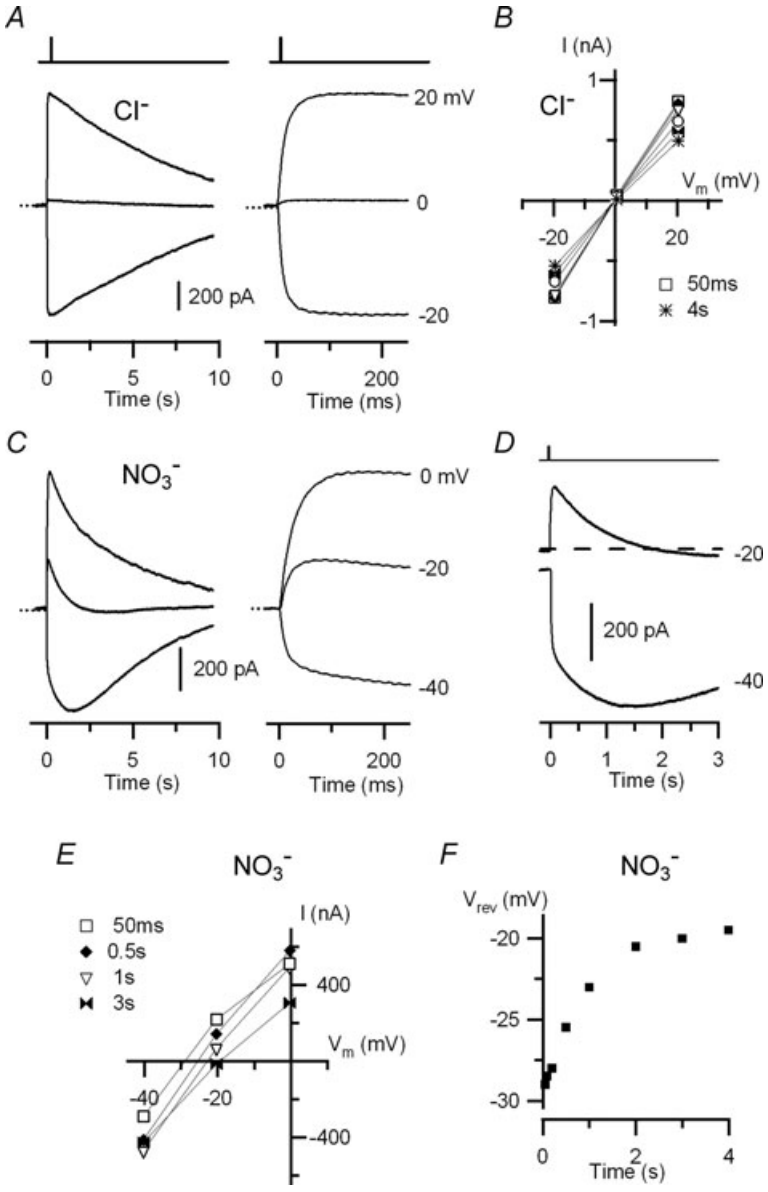

Figure 8. Anion selectivity of the TMEM16b/anoctamin2-mediated current in external Cl^- or NO_3^-
Currents recorded from HEK 293T cells expressing TMEM16b/anoctamin2 in the whole-cell voltage-clamp configuration in response to photorelease of caged Ca^{2+} at the time indicated by the vertical bars at the top. *A*, currents from a cell were recorded in almost symmetrical Cl^- solutions at the indicated holding potentials and plotted on different time scales. The dotted line indicates the zero current level. *B*, current–voltage relations measured from recordings in *A* at different times from the flash: 50 ms square, 0.5 s diamond, 1 s triangle, 2 s circle, 3 s double triangle, 4 s asterisk. *C*, currents from another cell were recorded in the presence of external NO_3^- at the indicated holding potentials and plotted on different time scales. The dotted line indicates the zero current level. *D*, recordings in external NO_3^- at −40 and −20 mV are shown on a different scale to better illustrate the time dependence of V_{rev}. *E*, current–voltage relations in external NO_3^- measured from recordings in *C* at different times from the flash: 50 ms square, 0.5 s diamond, 1 s triangle, 3 s double triangle. *F*, V_{rev} as a function of time for external NO_3^- from the recordings in *C*.

Extracellular blockers

In previous studies, the pharmacological profile of the native olfactory Ca^{2+}-activated Cl^- current has been investigated in detail only by applying Cl^- channel inhibitors at the cytoplasmic side of isolated cilia from frog olfactory sensory neurons (Kleene & Gesteland, 1991; Kleene, 1993; reviewed by Frings *et al.* 2000). However, it is well known that some compounds have very different effects when applied to the extracellular or to the intracellular side of the membrane. The most commonly used extracellular blockers for Ca^{2+}-activated Cl^- currents in olfactory sensory neurons are NFA (Lowe & Gold, 1993; Reisert *et al.* 2005; Boccaccio *et al.* 2006; Boccaccio & Menini, 2007; Antolin *et al.* 2010), which blocks also from the intracellular side (Kleene & Gesteland, 1991; Kleene, 1993; Reisert *et al.* 2003; Pifferi *et al.* 2006*b*), and SITS (Kurahashi & Yau, 1993; Lowe & Gold, 1993), which is a much less effective blocker from the intracellular side (Kleene & Gesteland, 1991; Pifferi *et al.* 2006*b*). We determined that the blocking properties of two other compounds, NPPB and DIDS, are side-specific with extracellular inhibition of 85% for 100 μM NPPB and 76% for 1 mM DIDS, while Kleene and Gesteland (1991) measured a very poor intracellular inhibition: 32% for 300 μM NPPB, and 5% for 100 μM DIDS (see Table 2 of Frings *et al.* 2000).

Similar side-specific effects of NPPB and DIDS on TMEM16b-induced currents were obtained in this and in a previous study (Pifferi *et al.* 2009*a*). Moreover, we found that the average percentages of current inhibition of TMEM16b-induced currents were similar to those we measured in olfactory sensory neurons. Taken together, the results on intracellular (Kleene & Gesteland, 1991; Kleene, 1993; Pifferi *et al.* 2009*a*) and extracellular blockage of native olfactory and TMEM16b-induced currents indicate that NPPB and DIDS block the two currents in a similar side-specific manner.

It is of interest to note that in some neurons NPPB or DIDS blocked the current almost completely, while such a large inhibition was never observed in TMEM16b-induced currents in HEK cells. A small difference in results between native and expressed channels has also been pointed out by Saidu *et al.* (2010). In fact, in excised patches the native current slightly inactivates at positive

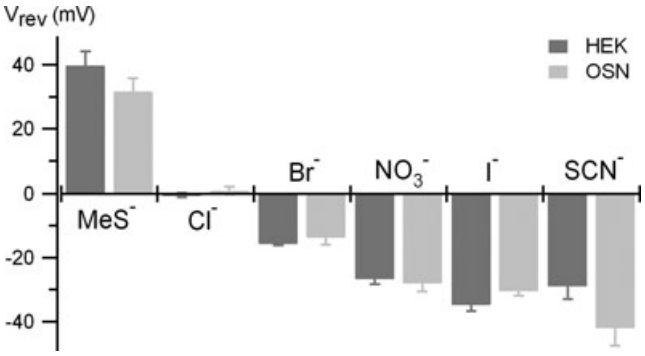

Figure 10. Comparison of anion selectivity for native and TMEM16b/anoctamin2-mediated current
Average V_{rev} for the fast component measured in the presence of the indicated external anions. Experiments were from olfactory sensory neurons (OSN, $n = 4$–13) or from HEK 293T cells transfected with TMEM16b/anoctamin2 (HEK, $n = 4$–21). V_{rev} in olfactory sensory neurons and in HEK 293T cells were not significantly different (unpaired *t* test).

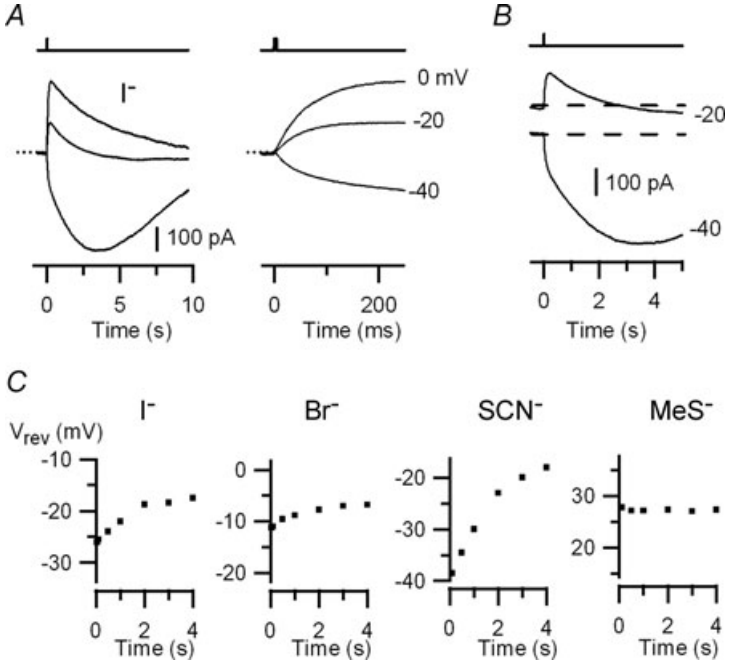

Figure 9. Anion selectivity of the TMEM16b/anoctamin2-mediated current in external I^-, SCN^-, Br^- or MeS^-
A, currents from a HEK 293T cell expressing TMEM16b/anoctamin2 were recorded in external iodide Ringer solution at the indicated holding potentials. The dotted line indicates the zero current level. *B*, recordings in external I^- at −20 and −40 mV are shown on a different scale to better illustrate the time dependence of V_{rev}. *C*, V_{rev} as a function of time for external I^- (from recordings in *A*), Br^-, SCN^- and MeS^-, each from a different cell.

membrane potentials (Reisert *et al.* 2003), whereas the TMEM16b/anoctamin2-induced current in HEK cells does not (Stephan *et al.* 2009; Saidu *et al.* 2010). These differences may point to the possibility that additional subunits and/or splice variants constitute the native channel, as recently suggested by Saidu *et al.* (2010).

Dynamic ion selectivity

Another important property of ion channels is ion selectivity. In previous reports, the ion selectivity of native olfactory Ca^{2+}-activated Cl^- currents has been measured only from inside-out membrane patches excised from the knob/ciliary region of olfactory sensory neurons, exchanging ions at the intracellular side of the membrane (Reisert *et al.* 2003; Pifferi *et al.* 2006*b*). The ion selectivity of native channels in isolated olfactory sensory neurons, replacing extracellular Cl^- with other ions, has not been estimated yet with the exception of substitution of Cl^- with the largely impermeant gluconate to demonstrate that the Ca^{2+}-activated current was carried by Cl^- (Takeuchi *et al.* 2009).

We found that some anions larger than Cl^-, such as NO_3^-, I^-, SCN^- and Br^-, were more permeant than Cl^-, while MeS^- was less permeant. Interestingly, in the presence of NO_3^-, SCN^- and I^-, a gradual time-dependent shift of V_{rev} was clearly evident. Indeed, V_{rev} in the presence of these anions changed with time, shifting about 10 mV toward less negative values over a few seconds after photorelease of Ca^{2+}, indicating that channels became less permeant to some foreign anions. To the best of our knowledge, this is the first demonstration that the native olfactory Ca^{2+}-activated Cl^- current exhibits dynamic ion selectivity.

What is the origin of the dynamic ion selectivity? A possibility is that V_{rev} changes with time because of a restricted anion diffusion: if anions accumulate at the intracellular mouth of the channel, the local concentration gradient will change modifying V_{rev}. In the narrow ciliary compartment, restricted anion diffusion might cause the accumulation of anions flowing into the cilia near the intracellular mouth of the channel, therefore leading to a different concentration gradient and a modification of V_{rev}. However, it is unlikely that this effect is the origin of the time-dependent change in V_{rev}, because such an effect is expected to be present with all anions, whereas it was not observed in the presence of Cl^- or of MeS^-. Furthermore, in some experiments (Figs 6*D* and 7*B*) the current reversed direction, which should not result from restricted diffusion. In fact, if the initial NO_3^- or I^- influx (outward current) causes an accumulation of NO_3^- or I^- inside the cilium, this should only proceed until equilibrium (zero current) and it cannot account for the Cl^- efflux (inward current) measured subsequently. Finally, an environmental-mediated restriction of anion diffusion, typical of the olfactory ciliary compartment, is unlikely to exist in TMEM16b/anoctamin2-transfected HEK 293T cells that, in turn, display a similar dynamic ion selectivity.

Since olfactory sensory neurons contain several types of channels, we cannot exclude that multiple current components might be due to the activation of different types of channels. Again, however, when the same experimental protocols were applied to HEK 293T cells expressing TMEM16b/anoctamin2, we obtained results very similar to those observed in the native olfactory channels. In HEK 293T cells, multiple current components were clearly evident in the presence of the same anions: NO_3^-, I^- and SCN^-, and absent with Cl^- or MeS^-. Moreover, the average V_{rev} for each anion was not significantly different between the two systems.

Our results have at least two important consequences: on one side they show that Ca^{2+}-activated Cl^- currents in olfactory sensory neurons have multiple components with different anion selectivity and, on the other side they show that heterologous expression of TMEM16b/anoctamin2 in HEK 293T cells reproduced similar results, indicating that time-dependent ion selectivity is not due to different types of channels.

The presence of multiple current components is not unique to the Ca^{2+}-activated Cl^- current present in olfactory sensory neurons since, for example, it has been found in *Xenopus* oocytes (Boton *et al.* 1989; Kuruma & Hartzell, 1999). More recently, Schroeder *et al.* (2008) clearly showed the presence of multiple current components with different anion selectivity, activating Ca^{2+}-activated Cl^- currents in *Xenopus* oocytes by photorelease of caged IP_3. Moreover, Schroeder *et al.* (2008) demonstrated that the TMEM16a/anoctamin1 channel expressed in *Axolotl* oocytes, which do not have endogenous Ca^{2+}-activated Cl^- currents, also exhibited current components with different V_{rev}, suggesting that the multiple components originated from different states of the same channel.

Furthermore, it is of interest to note that dynamic changes in ion selectivity are not a peculiarity of anion channels, and they have been revealed in cation channels (Khakh & Lester, 1999). For example, the P2X receptor of mast cells allows a time-dependent membrane permeability to large molecules (Cockcroft & Gomperts, 1979), the transient receptor potential vanilloid 1 (TRPV1) channel shows a time- and concentration-dependent change in ion selectivity in the presence of prolonged exposure to chemical agonists (Chung *et al.* 2008), and a mutant *N*-methyl-D-aspartate (NMDA) channel exhibits multiple current components with time-dependent ion selectivity (Schneggenburger & Ascher, 1997). Single-channel analysis of the mutant NMDA channel revealed the existence of at least two

subconductance states with different ion selectivity, indicating a strong coupling between permeation and gating (Schneggenburger & Ascher, 1997). Zheng and Sigworth (1997) also showed by single-channel analysis that a mutant *Shaker* K^+ channel exhibits two subconductance states with different ion selectivity.

Another example of coupling between gating and permeation occurs in the cyclic nucleotide-gated channel in retinal rods. Indeed, it has been shown that in intact rod photoreceptors, selectivity among divalent cations changes with different levels of cGMP (Cervetto *et al.* 1988), and that in inside-out patches from photoreceptors, both the channel open probability and the selectivity of Ca^{2+} over Na^+ increases with cGMP concentration (Hackos & Korenbrot, 1999). In addition, the linkage between selectivity and gating is specific for divalent cations, whereas it does not occur if only monovalent cations are present (Hackos & Korenbrot, 1999).

Previous studies on Ca^{2+}-activated Cl^- currents from various cell types showed that some foreign anions at the extracellular side affect gating by modifying channel kinetics (Evans & Marty, 1986; Greenwood & Large, 1999; Perez-Cornejo *et al.* 2004). Greenwood and Large (1999) suggested that some permeant anions might modulate the kinetics of Ca^{2+}-activated Cl^- channels in smooth muscle cells by binding to a site located on the external surface of the channel, which may be part of the channel representing the selectivity filter.

Our experiments were obtained by activating channels by a fast jump in Ca^{2+} concentration that decreased with time by diffusion and/or by active extrusion. In the presence of some anions, we observed a time-dependent shift of V_{rev} toward less negative values, corresponding to a decreased ion selectivity. A possible mechanism explaining the dynamic ion selectivity of native olfactory and TMEM16b/anoctamin2-induced Ca^{2+}-activated Cl^- currents is the presence of at least two open states with different ion selectivity and Ca^{2+}-dependent open probability. Indeed, our results are consistent with a model in which the more selective open state is favoured by high Ca^{2+} concentrations and the less selective open state by low Ca^{2+} concentrations.

The understanding of this phenomenon at the molecular level by future mutational and structural analyses, will clarify the molecular mechanisms of gating and permeation of Ca^{2+}-activated Cl^- channels, contributing to increase the knowledge about their functioning in physiological and pathophysiological processes.

Conclusions

In conclusion, we confirmed by immunohistochemistry that TMEM16b/anoctamin2 is expressed in the ciliary layer, and showed that TMEM16b/anoctamin2 reproduced the phenotypes of the native olfactory Ca^{2+}-activated Cl^- currents, including the time-dependent change in selectivity. Taken together with previous studies on inside-out patches (Pifferi *et al.* 2009*a*; Stephan *et al.* 2009), these results contribute to strongly indicate that TMEM16b/anoctamin2 is likely to be the major subunit of the native olfactory Ca^{2+}-activated Cl^- current. Future studies should examine the presence of olfactory Ca^{2+}-activated Cl^- currents in mice in which the TMEM16b/anoctamin2 gene is deleted. Moreover, the combination of molecular biology studies and functional measurements will clarify if additional subunits and/or splice variants belonging to the TMEM16/anoctamin or to other protein families are also part of the native Ca^{2+}-activated Cl^- channel.

References

Antolin S, Reisert J & Matthews HR (2010). Olfactory response termination involves Ca^{2+}-ATPase in vertebrate olfactory receptor neuron cilia. *J Gen Physiol* **135**, 367–378.

Bader CR, Bertrand D & Schwartz EA (1982). Voltage-activated and calcium-activated currents studied in solitary rod inner segments from the salamander retina. *J Physiol* **331**, 253–284.

Barish ME (1983). A transient calcium-dependent chloride current in the immature *Xenopus* oocyte. *J Physiol* **342**, 309–325.

Barry P (1994). JPCalc, a software package for calculating liquid junction potential corrections in patch-clamp, intracellular, epithelial and bilayer measurements and for correcting junction potential measurements. *J Neurosci Methods* **51**, 107–116.

Boccaccio A, Lagostena L, Hagen V & Menini A (2006). Fast adaptation in mouse olfactory sensory neurons does not require the activity of phosphodiesterase. *J Gen Physiol* **128**, 171–184.

Boccaccio A & Menini A (2007). Temporal development of cyclic nucleotide-gated and Ca^{2+}-activated Cl^- currents in isolated mouse olfactory sensory neurons. *J Neurophysiol* **98**, 153–160.

Boton R, Dascal N, Gillo B & Lass Y (1989). Two calcium-activated chloride conductances in *Xenopus laevis* oocytes permeabilized with the ionophore A23187. *J Physiol* **408**, 511–534.

Caputo A, Caci E, Ferrera L, Pedemonte N, Barsanti C, Sondo E, Pfeffer U, Ravazzolo R, Zegarra-Moran O & Galietta LJV (2008). TMEM16A, a membrane protein associated with calcium-dependent chloride channel activity. *Science* **322**, 590–594.

Cervetto L, Menini A, Rispoli G & Torre V (1988). The modulation of the ionic selectivity of the light-sensitive current in isolated rods of the tiger salamander. *J Physiol* **406**, 181–198.

Chung M, Güler AD & Caterina MJ (2008). TRPV1 shows dynamic ionic selectivity during agonist stimulation. *Nat Neurosci* **11**, 555–564.

Cockcroft S & Gomperts BD (1979). Activation and inhibition of calcium-dependent histamine secretion by ATP ions applied to rat mast cells. *J Physiol* **296**, 229–243.

Duran C, Thompson CH, Xiao Q & Hartzell HC (2010). Chloride channels: often enigmatic, rarely predictable. *Annu Rev Physiol* **72**, 95–121.

Evans MG & Marty A (1986). Calcium-dependent chloride currents in isolated cells from rat lacrimal glands. *J Physiol* **378**, 437–460.

Flores CA, Cid LP, Sepúlveda FV & Niemeyer MI (2009). TMEM16 proteins: the long awaited calcium-activated chloride channels?. *Braz J Med Biol Res* **42**, 993–1001.

Franciolini F & Nonner W (1994). A multi-ion permeation mechanism in neuronal background chloride channels. *J Gen Physiol* **104**, 725–746.

Frings S (2009*a*). Chloride-based signal amplification in olfactory sensory neurons. In *Physiology and Pathology of Chloride Transporters and Channels in the Nervous System. From Molecules to Diseases*, ed. Alvarez-Leefmans FJ & Delpire E. Elsevier-Academic Press, San Diego, CA.

Frings S (2009*b*). Primary processes in sensory cells: current advances. *J Comp Physiol A Neuroethol Sens Neural Behav Physiol* **195**, 1–19.

Frings S, Reuter D & Kleene SJ (2000). Neuronal Ca^{2+}-activated Cl^- channels–homing in on an elusive channel species. *Prog Neurobiol* **60**, 247–289.

Galietta LJV (2009). The TMEM16 protein family: a new class of chloride channels?. *Biophys J* **97**, 3047–3053.

Greenwood IA & Large WA (1999). Modulation of the decay of Ca^{2+}-activated Cl^- currents in rabbit portal vein smooth muscle cells by external anions. *J Physiol* **516**, 365–376.

Hackos DH & Korenbrot JI (1999). Divalent cation selectivity is a function of gating in native and recombinant cyclic nucleotide-gated ion channels from retinal photoreceptors. *J Gen Physiol* **113**, 799–818.

Hartzell C, Putzier I & Arreola J (2005). Calcium-activated chloride channels. *Annu Rev Physiol* **67**, 719–758.

Hartzell HC, Yu K, Xiao Q, Chien L & Qu Z (2009). Anoctamin/TMEM16 family members are Ca^{2+}-activated Cl^-channels. *J Physiol* **587**, 2127–2139.

Hengl T, Kaneko H, Dauner K, Vocke K, Frings S & Möhrlen F (2010). Molecular components of signal amplification in olfactory sensory cilia. *Proc Natl Acad Sci U S A* **107**, 6052–6057.

Hille B (2001). *Ionic Channels of Excitable Membranes*. Sinauer Associates, Inc., Sunderland, MA.

Kaneko H, Nakamura T & Lindemann B (2001). Noninvasive measurement of chloride concentration in rat olfactory receptor cells with use of a fluorescent dye. *Am J Physiol Cell Physiol* **280**, C1387–C1393.

Kaneko H, Putzier I, Frings S, Kaupp UB & Gensch T (2004). Chloride accumulation in mammalian olfactory sensory neurons. *J Neurosci* **24**, 7931–7938.

Khakh BS & Lester HA (1999). Dynamic selectivity filters in ion channels. *Neuron* **23**, 653–658.

Kleene SJ (1993). Origin of the chloride current in olfactory transduction. *Neuron* **11**, 123–132.

Kleene SJ (1997). High-gain, low-noise amplification in olfactory transduction. *Biophys J* **73**, 1110–1117.

Kleene SJ (2008). The electrochemical basis of odor transduction in vertebrate olfactory cilia. *Chem Senses* **33**, 839–859.

Kleene SJ & Gesteland RC (1991). Calcium-activated chloride conductance in frog olfactory cilia. *J Neurosci* **11**, 3624–3629.

Kunzelmann K, Kongsuphol P, Aldehni F, Tian Y, Ousingsawat J, Warth R & Schreiber R (2009). Bestrophin and TMEM16-Ca^{2+} activated Cl^- channels with different functions. *Cell Calcium* **46**, 233–241.

Kurahashi T & Yau KW (1993). Co-existence of cationic and chloride components in odorant-induced current of vertebrate olfactory receptor cells. *Nature* **363**, 71–74.

Kuruma A & Hartzell HC (1999). Dynamics of calcium regulation of chloride currents in *Xenopus* oocytes. *Am J Physiol Cell Physiol* **276**, C161–C175.

Lagostena L & Menini A (2003). Whole-cell recordings and photolysis of caged compounds in olfactory sensory neurons isolated from the mouse. *Chem Senses* **28**, 705–716.

Lowe G & Gold GH (1993). Nonlinear amplification by calcium-dependent chloride channels in olfactory receptor cells. *Nature* **366**, 283–286.

Matthews HR & Reisert J (2003). Calcium, the two-faced messenger of olfactory transduction and adaptation. *Curr Opin Neurobiol* **13**, 469–475.

Mayer U, Küller A, Daiber PC, Neudorf I, Warnken U, Schnölzer M, Frings S & Möhrlen F (2009). The proteome of rat olfactory sensory cilia. *Proteomics* **9**, 322–334.

Menco BP (1997). Ultrastructural aspects of olfactory signaling. *Chem Senses* **22**, 295–311.

Menco BP, Bruch RC, Dau B & Danho W (1992). Ultrastructural localization of olfactory transduction components: the G protein subunit $G_{olf\alpha}$ and type III adenylyl cyclase. *Neuron* **8**, 441–453.

Menco BP, Tekula FD, Farbman AI & Danho W (1994). Developmental expression of G-proteins and adenylyl cyclase in peripheral olfactory systems. Light microscopic and freeze-substitution electron microscopic immunocytochemistry. *J Neurocytol* **23**, 708–727.

Menini A (1999). Calcium signalling and regulation in olfactory neurons. *Curr Opin Neurobiol* **9**, 419–426.

Menini A, Lagostena L & Boccaccio A (2004). Olfaction: from odorant molecules to the olfactory cortex. *News Physiol Sci* **19**, 101–104.

Miledi R (1982). A calcium-dependent transient outward current in *Xenopus laevis* oocytes. *Proc R Soc Lond B Biol Sci* **215**, 491–497.

Perez-Cornejo P, De Santiago JA & Arreola J (2004). Permeant anions control gating of calcium-dependent chloride channels. *J Membr Biol* **198**, 125–133.

Pifferi S, Boccaccio A & Menini A (2006*a*). Cyclic nucleotide-gated ion channels in sensory transduction. *FEBS Lett* **580**, 2853–2859.

Pifferi S, Dibattista M & Menini A (2009*a*). TMEM16B induces chloride currents activated by calcium in mammalian cells. *Pflugers Arch* **458**, 1023–1038.

Pifferi S, Dibattista M, Sagheddu C, Boccaccio A, Al Qteishat A, Ghirardi F, Tirindelli R & Menini A (2009*b*).

Calcium-activated chloride currents in olfactory sensory neurons from mice lacking bestrophin-2. *J Physiol* **587**, 4265–4279.

Pifferi S, Menini A & Kurahashi T (2009*c*). Signal transduction in vertebrate olfactory cilia. In *The Neurobiology of Olfaction*, ed. Menini A, pp. 203–224. CRC Press, Taylor & Francis Group, Boca Raton, FL.

Pifferi S, Pascarella G, Boccaccio A, Mazzatenta A, Gustincich S, Menini A & Zucchelli S (2006*b*). Bestrophin-2 is a candidate calcium-activated chloride channel involved in olfactory transduction. *Proc Natl Acad Sci U S A* **103**, 12929–12934.

Qu Z & Hartzell HC (2000). Anion permeation in Ca^{2+}-activated Cl^- channels. *J Gen Physiol* **116**, 825–844.

Rasche S, Toetter B, Adler J, Tschapek A, Doerner JF, Kurtenbach S, Hatt H, Meyer H, Warscheid B & Neuhaus EM (2010). Tmem16b is specifically expressed in the cilia of olfactory sensory neurons. *Chem Senses* **35**, 239–245.

Reisert J, Bauer PJ, Yau K & Frings S (2003). The Ca-activated Cl channel and its control in rat olfactory receptor neurons. *J Gen Physiol* **122**, 349–363.

Reisert J, Lai J, Yau K & Bradley J (2005). Mechanism of the excitatory Cl^- response in mouse olfactory receptor neurons. *Neuron* **45**, 553–561.

Reuter D, Zierold K, Schröder WH & Frings S (1998). A depolarizing chloride current contributes to chemoelectrical transduction in olfactory sensory neurons *in situ*. *J Neurosci* **18**, 6623–6630.

Saidu SP, Stephan AB, Caraballo SM, Zhao H & Reisert J (2010). Splice variants of the Ca^{2+}-activated Cl^- channel anoctamin 2. Association for Chemoreception Sciences Meeting 2010, abstract P68.

Schild D & Restrepo D (1998). Transduction mechanisms in vertebrate olfactory receptor cells. *Physiol Rev* **78**, 429–466.

Schneggenburger R & Ascher P (1997). Coupling of permeation and gating in an NMDA-channel pore mutant. *Neuron* **18**, 167–177.

Schroeder BC, Cheng T, Jan YN & Jan LY (2008). Expression cloning of TMEM16A as a calcium-activated chloride channel subunit. *Cell* **134**, 1019–1029.

Stephan AB, Shum EY, Hirsh S, Cygnar KD, Reisert J & Zhao H (2009). ANO2 is the cilial calcium-activated chloride channel that may mediate olfactory amplification. *Proc Natl Acad Sci U S A* **106**, 11776–11781.

Stöhr H, Heisig JB, Benz PM, Schöberl S, Milenkovic VM, Strauss O, Aartsen WM, Wijnholds J, Weber BHF & Schulz HL (2009). TMEM16B, a novel protein with calcium-dependent chloride channel activity, associates with a presynaptic protein complex in photoreceptor terminals. *J Neurosci* **29**, 6809–6818.

Takeuchi H, Ishida H, Hikichi S & Kurahashi T (2009). Mechanism of olfactory masking in the sensory cilia. *J Gen Physiol* **133**, 583–601.

Tirindelli R, Dibattista M, Pifferi S & Menini A (2009). From pheromones to behavior. *Physiol Rev* **89**, 921–956.

Yang YD, Cho H, Koo JY, Tak MH, Cho Y, Shim W, Park SP, Lee J, Lee B, Kim B, Raouf R, Shin YK & Oh U (2008). TMEM16A confers receptor-activated calcium-dependent chloride conductance. *Nature* **455**, 1210–1215.

Yu T, McIntyre JC, Bose SC, Hardin D, Owen MC & McClintock TS (2005). Differentially expressed transcripts from phenotypically identified olfactory sensory neurons. *J Comp Neurol* **483**, 251–262.

Zheng J & Sigworth FJ (1997). Selectivity changes during activation of mutant Shaker potassium channels. *J Gen Physiol* **110**, 101–117.

Author contributions

All authors contributed to the conception and design of the experiments and approved the final version of the manuscript. RT-PCR experiments were performed by G.M. and R.T. at the University of Parma. Immunohistochemistry was done by M.D. and electrophysiological experiments were performed by C.S. and A.B. at SISSA, Trieste.

Acknowledgements

We thank H. Zhao (The Johns Hopkins University School of Medicine, Baltimore, MD, USA) for kindly providing the mouse olfactory TMEM16b/anoctamin2 DNA construct; H. Stöhr (Universitat Regensburg, Regensburg, Germany) for the gift of the TMEM16b monoclonal antibody; S. Pifferi, F. Celsi and all members of the laboratory for discussions. This study was supported by grants from the Italian Ministry of Education, University and Research (MIUR) and from the Italian Institute of Technology.

4 DISCUSSION

The Ca^{2+}-activated Cl^- current in the cilia of olfactory sensory neurons accounts for most of the depolarizing current in olfactory transduction (Boccaccio & Menini, 2007; Kleene, 2008). Despite its important role, the molecular identity of olfactory Ca^{2+}-activated Cl^- current is not definitely established. Bestrophin2 (Pifferi *et al.*, 2006*b*; Klimmeck *et al.*, 2009) and TMEM16b (Yu *et al.*, 2005; Mayer *et al.*, 2009; Stephan *et al.*, 2009; Hengl *et al.*, 2010; Rasche *et al.*, 2010) are expressed in the cilia of mature olfactory sensory neurons and they have been shown to induce Ca^{2+}-activated Cl^- conductance when expressed in heterologous systems (Qu & Hartzell, 2004; Qu *et al.*, 2004; Pifferi *et al.*, 2006*b*; Schroeder *et al.*, 2008; Pifferi *et al.*, 2009*a*; Stephan *et al.*, 2009; Stöhr *et al.*, 2009). Both bestrophin2 and TMEM16b have been proposed to be a part of the Ca^{2+}-activated Cl^- channel involved in olfactory transduction.

In the first part of this Thesis we presented a comparison between the Ca^{2+}-activated Cl^- current in isolated olfactory sensory neurons from wild type and bestrophin2 knockout mice (Pifferi *et al.*, 2009*b*). In the second part of this Thesis we presented a comparison between the electrophysiological properties of the native Cl^- conductance and the Ca^{2+}-activated Cl^- currents induced by heterologous expression of TMEM16b olfactory splice variant (Sagheddu *et al.*, 2010).

Comparison between OSNs Ca^{2+}-activated Cl^- currents from wild type and bestrophin2 knockout mice.

Bestrophin2 protein is specifically localized in the cilia of mature olfactory sensory neurons (Pifferi *et al.*, 2006*b*; Klimmeck *et al.*, 2009). It has been indicated by Pifferi *et al.* (2006*b*) as a candidate for the Cl^- channel involved in olfactory transduction; indeed the Ca^{2+}-activated Cl^- currents of native olfactory channels and of bestrophin2 expressed in HEK 293 cells showed the same anion permeability sequence, current–voltage relations quite close to linearity, voltage-independent and side-specific blockage by NFA and SITS. Nonetheless for bestrophin2 currents $K_{½}$ was 0.4 μM, whereas for native currents $K_{½}$ was 4.7 μM showing a difference of one order of magnitude from the native current (Pifferi *et al.*, 2006*b*).

We analyzed more in detail the role of bestrophin 2 in olfactory transduction comparing wild type and knockout mice for this protein (Pifferi *et al.*, 2009*a*). We obtained similar EOG recordings in olfactory epithelium from wild type and knockout mice, indicating that the lack of bestrophin2 does not produce a big impairment in the odorant sensitivity. Ca^{2+}-activated Cl^- currents measured by using photolysis of caged 8-Br-cAMP or of caged Ca^{2+} within the cilia of isolated olfactory sensory neurons from wild type and knockout mice did not show significant differences. Finally, a Ca^{2+}-activated Cl^- current was still present in excised inside-out patches from knob/cilia of olfactory sensory neurons of knockout mice. From these results we concluded that the absence of bestrophin2 in the ciliary layer of the olfactory epithelium does not significantly alter the olfactory transduction, although the possibility that some compensatory mechanisms occur in bestrophin2 knockout mice cannot be excluded.

Bestrophin2 expression pattern in olfactory sensory neurons have been recently investigated by Klimmeck *et al.* (2009). In adult mice, bestrophin2 expression has been specifically found in the cilia of mature olfactory sensory neurons, whereas in postnatal day 1 (P1) mice, bestrophin2 expression has been detected at all subcellular levels in developing neurons. Therefore Klimmeck *et al.* (2009) suggested that bestrophin2 has a role in neurogenesis, maybe as a volume-regulated anion channel contributing to the coordinated extension of cell volume in developing sensory neurons.

Bestrophin2 may also have a role in the maintenance of the intraciliary ionic homeostasis since bestrophin2 and other bestrophins have been shown to be activated by osmotic cell swelling even in the absence of Ca^{2+}, indicating that they may be cell volume regulators (Fischmeister & Hartzell, 2005; Chien & Hartzell, 2007). Therefore the presence of bestrophin2 protein in the cilia of mature olfactory sensory neurons has been definitely confirmed (Pifferi *et al.*, 2006*b*; Klimmeck *et al.*, 2009; Pifferi *et al.*, 2009*b*), but further studies are required to better define its role in physiology of olfactory epithelium.

Comparison of functional properties of Ca^{2+}-activated Cl^- currents from OSNs and TMEM16b expressed in HEK 293 cells.

TMEM16b, a member of the recently characterized protein family TMEM16/Anoctamin, produces Ca^{2+}-activated Cl^- currents when expressed in different cell types (Schroeder *et al.*, 2008; Pifferi *et al.*, 2009*a*; Stephan *et al.*, 2009). TMEM16b mRNA has been shown to be specifically expressed in mature olfactory sensory neurons by in situ hybridization (Yu *et al.*, 2005; Hengl *et al.*, 2010); moreover proteomic screenings of ciliary membranes (Stephan *et al.*, 2009; Mayer *et al.*, 2009; Rasche *et al.*, 2010) and immunohistochemistry experiments (Rasche *et al.*, 2010; Hengl *et al.*, 2010) revealed that TMEM16b protein is localized in the olfactory cilia.

It has been shown that some electrophysiological properties of Ca^{2+}-activated Cl^- currents induced by mTMEM16b expressed in HEK 293 and of native currents in the cilia of olfactory sensory neurons are remarkably similar. Currents in olfactory cilia (Kleene & Gesteland, 1991; Kleene, 1993*b*; Kurahashi & Yau, 1993, Reisert *et al.*, 2003; Pifferi *et al.*, 2006*b*; reviewed by Kleene, 2008) and induced by TMEM16b (Pifferi *et al.*, 2009*a*; Stephan *et al.*, 2009) showed similar sensitivity to Ca^{2+} and other divalent cations, similar small channel conductance (~1 pS), similar current-voltage relationship at saturating concentration of Ca^{2+} and the same permeability sequence.

At present TMEM16b protein is the best molecular candidate for the Ca^{2+}-activated Cl^- current in olfactory transduction.

In this Thesis we provided a further comparison between the electrophysiological properties of the Ca^{2+}-activated Cl^- current in isolated olfactory sensory neurons and in

HEK 293 transfected with mTMEM16b. We used the whole-cell voltage clamp technique to record currents elicited by flash photolysis of caged calcium in the cilia of olfactory sensory neurons and in HEK 293 cells heterologously expressing the olfactory splice variant (Stephan *et al.*, 2009) of mTMEM16b.

The presence of TMEM16b at the surface of the olfactory epithelium was confirmed in immunohistochemistry experiments by using an anti-TMEM16b antibody (Stöhr *et al.*, 2009). In our pharmacology experiments the native current and the current induced by TMEM16b are strongly inhibited by extracellular application of NFA, DIDS and NPPB. In OSNs we confirmed extracellular blockage by NFA and showed extracellular blocking effects for NPPB and DIDS, two compounds that have been shown to be poorly effective when applied to the intracellular side of the membrane (Kleene & Gesteland, 1991). Similar side-specific effects of NPPB and DIDS on TMEM16b currents were obtained also in a previous study (Pifferi *et al.*, 2009*a*).

Ion selectivity of olfactory and mTMEM16b channels was determined by exchanging anions at the extracellular side of the membrane. We obtained for both channels the same permeability sequence, for some anions we also observed a gradual time-dependent shift of V_{rev} toward less negative values, indicating a decreased permeation through the channel. The finding that both native channel and TMEM16b display similar dynamic ion selectivity is a further point supporting the hypothesis that TMEM16b is a major subunit of the ciliary Ca^{2+}-activated Cl^- channel.

Conclusions

The molecular identity of the Ca^{2+}-activated Cl^- channel involved in olfactory transduction has not been definitely established. Bestrophin2 and TMEM16b proteins are expressed in the cilia of OSNs and they have been proposed as candidates for the olfactory Ca^{2+}-activated Cl^- channel. In this Thesis we showed that olfactory OSNs from bestrophin2 knockout mice still have Ca^{2+}-dependent Cl^- currents in the olfactory cilia and they do not show significant impairments in the electrical properties of olfactory transduction; therefore the role of bestrophin2 in the cilia of OSNs remains to be further investigated. We found specific similarities between the electrophysiological properties

of the native olfactory channel and TMEM16b, supporting the hypothesis that TMEM16b is likely to be the main molecular component of the Ca^{2+}-activated Cl^- channel.

Future studies should examine the presence of olfactory Ca^{2+}-activated Cl^- currents in mice in which the TMEM16b/anoctamin2 gene is deleted. Moreover, the combination of molecular biology studies and functional measurements will clarify if additional subunits and/or splice variants belonging to the TMEM16/Anoctamin or to other protein families are also part of the native Ca^{2+}-activated Cl^- channel.

5 REFERENCES

Adamek GD, Gesteland RC, Mair RG & Oakley B (1984). Transduction physiology of olfactory receptor cilia. *Brain Res* **310**, 87-97.

Angermann JE, Sanguinetti AR, Kenyon JL, Leblanc N & Greenwood IA (2006). Mechanism of the inhibition of Ca^{2+}-activated Cl^- currents by phosphorylation in pulmonary arterial smooth muscle cells. *J Gen Physiol* **128**, 73-87.

Anselmo AN, Earnest S, Chen W, Juang Y, Kim SC, Zhao Y & Cobb MH (2006). WNK1 and OSR1 regulate the Na^+, K^+, $2Cl^-$ cotransporter in HeLa cells. *Proc Natl Acad Sci U S A* **103**, 10883-10888.

Antolin S & Matthews HR (2007). The effect of external sodium concentration on sodium-calcium exchange in frog olfactory receptor cells. *J Physiol* **581**, 495-503.

Antolin S, Reisert J & Matthews HR (2010). Olfactory response termination involves Ca^{2+}-ATPase in vertebrate olfactory receptor neuron cilia. *J Gen Physiol* **135**, 367-378.

Arreola J, Begenisich T, Nehrke K, Nguyen H, Park K, Richardson L, Yang B, Schutte BC, Lamb FS & Melvin JE (2002). Secretion and cell volume regulation by salivary acinar cells from mice lacking expression of the Clcn3 Cl^- channel gene. *J Physiol* **545**, 207-216.

Arreola J, Melvin JE & Begenisich T (1998). Differences in regulation of Ca^{2+}-activated Cl- channels in colonic and parotid secretory cells. *Am J Physiol* **274**, C161-6.

Bader CR, Bertrand D & Schwartz EA (1982). Voltage-activated and calcium-activated currents studied in solitary rod inner segments from the salamander retina. *J Physiol* **331**, 253-284.

Bakall B, Marmorstein LY, Hoppe G, Peachey NS, Wadelius C & Marmorstein AD (2003). Expression and localization of bestrophin during normal mouse development. *Invest Ophthalmol Vis Sci* **44**, 3622-3628.

Bakall B, McLaughlin P, Stanton JB, Zhang Y, Hartzell HC, Marmorstein LY & Marmorstein AD (2008). Bestrophin-2 is involved in the generation of intraocular pressure. *Invest Ophthalmol Vis Sci* **49**, 1563-1570.

Bakalyar HA & Reed RR (1990). Identification of a specialized adenylyl cyclase that may mediate odorant detection. *Science* **250**, 1403-1406.

Bao L, Kaldany C, Holmstrand EC & Cox DH (2004). Mapping the BK_{Ca} channel's "Ca^{2+} bowl": side-chains essential for Ca^{2+} sensing. *J Gen Physiol* **123**, 475-489.

Barish ME (1983). A transient calcium-dependent chloride current in the immature *Xenopus* oocyte. *J Physiol* **342**, 309-325.

Barnes S & Hille B (1989). Ionic channels of the inner segment of tiger salamander cone photoreceptors. *J Gen Physiol* **94**, 719-743.

Barro Soria R, Spitzner M, Schreiber R & Kunzelmann K (2009). Bestrophin-1 enables Ca^{2+}-activated Cl^- conductance in epithelia. *J Biol Chem* **284**, 29405-29412.

Barro-Soria R, Aldehni F, Almaça J, Witzgall R, Schreiber R & Kunzelmann K (2010). ER-localized bestrophin 1 activates Ca^{2+}-dependent ion channels TMEM16A and SK4 possibly by acting as a counterion channel. *Pflugers Arch* **459**, 485-497.

Barro-Soria R, Schreiber R & Kunzelmann K (2008). Bestrophin 1 and 2 are components of the Ca^{2+} activated Cl^- conductance in mouse airways. *Biochim Biophys Acta* **1783**, 1993-2000.

Belluscio L, Gold GH, Nemes A & Axel R (1998). Mice deficient in G_{olf} are anosmic. *Neuron* **20**, 69-81.

Bera TK, Das S, Maeda H, Beers R, Wolfgang CD, Kumar V, Hahn Y, Lee B & Pastan I (2004). NGEP, a gene encoding a membrane protein detected only in prostate cancer and normal prostate. *Proc Natl Acad Sci U S A* **101**, 3059-3064.

Boccaccio A & Menini A (2007). Temporal development of cyclic nucleotide-gated and Ca^{2+} -activated Cl^- currents in isolated mouse olfactory sensory neurons. *J Neurophysiol* **98**, 153-160.

Boccaccio A, Lagostena L, Hagen V & Menini A (2006). Fast adaptation in mouse olfactory sensory neurons does not require the activity of phosphodiesterase. *J Gen Physiol* **128**, 171-184.

Borisy FF, Ronnett GV, Cunningham AM, Juilfs D, Beavo J & Snyder SH (1992). Calcium/calmodulin-activated phosphodiesterase expressed in olfactory receptor neurons. *J Neurosci* **12**, 915-923.

Bradley J, Li J, Davidson N, Lester HA & Zinn K (1994). Heteromeric olfactory cyclic nucleotide-gated channels: a subunit that confers increased sensitivity to cAMP. *Proc Natl Acad Sci U S A* **91**, 8890-8894.

Breer H, Fleischer J & Strotmann J (2006). The sense of smell: multiple olfactory subsystems. *Cell Mol Life Sci* **63**, 1465-1475.

Brennan PA & Zufall F (2006). Pheromonal communication in vertebrates. *Nature* **444**, 308-315.

Brunet LJ, Gold GH & Ngai J (1996). General anosmia caused by a targeted disruption of the mouse olfactory cyclic nucleotide-gated cation channel. *Neuron* **17**, 681-693.

Buck L & Axel R (1991). A novel multigene family may encode odorant receptors: a molecular basis for odor recognition. *Cell* **65**, 175-187.

Bönigk W, Bradley J, Müller F, Sesti F, Boekhoff I, Ronnett GV, Kaupp UB & Frings S (1999). The native rat olfactory cyclic nucleotide-gated channel is composed of three distinct subunits. *J Neurosci* **19**, 5332-5347.

Caggiano M, Kauer JS & Hunter DD (1994). Globose basal cells are neuronal progenitors in the olfactory epithelium: a lineage analysis using a replication-incompetent retrovirus. *Neuron* **13**, 339-352.

Calof AL, Bonnin A, Crocker C, Kawauchi S, Murray RC, Shou J & Wu H (2002). Progenitor cells of the olfactory receptor neuron lineage. *Microsc Res Tech* **58**, 176-188.

Caputo A, Caci E, Ferrera L, Pedemonte N, Barsanti C, Sondo E, Pfeffer U, Ravazzolo R, Zegarra-Moran O & Galietta LJV (2008). TMEM16A, a membrane protein associated with calcium-dependent chloride channel activity. *Science* **322**, 590-594.

Carafoli E & Brini M (2000). Calcium pumps: structural basis for and mechanism of calcium transmembrane transport. *Curr Opin Chem Biol* **4**, 152-161.

Carlson CB, Gunderson KA & Mosher DF (2008). Mutations targeting intermodular interfaces or calcium binding destabilize the thrombospondin-2 signature domain. *J Biol Chem* **283**, 27089-27099.

Castillo K, Delgado R & Bacigalupo J (2007). Plasma membrane Ca^{2+}-ATPase in the cilia of olfactory receptor neurons: possible role in Ca^{2+} clearance. *Eur J Neurosci* **26**, 2524-2531.

Chen TY & Yau KW (1994). Direct modulation by Ca^{2+}-calmodulin of cyclic nucleotide-activated channel of rat olfactory receptor neurons. *Nature* **368**, 545-548.

Cherry JA & Davis RL (1995). A mouse homolog of dunce, a gene important for learning and memory in Drosophila, is preferentially expressed in olfactory receptor neurons. *J Neurobiol* **28**, 102-113.

Chien L & Hartzell HC (2007). Drosophila bestrophin-1 chloride current is dually regulated by calcium and cell volume. *J Gen Physiol* **130**, 513-524.

Chien L, Zhang Z & Hartzell HC (2006). Single Cl^- channels activated by Ca^{2+} in Drosophila S2 cells are mediated by bestrophins. *J Gen Physiol* **128**, 247-259.

Chipperfield AR & Harper AA (2000). Chloride in smooth muscle. *Prog Biophys Mol Biol* **74**, 175-221.

Conti M & Beavo J (2007). Biochemistry and physiology of cyclic nucleotide phosphodiesterases: essential components in cyclic nucleotide signaling. *Annu Rev Biochem* **76**, 481-511.

Cygnar KD & Zhao H (2009). Phosphodiesterase 1C is dispensable for rapid response termination of olfactory sensory neurons. *Nat Neurosci* **12**, 454-462.

Cygnar KD, Stephan AB & Zhao H (2010). Analyzing responses of mouse olfactory sensory neurons using the air-phase electroolfactogram recording. *J Vis Exp* , .

Das S, Hahn Y, Nagata S, Willingham MC, Bera TK, Lee B & Pastan I (2007). NGEP, a prostate-specific plasma membrane protein that promotes the association of LNCaP cells. *Cancer Res* **67**, 1594-1601.

Das S, Hahn Y, Walker DA, Nagata S, Willingham MC, Peehl DM, Bera TK, Lee B & Pastan I (2008). Topology of NGEP, a prostate-specific cell:cell junction protein widely expressed in many cancers of different grade level. *Cancer Res* **68**, 6306-6312.

Davis MJ & Hill MA (1999). Signaling mechanisms underlying the vascular myogenic response. *Physiol Rev* **79**, 387-423.

De Castro F, Geijo-Barrientos E & Gallego R (1997). Calcium-activated chloride current in normal mouse sympathetic ganglion cells. *J Physiol* **498 (Pt 2)**, 397-408.

De La Fuente R, Namkung W, Mills A & Verkman AS (2008). Small-molecule screen identifies inhibitors of a human intestinal calcium-activated chloride channel. *Mol Pharmacol* **73**, 758-768.

Delgado R & Bacigalupo J (2004). Cilium-attached and excised patch-clamp recordings of odorant-activated Ca^{2+}-dependent K channels from chemosensory cilia of olfactory receptor neurons. *Eur J Neurosci* **20**, 2975-2980.

Delpire E (2009). The mammalian family of sterile 20p-like protein kinases. *Pflugers Arch* **458**, 953-967.

Delpire E & Gagnon KBE (2008). SPAK and OSR1: STE20 kinases involved in the regulation of ion homoeostasis and volume control in mammalian cells. *Biochem J* **409**, 321-331.

Dhallan RS, Yau KW, Schrader KA & Reed RR (1990). Primary structure and functional expression of a cyclic nucleotide-activated channel from olfactory neurons. *Nature* **347**, 184-187.

Dowd BFX & Forbush B (2003). PASK (proline-alanine-rich STE20-related kinase), a regulatory kinase of the Na^{+}-K^{+}-Cl^{-} cotransporter (NKCC1). *J Biol Chem* **278**, 27347-27353.

Duchamp-Viret P, Duchamp A & Chaput MA (2000). Peripheral odor coding in the rat and frog: quality and intensity specification. *J Neurosci* **20**, 2383-2390.

Edwards JC & Kahl CR (2010). Chloride channels of intracellular membranes. *FEBS Lett* **584**, 2102-2111.

Eggermont J (2004). Calcium-activated chloride channels: (un)known, (un)loved?. *Proc Am Thorac Soc* **1**, 22-27.

Eisenman G & Horn R (1983). Ionic selectivity revisited: the role of kinetic and equilibrium processes in ion permeation through channels. *J Membr Biol* **76**, 197-225.

Ferrera L, Caputo A, Ubby I, Bussani E, Zegarra-Moran O, Ravazzolo R, Pagani F & Galietta LJV (2009). Regulation of TMEM16A chloride channel properties by alternative splicing. *J Biol Chem* **284**, 33360-33368.

Firestein S (2001). How the olfactory system makes sense of scents. *Nature* **413**, 211-218.

Firestein S & Shepherd GM (1995). Interaction of anionic and cationic currents leads to a voltage dependence in the odor response of olfactory receptor neurons. *J Neurophysiol* **73**, 562-567.

Firestein S & Werblin F (1989). Odor-induced membrane currents in vertebrate-olfactory receptor neurons. *Science* **244**, 79-82.

Firestein S & Werblin FS (1987). Gated currents in isolated olfactory receptor neurons of the larval tiger salamander. *Proc Natl Acad Sci U S A* **84**, 6292-6296.

Firestein S, Picco C & Menini A (1993). The relation between stimulus and response in olfactory receptor cells of the tiger salamander. *J Physiol* **468**, 1-10.

Firestein S, Shepherd GM & Werblin FS (1990). Time course of the membrane current underlying sensory transduction in salamander olfactory receptor neurons. *J Physiol* **430**, 135-158.

Firestein S, Zufall F & Shepherd GM (1991). Single odor-sensitive channels in olfactory receptor neurons are also gated by cyclic nucleotides. *J Neurosci* **11**, 3565-3572.

Fischmeister R & Hartzell HC (2005). Volume sensitivity of the bestrophin family of chloride channels. *J Physiol* **562**, 477-491.

Flores CA, Cid LP, Sepúlveda FV & Niemeyer MI (2009). TMEM16 proteins: the long awaited calcium-activated chloride channels?. *Braz J Med Biol Res* **42**, 993-1001.

Frings S (2001). Chemoelectrical signal transduction in olfactory sensory neurons of air-breathing vertebrates. *Cell Mol Life Sci* **58**, 510-519.

Frings S & Lindemann B (1990). Single unit recording from olfactory cilia. *Biophys J* **57**, 1091-1094.

Frings S, Lynch JW & Lindemann B (1992). Properties of cyclic nucleotide-gated channels mediating olfactory transduction. Activation, selectivity, and blockage. *J Gen Physiol* **100**, 45-67.

Frings S, Reuter D & Kleene SJ (2000). Neuronal Ca^{2+}-activated Cl^- channels-homing in on an elusive channel species. *Prog Neurobiol* **60**, 247-289.

Gagnon KBE, England R & Delpire E (2007). A single binding motif is required for SPAK activation of the Na-K-2Cl cotransporter. *Cell Physiol Biochem* **20**, 131-142.

Galietta LJV (2009). The TMEM16 protein family: a new class of chloride channels?. *Biophys J* **97**, 3047-3053.

Galindo BE & Vacquier VD (2005). Phylogeny of the TMEM16 protein family: some members are overexpressed in cancer. *Int J Mol Med* **16**, 919-924.

Getchell TV (1986). Functional properties of vertebrate olfactory receptor neurons. *Physiol Rev* **66**, 772-818.

Gritli-Linde A, Vaziri Sani F, Rock JR, Hallberg K, Iribarne D, Harfe BD & Linde A (2009). Expression patterns of the Tmem16 gene family during cephalic development in the mouse. *Gene Expr Patterns* **9**, 178-191.

Grosmaitre X, Vassalli A, Mombaerts P, Shepherd GM & Ma M (2006). Odorant responses of olfactory sensory neurons expressing the odorant receptor MOR23: a patch clamp analysis in gene-targeted mice. *Proc Natl Acad Sci U S A* **103**, 1970-1975.

Gruber AD & Pauli BU (1999). Molecular cloning and biochemical characterization of a truncated, secreted member of the human family of Ca^{2+}-activated Cl^- channels. *Biochim Biophys Acta* **1444**, 418-423.

Hallani M, Lynch JW & Barry PH (1998). Characterization of calcium-activated chloride channels in patches excised from the dendritic knob of mammalian olfactory receptor neurons. *J Membr Biol* **161**, 163-171.

Hartzell C, Putzier I & Arreola J (2005). Calcium-activated chloride channels. *Annu Rev Physiol* **67**, 719-758.

Hartzell HC & Qu Z (2003). Chloride currents in acutely isolated *Xenopus* retinal pigment epithelial cells. *J Physiol* **549**, 453-469.

Hartzell HC, Qu Z, Yu K, Xiao Q & Chien L (2008). Molecular physiology of bestrophins: multifunctional membrane proteins linked to best disease and other retinopathies. *Physiol Rev* **88**, 639-672.

Hartzell HC, Yu K, Xiao Q, Chien L & Qu Z (2009). Anoctamin/TMEM16 family members are Ca^{2+}-activated Cl^- channels. *J Physiol* **587**, 2127-2139.

Hengl T, Kaneko H, Dauner K, Vocke K, Frings S & Möhrlen F (2010). Molecular components of signal amplification in olfactory sensory cilia. *Proc Natl Acad Sci U S A* **107**, 6052-6057.

Hennig B, Schultheiss G, Kunzelmann K & Diener M (2008). Ca^{2+}-induced Cl^- efflux at rat distal colonic epithelium. *J Membr Biol* **221**, 61-72.

Hille B (2001). *Ionic Channels of Excitable Membranes*. Sinauer Associates, Inc., Sunderland, MA.

Huang F, Rock JR, Harfe BD, Cheng T, Huang X, Jan YN & Jan LY (2009). Studies on expression and function of the TMEM16A calcium-activated chloride channel. *Proc Natl Acad Sci U S A* **106**, 21413-21418.

Huang X, Godfrey TE, Gooding WE, McCarty KSJ & Gollin SM (2006). Comprehensive genome and transcriptome analysis of the 11q13 amplicon in human oral cancer and synteny to the 7F5 amplicon in murine oral carcinoma. *Genes Chromosomes Cancer* **45**, 1058-1069.

Jones DT & Reed RR (1989). G_{olf}: an olfactory neuron specific-G protein involved in odorant signal transduction. *Science* **244**, 790-795.

Juilfs DM, Fülle HJ, Zhao AZ, Houslay MD, Garbers DL & Beavo JA (1997). A subset of olfactory neurons that selectively express cGMP-stimulated phosphodiesterase (PDE2) and guanylyl cyclase-D define a unique olfactory signal transduction pathway. *Proc Natl Acad Sci U S A* **94**, 3388-3395.

Jung A, Lischka FW, Engel J & Schild D (1994). Sodium/calcium exchanger in olfactory receptor neurons of *Xenopus laevis*. *Neuroreport* **5**, 1741-1744.

Kalay E, Caylan R, Kiroglu AF, Yasar T, Collin RWJ, Heister JGAM, Oostrik J, Cremers CWRJ, Brunner HG, Karaguzel A & Kremer H (2007). A novel locus for autosomal recessive nonsyndromic hearing impairment, DFNB63, maps to chromosome 11q13.2-q13.4. *J Mol Med* **85**, 397-404.

Kaneko H, Möhrlen F & Frings S (2006). Calmodulin contributes to gating control in olfactory calcium-activated chloride channels. *J Gen Physiol* **127**, 737-748.

Kaneko H, Nakamura T & Lindemann B (2001). Non invasive measurement of chloride concentration in rat olfactory receptor cells with use of a fluorescent dye. *Am J Physiol Cell Physiol* **280**, C1387-93.

Kaneko H, Putzier I, Frings S, Kaupp UB & Gensch T (2004). Chloride accumulation in mammalian olfactory sensory neurons. *J Neurosci* **24**, 7931-7938.

Katoh M & Katoh M (2003). FLJ10261 gene, located within the CCND1-EMS1 locus on human chromosome 11q13, encodes the eight-transmembrane protein homologous to C12orf3, C11orf25 and FLJ34272 gene products. *Int J Oncol* **22**, 1375-1381.

Katoh M & Katoh M (2004). Characterization of human TMEM16G gene *in silico. Int J Mol Med* **14**, 759-764.

Katoh M & Katoh M (2004). Identification and characterization of TMEM16E and TMEM16F genes *in silico. Int J Oncol* **24**, 1345-1349.

Katoh M & Katoh M (2004). GDD1 is identical to TMEM16E, a member of the TMEM16 family. *Am J Hum Genet* **75**, 927-8; author reply 928.

Katoh M & Katoh M (2005). Identification and characterization of TMEM16H gene *in silico. Int J Mol Med* **15**, 353-358.

Kaupp UB (2010). Olfactory signaling in vertebrates and insects: differences and commonalities. *Nat Rev Neurosci* **11**, 188-200.

Kaupp UB & Seifert R (2002). Cyclic nucleotide-gated ion channels. *Physiol Rev* **82**, 769-824.

Kaupp UB, Niidome T, Tanabe T, Terada S, Bönigk W, Stühmer W, Cook NJ, Kangawa K, Matsuo H, Hirose T & et al. (1989). Primary structure and functional expression from complementary DNA of the rod photoreceptor cyclic GMP-gated channel. *Nature* **342**, 762-766.

Kern RC, Kerr TP & Getchell TV (1991). Ultrastructural localization of Na^+/K^+-ATPase in rodent olfactory epithelium. *Brain Res* **546**, 8-17.

Kim Y, Chattopadhyay S, Locke S & Pearce DA (2005). Interaction among Btn1p, Btn2p, and Ist2p reveals potential interplay among the vacuole, amino acid levels, and ion homeostasis in the yeast *Saccharomyces cerevisiae*. *Eukaryot Cell* **4**, 281-288.

Kleene SJ (1993*a*). The cyclic nucleotide-activated conductance in olfactory cilia: effects of cytoplasmic Mg^{2+} and Ca^{2+}. *J Memebrane Biol* **131**, 237-243

Kleene SJ (1993*b*). Origin of the chloride current in olfactory transduction. *Neuron* **11**, 123-132.

Kleene SJ (1994). Inhibition of olfactory cyclic nucleotide-activated current by calmodulin antagonists. *Br J Pharmacol* **111**, 469-472.

Kleene SJ (1995). Block by external calcium and magnesium of the cyclic-nucleotide-activated current in olfactory cilia. *Neuroscience* **66**, 1001-1008.

Kleene SJ (1997). High-gain, low-noise amplification in olfactory transduction. *Biophys J* **73**, 1110-1117.

Kleene SJ (1999). Both external and internal calcium reduce the sensitivity of the olfactory cyclic-nucleotide-gated channel to cAMP. *J Neurophysiol* **81**, 2675-2682.

Kleene SJ (2008). The electrochemical basis of odor transduction in vertebrate olfactory cilia. *Chem Senses* **33**, 839-859.

Kleene SJ (2009). Limits of calcium clearance by plasma membrane calcium ATPase in olfactory cilia. *PLoS ONE* **4**, e5266.

Kleene SJ & Gesteland RC (1991). Calcium-activated chloride conductance in frog olfactory cilia. *J Neurosci* **11**, 3624-3629.

Klimmeck D, Daiber PC, Brühl A, Baumann A, Frings S & Möhrlen F (2009). Bestrophin 2: an anion channel associated with neurogenesis in chemosensory systems. *J Comp Neurol* **515**, 585-599.

Klimmeck D, Mayer U, Ungerer N, Warnken U, Schnölzer M, Frings S & Möhrlen F (2008). Calcium-signaling networks in olfactory receptor neurons. *Neuroscience* **151**, 901-912.

Kranjc A, Grillo FW, Rievaj J, Boccaccio A, Pietrucci F, Menini A, Carloni P & Anselmi C (2009). Regulation of bestrophins by Ca^{2+}: a theoretical and experimental study. *PLoS ONE* **4**, e4672.

Krämer F, Mohr N, Kellner U, Rudolph G & Weber BHF (2003). Ten novel mutations in VMD2 associated with Best macular dystrophy (BMD). *Hum Mutat* **22**, 418.

Krämer F, Stöhr H & Weber BHF (2004). Cloning and characterization of the murine Vmd2 RFP-TM gene family. *Cytogenet Genome Res* **105**, 107-114.

Kunzelmann K, Kongsuphol P, Aldehni F, Tian Y, Ousingsawat J, Warth R & Schreiber R (2009). Bestrophin and TMEM16-Ca^{2+} activated Cl^- channels with different functions. *Cell Calcium* **46**, 233-241.

Kunzelmann K, Milenkovic VM, Spitzner M, Soria RB & Schreiber R (2007). Calcium-dependent chloride conductance in epithelia: is there a contribution by Bestrophin?. *Pflugers Arch* **454**, 879-889.

Kurahashi T (1989). Activation by odorants of cation-selective conductance in the olfactory receptor cell isolated from the newt. *J Physiol* **419**, 177-192.

Kurahashi T (1990). The response induced by intracellular cyclic AMP in isolated olfactory receptor cells of the newt. *J Physiol* **430**, 355-371.

Kurahashi T & Kaneko A (1991). High density cAMP-gated channels at the ciliary membrane in the olfactory receptor cell. *Neuroreport* **2**, 5-8.

Kurahashi T & Yau KW (1993). Co-existence of cationic and chloride components in odorant-induced current of vertebrate olfactory receptor cells. *Nature* **363**, 71-74.

Kuruma A & Hartzell HC (2000). Bimodal control of a Ca^{2+}-activated Cl^- channel by different Ca^{2+} signals. *J Gen Physiol* **115**, 59-80.

Lagostena L & Menini A (2003). Whole-cell recordings and photolysis of caged compounds in olfactory sensory neurons isolated from the mouse. *Chem Senses* **28**, 705-716.

Lalonde MR, Kelly ME & Barnes S (2008). Calcium-activated chloride channels in the retina. *Channels (Austin)* **2**, 252-260.

Lancet D (1986). Vertebrate olfactory reception. *Annu Rev Neurosci* **9**, 329-355.

Large WA & Wang Q (1996). Characteristics and physiological role of the Ca^{2+}-activated Cl- conductance in smooth muscle. *Am J Physiol* **271**, C435-54.

Larsson HP, Kleene SJ & Lecar H (1997). Noise analysis of ion channels in non-space-clamped cables: estimates of channel parameters in olfactory cilia. *Biophys J* **72**, 1193-1203.

Leblanc N, Ledoux J, Saleh S, Sanguinetti A, Angermann J, O'Driscoll K, Britton F, Perrino BA & Greenwood IA (2005). Regulation of calcium-activated chloride channels in smooth muscle cells: a complex picture is emerging. *Can J Physiol Pharmacol* **83**, 541-556.

Lee S, Yoon B, Berglund K, Oh S, Park H, Shin H, Augustine GJ & Lee CJ (2010). Channel-Mediated Tonic GABA Release from Glia. *Science* , .

Leinders-Zufall T, Greer CA, Shepherd GM & Zufall F (1998). Imaging odor-induced calcium transients in single olfactory cilia: specificity of activation and role in transduction. *J Neurosci* **18**, 5630-5639.

Leinders-Zufall T, Rand MN, Shepherd GM, Greer CA & Zufall F (1997). Calcium entry through cyclic nucleotide-gated channels in individual cilia of olfactory receptor cells: spatiotemporal dynamics. *J Neurosci* **17**, 4136-4148.

Leung CT, Coulombe PA & Reed RR (2007). Contribution of olfactory neural stem cells to tissue maintenance and regeneration. *Nat Neurosci* **10**, 720-726.

Lidow MS & Menco BP (1984). Observations on axonemes and membranes of olfactory and respiratory cilia in frogs and rats using tannic acid-supplemented fixation and photographic rotation. *J Ultrastruct Res* **86**, 18-30.

Liman ER & Buck LB (1994). A second subunit of the olfactory cyclic nucleotide-gated channel confers high sensitivity to cAMP. *Neuron* **13**, 611-621.

Lin W, Arellano J, Slotnick B & Restrepo D (2004). Odors detected by mice deficient in cyclic nucleotide-gated channel subunit A2 stimulate the main olfactory system. *J Neurosci* **24**, 3703-3710.

Liu M, Chen TY, Ahamed B, Li J & Yau KW (1994). Calcium-calmodulin modulation of the olfactory cyclic nucleotide-gated cation channel. *Science* **266**, 1348-1354.

Lo YH, Bradley TM & Rhoads DE (1991). L-alanine binding sites and Na^+/ K^+-ATPase in cilia and other membrane fractions from olfactory rosettes of Atlantic salmon. *Comp Biochem Physiol B* **98**, 121-126.

Lowe G & Gold GH (1993). Contribution of the ciliary cyclic nucleotide-gated conductance to olfactory transduction in the salamander. *J Physiol* **462**, 175-196.

Lowe G & Gold GH (1993). Nonlinear amplification by calcium-dependent chloride channels in olfactory receptor cells. *Nature* **366**, 283-286.

Ludwig J, Margalit T, Eismann E, Lancet D & Kaupp UB (1990). Primary structure of cAMP-gated channel from bovine olfactory epithelium. *FEBS Lett* **270**, 24-29.

Ma M (2007). Encoding olfactory signals via multiple chemosensory systems. *Crit Rev Biochem Mol Biol* **42**, 463-480.

Ma M, Chen WR & Shepherd GM (1999). Electrophysiological characterization of rat and mouse olfactory receptor neurons from an intact epithelial preparation. *J Neurosci Methods* **92**, 31-40.

Malnic B, Hirono J, Sato T & Buck LB (1999). Combinatorial receptor codes for odors. *Cell* **96**, 713-723.

Maricq AV & Korenbrot JI (1988). Calcium and calcium-dependent chloride currents generate action potentials in solitary cone photoreceptors. *Neuron* **1**, 503-515.

Marmorstein AD, Cross HE & Peachey NS (2009). Functional roles of bestrophins in ocular epithelia. *Prog Retin Eye Res* **28**, 206-226.

Marmorstein AD, Marmorstein LY, Rayborn M, Wang X, Hollyfield JG & Petrukhin K (2000). Bestrophin, the product of the Best vitelliform macular dystrophy gene (VMD2), localizes to the basolateral plasma membrane of the retinal pigment epithelium. *Proc Natl Acad Sci U S A* **97**, 12758-12763.

Marmorstein LY, Wu J, McLaughlin P, Yocom J, Karl MO, Neussert R, Wimmers S, Stanton JB, Gregg RG, Strauss O, Peachey NS & Marmorstein AD (2006). The light peak of the electroretinogram is dependent on voltage-gated calcium channels and antagonized by bestrophin (best-1). *J Gen Physiol* **127**, 577-589.

Marquardt A, Stöhr H, Passmore LA, Krämer F, Rivera A & Weber BH (1998). Mutations in a novel gene, VMD2, encoding a protein of unknown properties cause juvenile-onset vitelliform macular dystrophy (Best's disease). *Hum Mol Genet* **7**, 1517-1525.

Mayer U, Küller A, Daiber PC, Neudorf I, Warnken U, Schnölzer M, Frings S & Möhrlen F (2009). The proteome of rat olfactory sensory cilia. *Proteomics* **9**, 322-334.

Mayer U, Ungerer N, Klimmeck D, Warnken U, Schnölzer M, Frings S & Möhrlen F (2008). Proteomic analysis of a membrane preparation from rat olfactory sensory cilia. *Chem Senses* **33**, 145-162.

Menco B (1992). Ultrastructural studies on membrane, cytoskeletal, mucous, and protective compartments in olfaction. *Microsc Res Tech* **22**, 215-224.

Menco BP (1980). Qualitative and quantitative freeze-fracture studies on olfactory and nasal respiratory structures of frog, ox, rat, and dog. I. A general survey. *Cell Tissue Res* **207**, 183-209.

Menco BP (1997). Ultrastructural aspects of olfactory signaling. *Chem Senses* **22**, 295-311.

Menco BP, Birrell GB, Fuller CM, Ezeh PI, Keeton DA & Benos DJ (1998). Ultrastructural localization of amiloride-sensitive sodium channels and Na^+/K^+-ATPase in the rat's olfactory epithelial surface. *Chem Senses* **23**, 137-149.

Menco BPM (2005). The fine-structural distribution of G-protein receptor kinase 3, beta-arrestin-2, Ca^{2+}/calmodulin-dependent protein kinase II and phosphodiesterase PDE1C2, and a Cl^--cotransporter in rodent olfactory epithelia. *J Neurocytol* **34**, 11-36.

Michalakis S, Reisert J, Geiger H, Wetzel C, Zong X, Bradley J, Spehr M, Hüttl S, Gerstner A, Pfeifer A, Hatt H, Yau K & Biel M (2006). Loss of CNGB1 protein leads to

olfactory dysfunction and subciliary cyclic nucleotide-gated channel trapping. *J Biol Chem* **281**, 35156-35166.

Miledi R (1982). A calcium-dependent transient outward current in *Xenopus laevis* oocytes. *Proc R Soc Lond B Biol Sci* **215**, 491-497.

Milenkovic VM, Rivera A, Horling F & Weber BHF (2007). Insertion and topology of normal and mutant bestrophin-1 in the endoplasmic reticulum membrane. *J Biol Chem* **282**, 1313-1321.

Mizuta K, Tsutsumi S, Inoue H, Sakamoto Y, Miyatake K, Miyawaki K, Noji S, Kamata N & Itakura M (2007). Molecular characterization of GDD1/TMEM16E, the gene product responsible for autosomal dominant gnathodiaphyseal dysplasia. *Biochem Biophys Res Commun* **357**, 126-132.

Mombaerts P (1999). Molecular biology of odorant receptors in vertebrates. *Annu Rev Neurosci* **22**, 487-509.

Mombaerts P (2001). The human repertoire of odorant receptor genes and pseudogenes. *Annu Rev Genomics Hum Genet* **2**, 493-510.

Mombaerts P (2004). Genes and ligands for odorant, vomeronasal and taste receptors. *Nat Rev Neurosci* **5**, 263-278.

Mori K, Nagao H & Yoshihara Y (1999). The olfactory bulb: coding and processing of odor molecule information. *Science* **286**, 711-715.

Morrison EE & Costanzo RM (1990). Morphology of the human olfactory epithelium. *J Comp Neurol* **297**, 1-13.

Mullins RF, Kuehn MH, Faidley EA, Syed NA & Stone EM (2007). Differential macular and peripheral expression of bestrophin in human eyes and its implication for best disease. *Invest Ophthalmol Vis Sci* **48**, 3372-3380.

Munger SD, Leinders-Zufall T & Zufall F (2009). Subsystem organization of the mammalian sense of smell. *Annu Rev Physiol* **71**, 115-140.

Nakamura T (2000). Cellular and molecular constituents of olfactory sensation in vertebrates. *Comp Biochem Physiol A Mol Integr Physiol* **126**, 17-32.

Nakamura T & Gold GH (1987). A cyclic nucleotide-gated conductance in olfactory receptor cilia. *Nature* **325**, 442-444.

Nakamura T, Kaneko H & Nishida N (1997). Direct measurement of the chloride concentration in newt olfactory receptors with the fluorescent probe. *Neurosci Lett* **237**, 5-8.

Nei M, Niimura Y & Nozawa M (2008). The evolution of animal chemosensory receptor gene repertoires: roles of chance and necessity. *Nat Rev Genet* **9**, 951-963.

Nickell WT, Kleene NK & Kleene SJ (2007). Mechanisms of neuronal chloride accumulation in intact mouse olfactory epithelium. *J Physiol* **583**, 1005-1020.

Nickell WT, Kleene NK, Gesteland RC & Kleene SJ (2006). Neuronal chloride accumulation in olfactory epithelium of mice lacking NKCC1. *J Neurophysiol* **95**, 2003-2006.

Nilius B, Prenen J, Szücs G, Wei L, Tanzi F, Voets T & Droogmans G (1997). Calcium-activated chloride channels in bovine pulmonary artery endothelial cells. *J Physiol* **498 (Pt 2)**, 381-396.

Noé J, Tareilus E, Boekhoff I & Breer H (1997). Sodium/calcium exchanger in rat olfactory neurons. *Neurochem Int* **30**, 523-531.

Otowa T, Yoshida E, Sugaya N, Yasuda S, Nishimura Y, Inoue K, Tochigi M, Umekage T, Miyagawa T, Nishida N, Tokunaga K, Tanii H, Sasaki T, Kaiya H & Okazaki Y (2009). Genome-wide association study of panic disorder in the Japanese population. *J Hum Genet* **54**, 122-126.

Ottoson D (1955). Analysis of the electrical activity of the olfactory epithelium. *Acta Physiol Scand Suppl* **35**, 1-83.

Ousingsawat J, Martins JR, Schreiber R, Rock JR, Harfe BD & Kunzelmann K (2009). Loss of TMEM16A causes a defect in epithelial Ca^{2+}-dependent chloride transport. *J Biol Chem* **284**, 28698-28703.

Pace U, Hanski E, Salomon Y & Lancet D (1985). Odorant-sensitive adenylyl cyclase may mediate olfactory reception. *Nature* **316**, 255-258.

Petrukhin K, Koisti MJ, Bakall B, Li W, Xie G, Marknell T, Sandgren O, Forsman K, Holmgren G, Andreasson S, Vujic M, Bergen AA, McGarty-Dugan V, Figueroa D, Austin CP, Metzker ML, Caskey CT & Wadelius C (1998). Identification of the gene responsible for Best macular dystrophy. *Nat Genet* **19**, 241-247.

Pifferi S, Boccaccio A & Menini A (2006*a*). Cyclic nucleotide-gated ion channels in sensory transduction. *FEBS Lett* **580**, 2853-2859.

Pifferi S, Dibattista M & Menini A (2009*a*). TMEM16B induces chloride currents activated by calcium in mammalian cells. *Pflugers Arch* **458**, 1023-1038.

Pifferi S, Dibattista M, Sagheddu C, Boccaccio A, Al Qteishat A, Ghirardi F, Tirindelli R & Menini A (2009*b*). Calcium-activated chloride currents in olfactory sensory neurons from mice lacking bestrophin-2. *J Physiol* **587**, 4265-4279.

Pifferi S, Menini A & Kurahashi T (2009*c*). Signal transduction in vertebrate olfactory cilia. In *The Neurobiology of Olfaction*, ed. Menini A, pp. 203-224. CRC Press, Taylor & Francis Group, Boca Raton, FL.

Pifferi S, Pascarella G, Boccaccio A, Mazzatenta A, Gustincich S, Menini A & Zucchelli S (2006*b*). Bestrophin-2 is a candidate calcium-activated chloride channel involved in olfactory transduction. *Proc Natl Acad Sci U S A* **103**, 12929-12934.

Pluznick JL, Zou D, Zhang X, Yan Q, Rodriguez-Gil DJ, Eisner C, Wells E, Greer CA, Wang T, Firestein S, Schnermann J & Caplan MJ (2009). Functional expression of the olfactory signaling system in the kidney. *Proc Natl Acad Sci U S A* **106**, 2059-2064.

Pusch M (2004). Ca^{2+}-activated chloride channels go molecular. *J Gen Physiol* **123**, 323-325.

Pyrski M, Koo JH, Polumuri SK, Ruknudin AM, Margolis JW, Schulze DH & Margolis FL (2007). Sodium/calcium exchanger expression in the mouse and rat olfactory systems. *J Comp Neurol* **501**, 944-958.

Qu Z & Hartzell C (2004). Determinants of anion permeation in the second transmembrane domain of the mouse bestrophin-2 chloride channel. *J Gen Physiol* **124**, 371-382.

Qu Z & Hartzell HC (2008). Bestrophin Cl^- channels are highly permeable to HCO_3^-. *Am J Physiol Cell Physiol* **294**, C1371-7.

Qu Z, Chien L, Cui Y & Hartzell HC (2006). The anion-selective pore of the bestrophins, a family of chloride channels associated with retinal degeneration. *J Neurosci* **26**, 5411-5419.

Qu Z, Fischmeister R & Hartzell C (2004). Mouse bestrophin-2 is a bona fide Cl^- channel: identification of a residue important in anion binding and conduction. *J Gen Physiol* **123**, 327-340.

Qu Z, Wei RW, Mann W & Hartzell HC (2003). Two bestrophins cloned from Xenopus laevis oocytes express Ca^{2+}-activated Cl^- currents. *J Biol Chem* **278**, 49563-49572.

Ran S, Fuller CM, Arrate MP, Latorre R & Benos DJ (1992). Functional reconstitution of a chloride channel protein from bovine trachea. *J Biol Chem* **267**, 20630-20637.

Rasche S, Toetter B, Adler J, Tschapek A, Doerner JF, Kurtenbach S, Hatt H, Meyer H, Warscheid B & Neuhaus EM (2010). Tmem16b is specifically expressed in the cilia of olfactory sensory neurons. *Chem Senses* **35**, 239-245.

Reisert J & Matthews HR (1998). Na^+-dependent Ca^{2+} extrusion governs response recovery in frog olfactory receptor cells. *J Gen Physiol* **112**, 529-535.

Reisert J & Matthews HR (1999). Adaptation of the odor-induced response in frog olfactory receptor cells. *J Physiol* **519 Pt 3**, 801-813.

Reisert J & Matthews HR (2001). Simultaneous recording of receptor current and intraciliary Ca^{2+} concentration in salamander olfactory receptor cells. *J Physiol* **535**, 637-645.

Reisert J, Bauer PJ, Yau K & Frings S (2003). The Ca^{2+}-activated Cl^- channel and its control in rat olfactory receptor neurons. *J Gen Physiol* **122**, 349-363.

Reisert J, Lai J, Yau K & Bradley J (2005). Mechanism of the excitatory Cl^- response in mouse olfactory receptor neurons. *Neuron* **45**, 553-561.

Reisert J, Yau K & Margolis FL (2007). Olfactory marker protein modulates the cAMP kinetics of the odor-induced response in cilia of mouse olfactory receptor neurons. *J Physiol* **585**, 731-740.

Ressler KJ, Sullivan SL & Buck LB (1993). A zonal organization of odorant receptor gene expression in the olfactory epithelium. *Cell* **73**, 597-609.

Restrepo D, Okada Y & Teeter JH (1993). Odorant-regulated Ca^{2+} gradients in rat olfactory neurons. *J Gen Physiol* **102**, 907-924.

Reuter D, Zierold K, Schröder WH & Frings S (1998). A depolarizing chloride current contributes to chemoelectrical transduction in olfactory sensory neurons in situ. *J Neurosci* **18**, 6623-6630.

Rock JR & Harfe BD (2008). Expression of TMEM16 paralogs during murine embryogenesis. *Dev Dyn* **237**, 2566-2574.

Rock JR, Futtner CR & Harfe BD (2008). The transmembrane protein TMEM16A is required for normal development of the murine trachea. *Dev Biol* **321**, 141-149.

Rock JR, O'Neal WK, Gabriel SE, Randell SH, Harfe BD, Boucher RC & Grubb BR (2009). Transmembrane protein 16A (TMEM16A) is a Ca^{2+}-regulated Cl^- secretory channel in mouse airways. *J Biol Chem* **284**, 14875-14880.

Rodriguez I (2007). Odorant and pheromone receptor gene regulation in vertebrates. *Curr Opin Genet Dev* **17**, 465-470.

Sagheddu C, Boccaccio A, Dibattista M, Montani G, Tirindelli R & Menini A (2010). Calcium concentration jumps reveal dynamic ion selectivity of calcium-activated chloride currents in mouse olfactory sensory neurons and TMEM16b-transfected HEK 293T cells. *J Physiol* **588**, 4189–4204.

Saidu SP, Weeraratne SD, Valentine M, Delay R & Van Houten JL (2009). Role of plasma membrane calcium ATPases in calcium clearance from olfactory sensory neurons. *Chem Senses* **34**, 349-358.

Sautter A, Zong X, Hofmann F & Biel M (1998). An isoform of the rod photoreceptor cyclic nucleotide-gated channel beta subunit expressed in olfactory neurons. *Proc Natl Acad Sci U S A* **95**, 4696-4701.

Schild D & Restrepo D (1998). Transduction mechanisms in vertebrate olfactory receptor cells. *Physiol Rev* **78**, 429-466.

Schneppenheim R, Castaman G, Federici AB, Kreuz W, Marschalek R, Oldenburg J, Oyen F & Budde U (2007). A common 253-kb deletion involving VWF and TMEM16B in German and Italian patients with severe von Willebrand disease type 3. *J Thromb Haemost* **5**, 722-728.

Schoenfeld TA & Cleland TA (2005). The anatomical logic of smell. *Trends Neurosci* **28**, 620-627.

Schreiber M & Salkoff L (1997). A novel calcium-sensing domain in the BK channel. *Biophys J* **73**, 1355-1363.

Schreiber R, Uliyakina I, Kongsuphol P, Warth R, Mirza M, Martins JR & Kunzelmann K (2010). Expression and function of epithelial anoctamins. *J Biol Chem* **285**, 7838-7845.

Schroeder BC, Cheng T, Jan YN & Jan LY (2008). Expression cloning of TMEM16A as a calcium-activated chloride channel subunit. *Cell* **134**, 1019-1029.

Schwob JE (2002). Neural regeneration and the peripheral olfactory system. *Anat Rec* **269**, 33-49.

Scott JW & Scott-Johnson PE (2002). The electroolfactogram: a review of its history and uses. *Microsc Res Tech* **58**, 152-160.

Scott RH, Woods AJ, Lacey MJ, Fernando D, Crawford JH & Andrews PL (1995). An electrophysiological investigation of the effects of cisplatin and the protective actions of dexamethasone on cultured dorsal root ganglion neurons from neonatal rats. *Naunyn Schmiedebergs Arch Pharmacol* **352**, 247-255.

Shirley SG, Robinson CJ, Dickinson K, Aujla R & Dodd GH (1986). Olfactory adenylyl cyclase of the rat. Stimulation by odorants and inhibition by Ca^{2+}. *Biochem J* **240**, 605-607.

Sicard G & Holley A (1984). Receptor cell responses to odorants: similarities and differences among odorants. *Brain Res* **292**, 283-296.

Sklar PB, Anholt RR & Snyder SH (1986). The odorant-sensitive adenylate cyclase of olfactory receptor cells. Differential stimulation by distinct classes of odorants. *J Biol Chem* **261**, 15538-15543.

Smith DW, Thach S, Marshall EL, Mendoza M & Kleene SJ (2008). Mice lacking NKCC1 have normal olfactory sensitivity. *Physiol Behav* **93**, 44-49.

Song Y, Cygnar KD, Sagdullaev B, Valley M, Hirsh S, Stephan A, Reisert J & Zhao H (2008). Olfactory CNG channel desensitization by Ca^{2+}/CaM via the B1b subunit affects response termination but not sensitivity to recurring stimulation. *Neuron* **58**, 374-386.

Spehr M, Gisselmann G, Poplawski A, Riffell JA, Wetzel CH, Zimmer RK & Hatt H (2003). Identification of a testicular odorant receptor mediating human sperm chemotaxis. *Science* **299**, 2054-2058.

Stephan AB, Shum EY, Hirsh S, Cygnar KD, Reisert J & Zhao H (2009). ANO2 is the cilial calcium-activated chloride channel that may mediate olfactory amplification. *Proc Natl Acad Sci U S A* **106**, 11776-11781.

Stöhr H, Heisig JB, Benz PM, Schöberl S, Milenkovic VM, Strauss O, Aartsen WM, Wijnholds J, Weber BHF & Schulz HL (2009). TMEM16B, a novel protein with calcium-dependent chloride channel activity, associates with a presynaptic protein complex in photoreceptor terminals. *J Neurosci* **29**, 6809-6818.

Stöhr H, Marquardt A, Nanda I, Schmid M & Weber BHF (2002). Three novel human VMD2-like genes are members of the evolutionary highly conserved RFP-TM family. *Eur J Hum Genet* **10**, 281-284.

Sun H, Tsunenari T, Yau K & Nathans J (2002). The vitelliform macular dystrophy protein defines a new family of chloride channels. *Proc Natl Acad Sci U S A* **99**, 4008-4013.

Suzuki M (2006). The *Drosophila* tweety family: molecular candidates for large-conductance Ca^{2+}-activated Cl^- channels. *Exp Physiol* **91**, 141-147.

Suzuki M & Mizuno A (2004). A novel human Cl^- channel family related to *Drosophila* flightless locus. *J Biol Chem* **279**, 22461-22468.

Takeuchi H & Kurahashi T (2002). Photolysis of caged cyclic AMP in the ciliary cytoplasm of the newt olfactory receptor cell. *J Physiol* **541**, 825-833.

Takeuchi H & Kurahashi T (2003). Identification of second messenger mediating signal transduction in the olfactory receptor cell. *J Gen Physiol* **122**, 557-567.

Takeuchi H & Kurahashi T (2005). Mechanism of signal amplification in the olfactory sensory cilia. *J Neurosci* **25**, 11084-11091.

Takeuchi H, Imanaka Y, Hirono J & Kurahashi T (2003). Cross-adaptation between olfactory responses induced by two subgroups of odorant molecules. *J Gen Physiol* **122**, 255-264.

Thoreson WB & Burkhardt DA (1991). Ionic influences on the prolonged depolarization of turtle cones in situ. *J Neurophysiol* **65**, 96-110.

Tirindelli R, Dibattista M, Pifferi S & Menini A (2009). From pheromones to behavior. *Physiol Rev* **89**, 921-956.

Tomaru A & Kurahashi T (2005). Mechanisms determining the dynamic range of the bullfrog olfactory receptor cell. *J Neurophysiol* **93**, 1880-1888.

Tsunenari T, Nathans J & Yau K (2006). Ca^{2+}-activated Cl^- current from human bestrophin-4 in excised membrane patches. *J Gen Physiol* **127**, 749-754.

Tsunenari T, Sun H, Williams J, Cahill H, Smallwood P, Yau K & Nathans J (2003). Structure-function analysis of the bestrophin family of anion channels. *J Biol Chem* **278**, 4114-4125.

Tsutsumi S, Kamata N, Vokes TJ, Maruoka Y, Nakakuki K, Enomoto S, Omura K, Amagasa T, Nagayama M, Saito-Ohara F, Inazawa J, Moritani M, Yamaoka T, Inoue H & Itakura M (2004). The novel gene encoding a putative transmembrane protein is mutated in gnathodiaphyseal dysplasia (GDD). *Am J Hum Genet* **74**, 1255-1261.

Webb DJ & Nuccitelli R (1985). Fertilization potential and electrical properties of the *Xenopus laevis* egg. *Dev Biol* **107**, 395-406.

Weeraratne SD, Valentine M, Cusick M, Delay R & Van Houten JL (2006). Plasma membrane calcium pumps in mouse olfactory sensory neurons. *Chem Senses* **31**, 725-730.

West RB, Corless CL, Chen X, Rubin BP, Subramanian S, Montgomery K, Zhu S, Ball CA, Nielsen TO, Patel R, Goldblum JR, Brown PO, Heinrich MC & van de Rijn M (2004). The novel marker, DOG1, is expressed ubiquitously in gastrointestinal stromal tumors irrespective of KIT or PDGFRA mutation status. *Am J Pathol* **165**, 107-113.

Whyte WL, Irick H, Arbel T, Yasuda G, French RL, Falk DR & Hawley RS (1993). The genetic analysis of achiasmate segregation in *Drosophila melanogaster*. III. The wild-type product of the Axs gene is required for the meiotic segregation of achiasmate homologs. *Genetics* **134**, 825-835.

Wong ST, Trinh K, Hacker B, Chan GC, Lowe G, Gaggar A, Xia Z, Gold GH & Storm DR (2000). Disruption of the type III adenylyl cyclase gene leads to peripheral and behavioral anosmia in transgenic mice. *Neuron* **27**, 487-497.

Wright EM & Diamond JM (1977). Anion selectivity in biological systems. *Physiol Rev* **57**, 109-156.

Yan C, Zhao AZ, Bentley JK & Beavo JA (1996). The calmodulin-dependent phosphodiesterase gene PDE1C encodes several functionally different splice variants in a tissue-specific manner. *J Biol Chem* **271**, 25699-25706.

Yan C, Zhao AZ, Bentley JK, Loughney K, Ferguson K & Beavo JA (1995). Molecular cloning and characterization of a calmodulin-dependent phosphodiesterase enriched in olfactory sensory neurons. *Proc Natl Acad Sci U S A* **92**, 9677-9681.

Yang YD, Cho H, Koo JY, Tak MH, Cho Y, Shim W, Park SP, Lee J, Lee B, Kim B, Raouf R, Shin YK & Oh U (2008). TMEM16A confers receptor-activated calcium-dependent chloride conductance. *Nature* **455**, 1210-1215.

Yau KW (1994). Phototransduction mechanism in retinal rods and cones. The Friedenwald Lecture. *Invest Ophthalmol Vis Sci* **35**, 9-32.

Yu K, Lujan R, Marmorstein A, Gabriel S & Hartzell HC (2010). Bestrophin-2 mediates bicarbonate transport by goblet cells in mouse colon. *J Clin Invest* **120**, 1722-1735.

Yu T, McIntyre JC, Bose SC, Hardin D, Owen MC & McClintock TS (2005). Differentially expressed transcripts from phenotypically identified olfactory sensory neurons. *J Comp Neurol* **483**, 251-262.

Zhainazarov AB & Ache BW (1995). Odor-induced currents in *Xenopus* olfactory receptor cells measured with perforated-patch recording. *J Neurophysiol* **74**, 479-483.

Zhang Y, Patil RV & Marmorstein AD (2010). Bestrophin 2 is expressed in human non-pigmented ciliary epithelium but not retinal pigment epithelium. *Mol Vis* **16**, 200-206.

Zhao H & Reed RR (2001). X inactivation of the OCNC1 channel gene reveals a role for activity-dependent competition in the olfactory system. *Cell* **104**, 651-660.

Zhao H, Ivic L, Otaki JM, Hashimoto M, Mikoshiba K & Firestein S (1998). Functional expression of a mammalian odorant receptor. *Science* **279**, 237-242.

Zitron AE & Hawley RS (1989). The genetic analysis of distributive segregation in *Drosophila melanogaster*. I. Isolation and characterization of Aberrant X segregation (Axs), a mutation defective in chromosome partner choice. *Genetics* **122**, 801-821.

Zufall F & Firestein S (1993). Divalent cations block the cyclic nucleotide-gated channel of olfactory receptor neurons. *J Neurophysiol* **69**, 1758-1768.

Zufall F, Firestein S & Shepherd GM (1991). Analysis of single cyclic nucleotide-gated channels in olfactory receptor cells. *J Neurosci* **11**, 3573-3580.

Acknowledgments

I would like to first express my gratitude to my woman guides.
To my supervisor Anna Menini for her faith in this project, for her constant, patient and expert guidance. She highlighted for me the importance of devoted attitude in our extraordinary job and I have learnt very much from working with her.
To Anna Boccaccio, who have taught me a lot with patience, for her support and perceptive and enlightening advices.

I feel very much indebted to Michele Dibattista for his daily help and discussions to improve my knowledge in the field; to Valentina Cenedese for her comments, and more generally for exploring with me the boundaries of professional friendship; to Fulvio Celsi for the discussions which helped me develop the ideas, in challenging me with alternative views; to several other colleagues, technicians and friends at SISSA, who have assisted me one way or another.

I am particularly grateful to my parents, Andrea, Sergio, Tore and especially Roberta, even though they are far away they have always trust me.
Also, my in-laws and my long standing friends support meant a great deal to me.

I am very thankful to my friends Marilena and Assunta, who have shared their ideas, free time and emotions with me over the years.

And most importantly I owe much to Giuseppe, his love in full support of my research has been vital energy for me and it is the best hope for our future together.

It would not have been possible without your help.

Thank you all,

Claudia